TESLA - COLLABORATION

R & D Issues in the Field of Superconducting Cavities

Feb. 29, 1996, DESY

March 1996, TESLA 96-03

Contents

R&D Meeting, Thursday, Feb. 29, Bldg. 30B, Rm 459

It is the idea to report/discuss about the following subjects and to stimulate further experimental investigations:

A: Quench limitations

1. Review model calculations of quench fields as function of
- defect size (including defect-free case)
- wall thickness
- RRR
- Kapitza resistance

Model calculations have been done at Cornell,Wuppertal (finite element) and at Saclay (analytic) - Reschke Safa
2. Experimental verification of Kapitza resistance - Saclay/Orsay
3. Compare measured results of quench limitations vs. RRR - Moeller
4. Experimental evidence of importance of material parameters other than RRR on cavity performance - (discussion)
5. Correlation between Qo at low field and max Eacc - (discussion)

B: Ti heat treatment

1. Theoretical diffusion (grain boundary diffusion) of Ti into Nb as function of temperature and time - Singer
2. Experimental data on Ti diffusion into Nb - Matheisen, Safa
3. Temperature and time profile during Ti treatment: experience with cavities and samples. - (Saclay/Desy)
4. Lowering of yield strength by heat treatment - Kaiser, Singer

C: Quality control of Nb

1. First results/conclusion from magnetization measurements - Schmueser
2. First results/conclusions from Hc2 measurements - Müller
3. Results from eddy current measurements: is this a method to scan Nb sheet material - Singer
4. Material properties of Tokyo Denkai Nb material - (NN)

D: Field emission

1. Correlation of field emission properties with treatment of TTF cavities - Kuzminski
2. Strategy to achieve high gradients without HPP - (discussion)
3. Do we gain permanent improvement after HPP? - (discussion)
4. Understanding of Q degradation after HPP. - Pekeler, NN
5. DC field emission from naturally rough particles - Habermann

Summary of workshop on niobium properties and cavity treatment

P.Schmüser

A) Quality control of niobium

1) First results/conclusions from B_{c2} measurements (G. Müller, Wuppertal).

In the apparatus built at Wuppertal, a niobium sample of 30x10x3 mm^3 size is inserted between two small coils of 8 mm diameter. The first coil produces an a.c. magnetic field of up to 50 Gauss transverse to the surface of the sample, the second coil serves as induction coil. The signal is processed with a lock-in analyzer. The optimum frequency is about 160 Hz, higher frequencies lead to microphonics. There is some stray flux around the sample, so the pick-up coil receives also a signal when the sample is superconductive. The arrangement is positioned inside a superconducting solenoid coil providing a longitudinal field B_0 of up to 8 T. A standard measurement consists in recording the amplitude of the pick-up signal as a function of the field B_0. When the upper critical field of Nb is exceeded one observes a steep increase in signal amplitude since the field attenuation in normal-conducting Nb is weak. The position of the step determines B_{c2} . For a pure niobium surface one obtains B_{c2}=0.27 T. The height of the step is a measure of RRR, large RRR values (high conductivity Nb) give a small step.

Two Heraeus samples show this nicely, sample (a) with 770°C heat treatment and 100 μm chemical polishing, sample (b) with 1400°C heat treatment (titanium getter) and 200 μm chemical polishing. In a Wah Chang sample (c) the transition starts at the same field but is wider, indicating some surface damage. The Wuppertal 'reference sample' (d) from old Kawecki material has a wide transition above 0.4 T which implies surface contamination.

Using a very small a.c. field of 50 mG the technique is extremely sensitive to thin surface layers. The data show clearly that after a 1400°C heat treatment with titanium getter a NbTi surface layer is present which needs at least 200 μm of BCP to be removed. A chemical polishing of 200 μm appears also recommendable for the new heat treatment (1 hour at 1400°C, 3 hours at 1250°C) but the B_{c2} data are not yet conclusive.

2) Eddy current check of niobium at BAM (W. Singer, DESY).

The Bundesanstalt für Materialforschung in Berlin has developed a high-resolution scanning head which is capable of resolving defects in the few 100 μm range. The eddy-current penetration depth depends on the conductivity of the sample and on frequency. Voids and scratches of at least 100 μm can be detected in a surface layer up to 300 μm deep. For a larger depth up to 3 mm the minimum defect size is 500 μm. In cell 5 of cavity D6 a large defect was found. Scanning of entire niobium sheets takes very long with the present setup.

3) First results on Nb magnetization hysteresis (P. Schmüser, Uni Hamburg).

Following a design at KEK an apparatus was built at DESY for measuring the magnetic hysteresis of 9x9mm^2 samples from the Nb sheets used for cavity production. The basic idea is that pure niobium should have no flux pinning and hence follow a reversible magnetization curve while the observation of a magnetic hysteresis is a proof of magnetic flux pinning. Pinning centers (lattice defects or impurities) at the surface can be expected to increase the surface RF resistance. The Japanese data show a large hysteresis after heat treatment with titanium gettering which vanishes after chemical polishing. This is an indication that a NbTi surface layer was formed by the heat treatment with Ti getter. The Heraeus Nb sheets exhibit a large hysteresis loop in the raw material. After heat treatment (1 hour at 1400°C, 3 hours at 1250°C with Ti getter) but without subsequent chemical polishing the enclosed area of the hysteresis loop is reduced by factor of 10. Additional chemistry (50 μm removal) does not change the hysteresis. These results are surprising in view of the KEK results. Investigations on the sensitivity of the DESY setup to NbTi surface layers are needed.

B) Quench limitations

1) Thermal model calculations (D. Reschke, DESY).

At Wuppertal a program has been written to solve the heat equation for a cylindrical disk on a discrete lattice. The mesh size is variable and can be made finer close to a possible hot spot at r=0. The heat conductivity of niobium is treated as temperature dependent. Data on $\lambda(T)$ for Nb of different RRR values are used as input. The Kapitza conductance is taken from measurements of Mittag and from Orsay, the uncertainty is estimated to be around 30%. Calculations were done at Wuppertal for 3 Ghz cavities. The calculated quench fields agree with experimental data. At low RRR the heat conductivity scales with the square root of RRR but above RRR=300 there is a weaker dependence of $\lambda(T)$ on RRR. This observation is supported by analytical calculations by H. Safa which are based on a constant average heat conductivity. It appears questionable whether an increase in RRR beyond 500 will improve the cavity performance. It was agreed that thermal calculations should be done for the TESLA 1.3 Ghz cavities.

2) Kapitza conductance at Cu-HeII interface and critical heat flux in saturated superfluid helium (M. Fouaidy, IPN-Orsay)
Precise data were presented for the heat transfer between copper and superfluid helium and on the heat flux in He II.

3) Experimental results on quench limitations (W.-D. Möller, DESY).

In test results from 40 single cell cavities (excluding the KEK cavities) the quench field is found to increase with $\sqrt{RRR}$ for RRR up to 300 and then to level off. For multicell cavities a clear rise between RRR=300 and 500 is seen. Several KEK single-cell cavities achieve very high quench field at moderate RRR (200-350). Model

calculations show that in case of large defects a significant improvement is expected by increasing RRR while for small defects the improvement is only moderate.

C) Heat treatment procedure of niobium cavities

1) Diffusion of O, C, N and Ti in niobium (W.Singer, DESY).

The elements O, C, N are dissolved in the bulk niobium and have to be removed by a suitable heat treatment. In material with RRR=300 the contamination amounts to around 5 μg oxygen per g Nb (5 weight ppm) and similarly for C and N. Heat treatment at 1400°C for 4 hours reduces the oxygen content to less than 0.1 wt ppm. The diffusion coefficients of O, C, N in Nb depend exponentially on temperature. A 4 hour heat treatment at 1400°C removes 98% of the oxygen, at 1200°C only 78%. The vacuum in the furnace (a few 10^{-7} mbar) is insufficient to perform heat treatment without titanium gettering because otherwise the oxygen content in the niobium would be enhanced. A reasonable vapour pressure of Ti requires high temperature, 1400°C being much more favourable than 1200°C. Titanium diffusion in pure Nb is very slow but as soon as a NbTi layer is formed the diffusion coefficient increases with increasing Ti concentration. For 4 hours at 1400°C Ti diffuses to about 100 μm depth but it should be noted that the diffusion occurs mainly at grain boundaries and may be deeper there. Hence 4 hours at 1400°C may be too much.

2) Experimenta data on titanium diffusion into niobium (A. Matheisen, DESY).

The heat treatment cycle I for TESLA cavities involves two pre-heating steps at 550°C and 1100°C for outgassing. Heating the furnace to these temperature levels requires 8 hours each. The oven is cooled down overnight. Then it is heated to 1400°C in 8 hours and stays at 1400°C for 4 hours. With titanium getter the RRR improves from 250-280 to about 550. The new cycle II involves 3 preheating steps (550°C, 1000°C and 1400°C with cooldown overnight in between). Then the furnace is heated up to 1400°C in 4 hours, stays at 1400°C for 1 hour, followed by 3 hours at 1250°C and cooldown. With cycle II the RRR increases somewhat less, to about 490. The preheating steps are needed because of heavy outgassing.

The titanium layer deposited in cycle I was measured by MAN to be about 16 μm thick. X ray analysis at MAN was not sensitive enough to reveal Ti penetration into deeper layers. A measurement at Hasylab which yielded a penetration depth of about 70 μm.

The heat treatment cycle for the TTF cavities should be reexamined. It appears that in the 3-hour period the temperature of 1250°C may be too low for an effective oxygen removal and that 1300°C or 1350°C (but less than 1400°C) might be more appropriate. Also a moderate extension of the time spent at high temperature may be favourable. Calculations and tests measurements are needed.

3) Softening of Nb during heat treatment (H. Kaiser, DESY).

Creep measurements on a heat-treated Nb sample show that the plastic limit is only 5 MPa (5 N/mm^2). When a load is applied one observes creep which leads to a lenghtening and a certain hardening of the material. Due to this extreme softness the

heat-treated cavity is very sensitive and can be plastically deformed by improper handling and during mounting in the test dewar or in the tuning apparatus. Measures have been taken to avoid this. Another concern is that the cavity might sag in the horizontal cryostat. If it is supported at the end flanges the maximum computed stress of 14 MPa clearly exceeds the plastic limit of 5 MPa. The measured plastic sag is found to follow a logarithmic time dependence. For a support at the end flanges a sag of 0.5 mm is expected in the first year and almost no sag afterwards. In the titanium cylinder the cavity is supported further inside and the expected sag is significantly lower. Hence a center support is not needed. However, extreme care must be excercised during handling and welding to prevent permanent deformation and detuning of the cavity.

D) Field emission

1) Correlation of field emission properties and cavity performance (J. Kusminski, DESY, M. Pekeler, Uni Hamburg).

The Dornier 9-cell cavities exhibited some field emission which could be removed by high power processing. The present limitations seen in D4, D5 and D6 are probably not due to field emission. The removal of emitters by HPP is usually accompanied with a Q degradation (if the initial Q was in the 10^{10} range). The interpration is that material evaporating from the emitting site is deposited elsewhere on the cavity surface and degrades the surface resistance. Hence HPP may be a viable method for removing field emitters from an already installed cavity but it is not considered a good tool for conditioning the cavity in the preparatory phase. There is general agreement that field emitters should and can be avoided by several high pressure rinsing steps and extremely careful handling. The standard RF test of the TTF cavities is now carried out with an input antenna that is matched to a high Q and does not allow HPP.
An improvement of Q by HPP was only observed when the initial Q was fairly low.

2) Field emission from natural rough particles (T. Habermann, Wuppertal).

The experiment has been designed to check the validity of the "tip-on-tip" model for large field enhancement factors. Field emission from dust particles were studied in a d.c. field. The emitting particles were investigated with a scanning electron miscroscope and their size, shape geometrical field enhancement factors were determined. By evaporating a gold film these geometrical quantities are modified in a well-defined way. Although there is a considerable spread in the correlation plots the data show clearly that with natural particles field enhancement factors in the range 50-200 can be realized.

3) Impact of dark current on the performance of 9-cell cavities (C. Stolzenburg, DESY).

A program has been written to track the trajectories of field-emitted electrons through the
9-cell cavity. It is obvious that the electrons emitted in a given cell extract energy not only from this cell but also from other cells. Hence, for identical field emission properties, the Q(E) curve of a 9-cell cavity will start to drop at an accelerating field that is roughly 5 MV/m lower than for a single-cell cavity. The Q(E) curves of the Dornier cavities D1 and D2 (without heavy field emission) can be well parametrized by a model in which many small field emitters are assumed with a gaussian distribution of field enhancement factors. The initial tests of these cavities were often dominated by single strong field emitter. Choosing an appropriate β value also the Q(E) curve of such a cavity is well reproduced. It appears that these calculations offer a nice way to parametrize cavity performance.

Hamburg, 29.2.96

FIRST RESULTS/CONCLUSIONS from H_{c2}-MEASUREMENTS on various Nb-samples from DESY

G. Müller
Univ. WUPPERTAL - CRYOELECTRA GmbH

I Measurement Technique

II Experimental Set-up

III Results

a) raw Nb from different producers

b) Nb after Ti-treatments + BCP

c) Surface Effects at low Test-Field

IV Conclusions

I Principle of H_{c2}-Measurement Technique

Abbildung 2.7 Der Meßaufbau

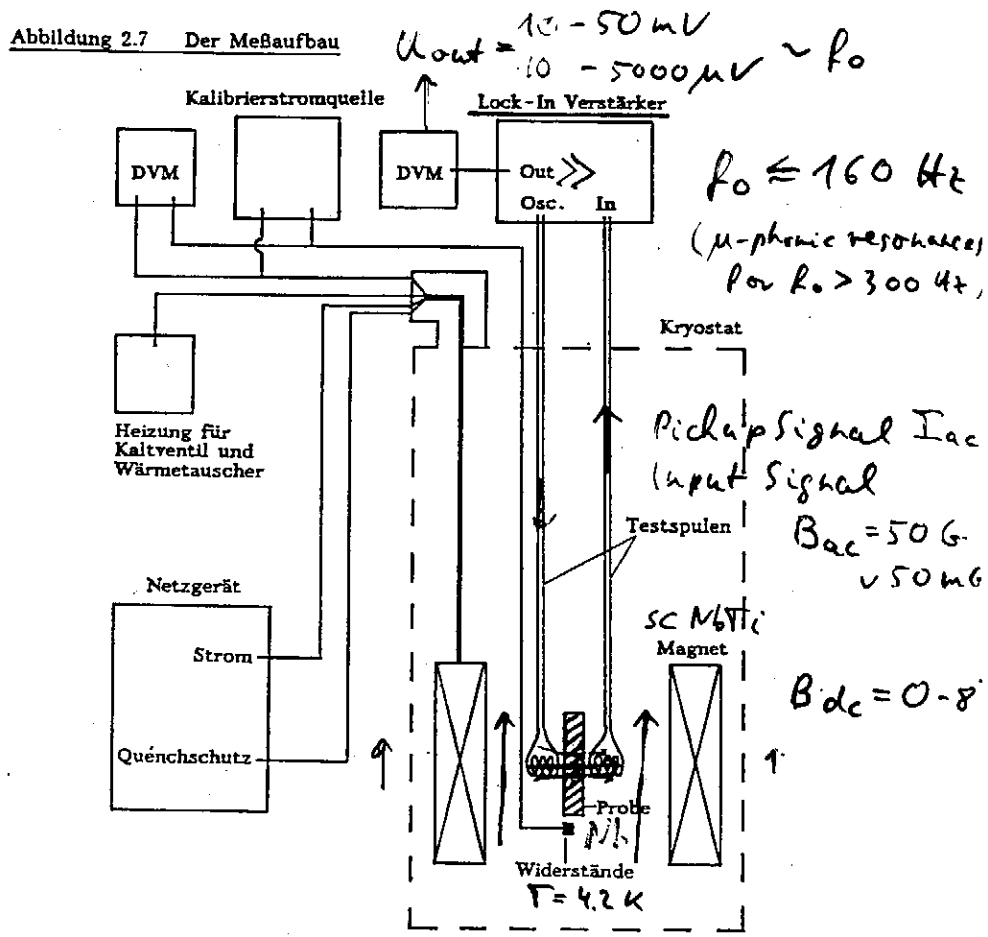

tesla 1996-03

a) non-destructive T_c-measurement of SC

Die Abschirmwirkung eines Supraleiters

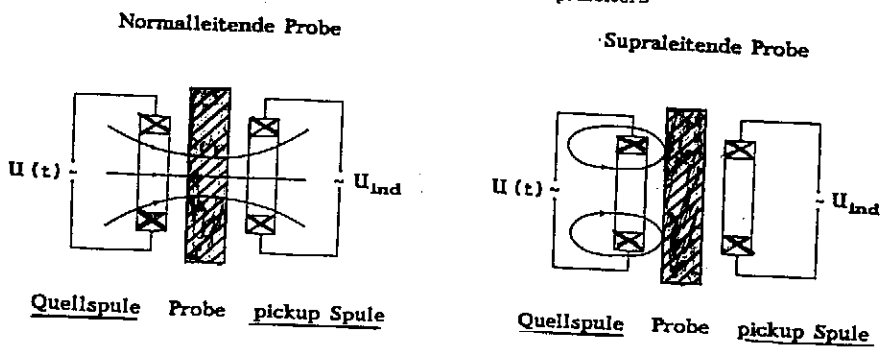

$B_{dc} = 0$

Induktive T_c-Messung an einer ausgeheizten Niobprobe (Nb1)
mit H_{ac} = 60 mOe, F = 15 Hz

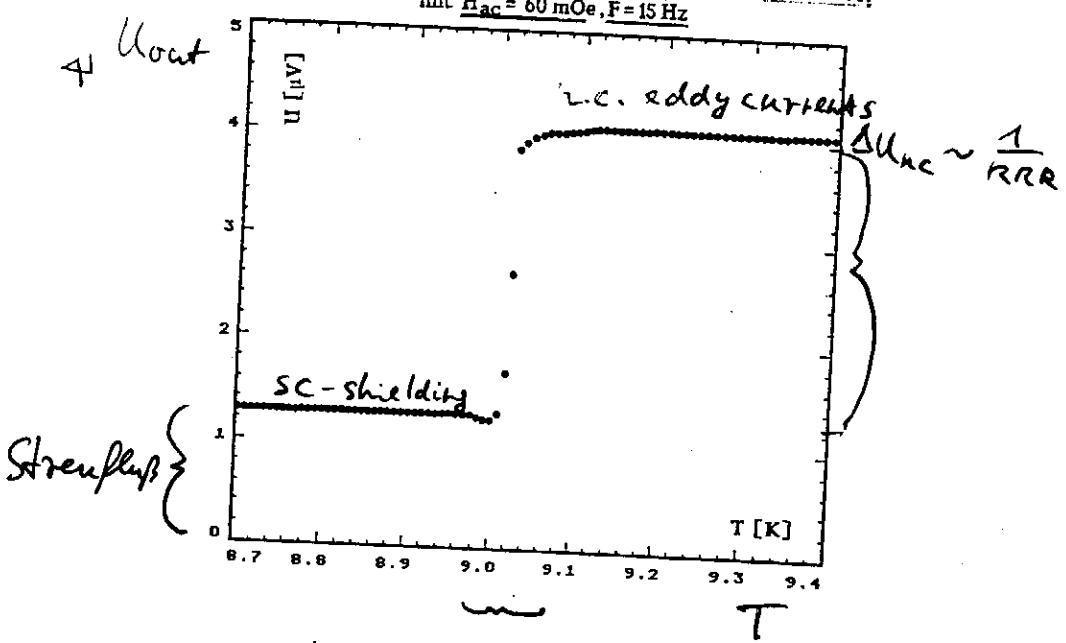

ΔU_{out}

e.c. eddy currents

$\Delta U_{ec} \sim \frac{1}{RRR}$

ΔT

transition width/shape

T_c - Homogeneity of SC-sample

$\overline{RRR}$ - determination from transition height ΔU_{ac}
(for homogenous samples only!)

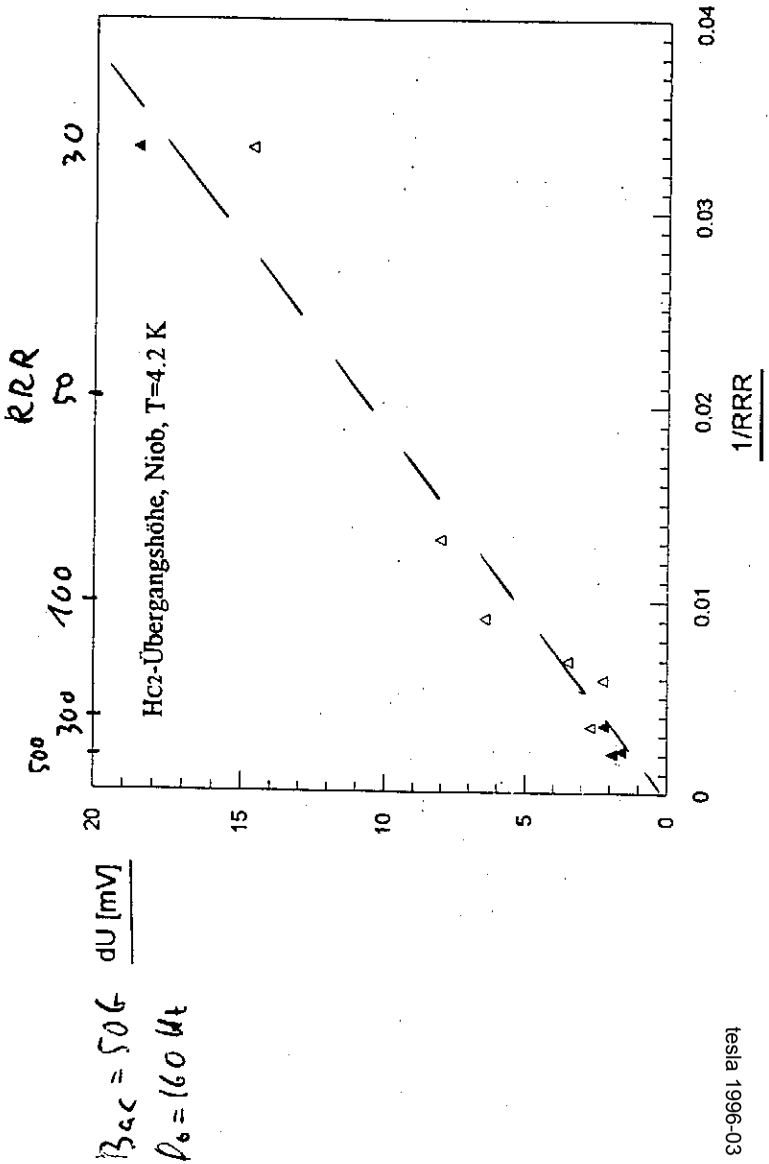

b) non-destructive H_{c2}-measurement of SC

$T_c = 4.2\,K$ $\quad B_{dc} = 0 - 8\,T > H_{c2}(Nb)$

⇓

- $B_{ac} < B_{c1} \Rightarrow$ Meißner-state – perfect SC shielding
- $B_{c1} < B_{dc} < B_{c2}$:

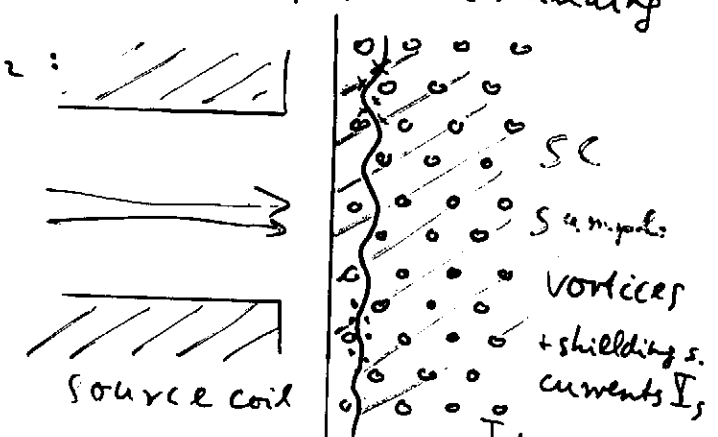

∞

Critical vortex state (Bean-Model) $\quad -\frac{dI_s}{dx} = j_c$

$B_{ac} = 50\,mG$ ⇒ $x \approx 10 - 1000\,\mu m$

Surface shielding

×1000 $\quad B_{ac} = 50\,G \Rightarrow x = 10 - 1000\,\mu m$ bulk shielding

- $B_{c2} < B_{dc} \Rightarrow$ NC eddy currents

Homogeneous sample ⇒ sharp Transition ΔB_{c2}

Coated sample or surface damage ⇒ Broad Transition

$B_{ac} = 50\,mG \Rightarrow$ surface layer dominates

$B_{ac} = 50\,G \Rightarrow j_c$(surface layer/passiv) bulk dominates

II Evaporation Cryostat with NbTi-Magnet

Abbildung 2.1

Der Verdampferkryostat mit supraleitendem 8 T Magnet

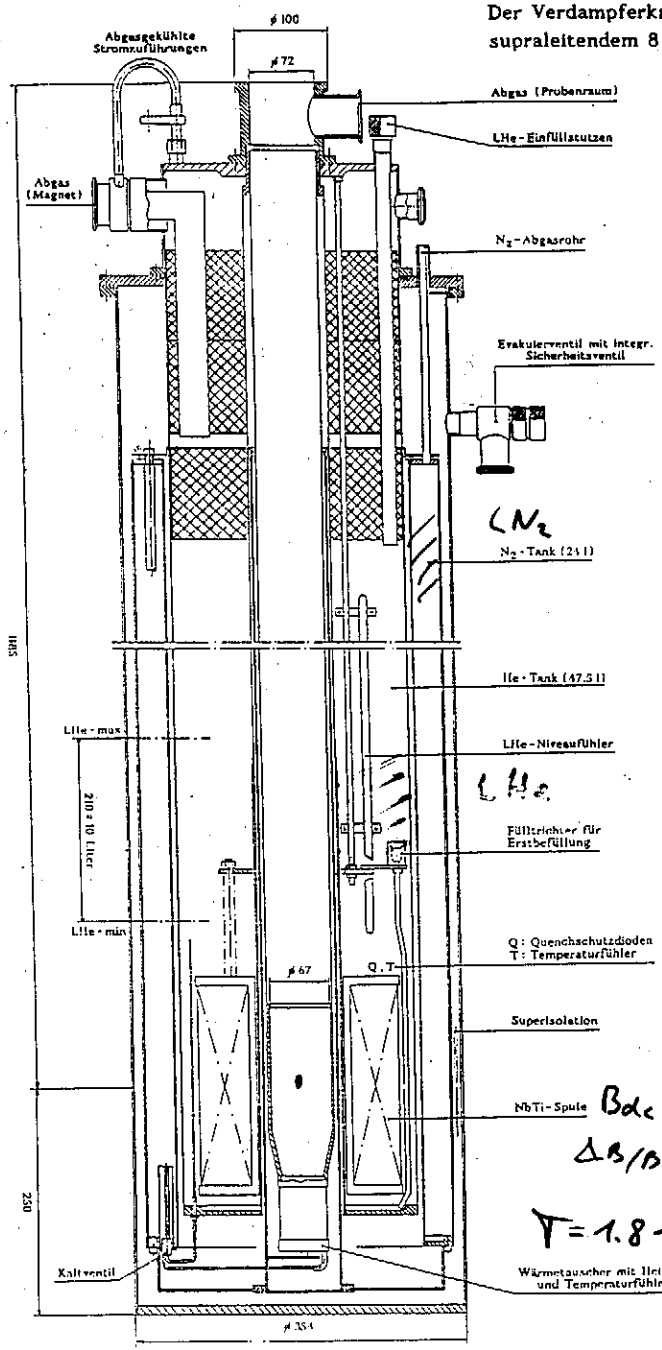

ca. 1.5 m

Tesla-1996-03

Bore ϕ = 67 mm

Test-Insert for quick sample exchange

Abbildung 2.5

Der Kryostateinsatz für induktive H_{c2} - Messungen

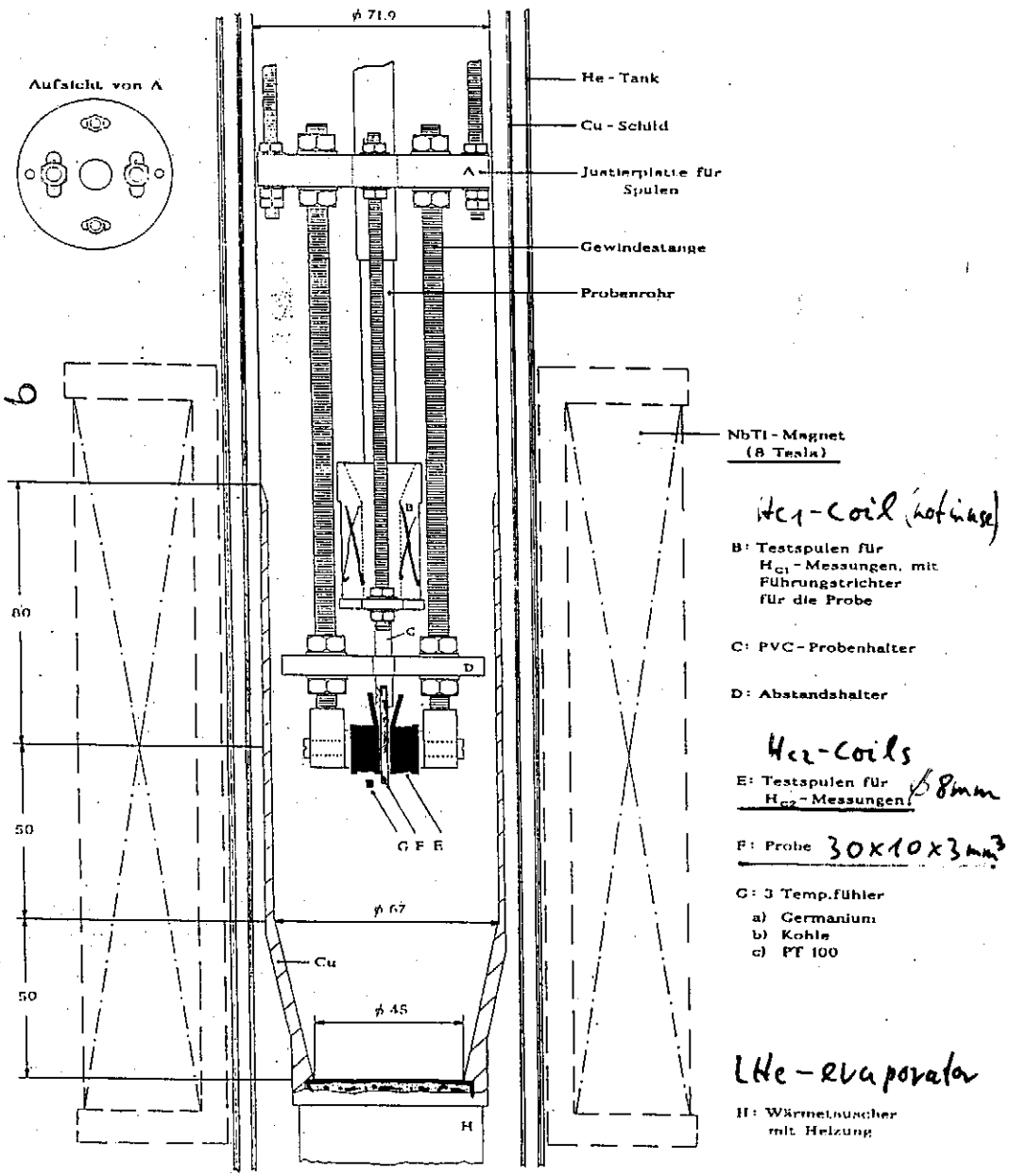

Hc1-coil (notinse)

B: Testspulen für H_{c1} - Messungen, mit Führungstrichter für die Probe

C: PVC - Probenhalter

D: Abstandshalter

Hc2-Coils

E: Testspulen für H_{c2} - Messungen ϕ 8mm

F: Probe 30x10x3mm³

G: 3 Temp.fühler
a) Germanium
b) Kohle
c) PT 100

LHe-evaporator

H: Wärmetauscher mit Heizung

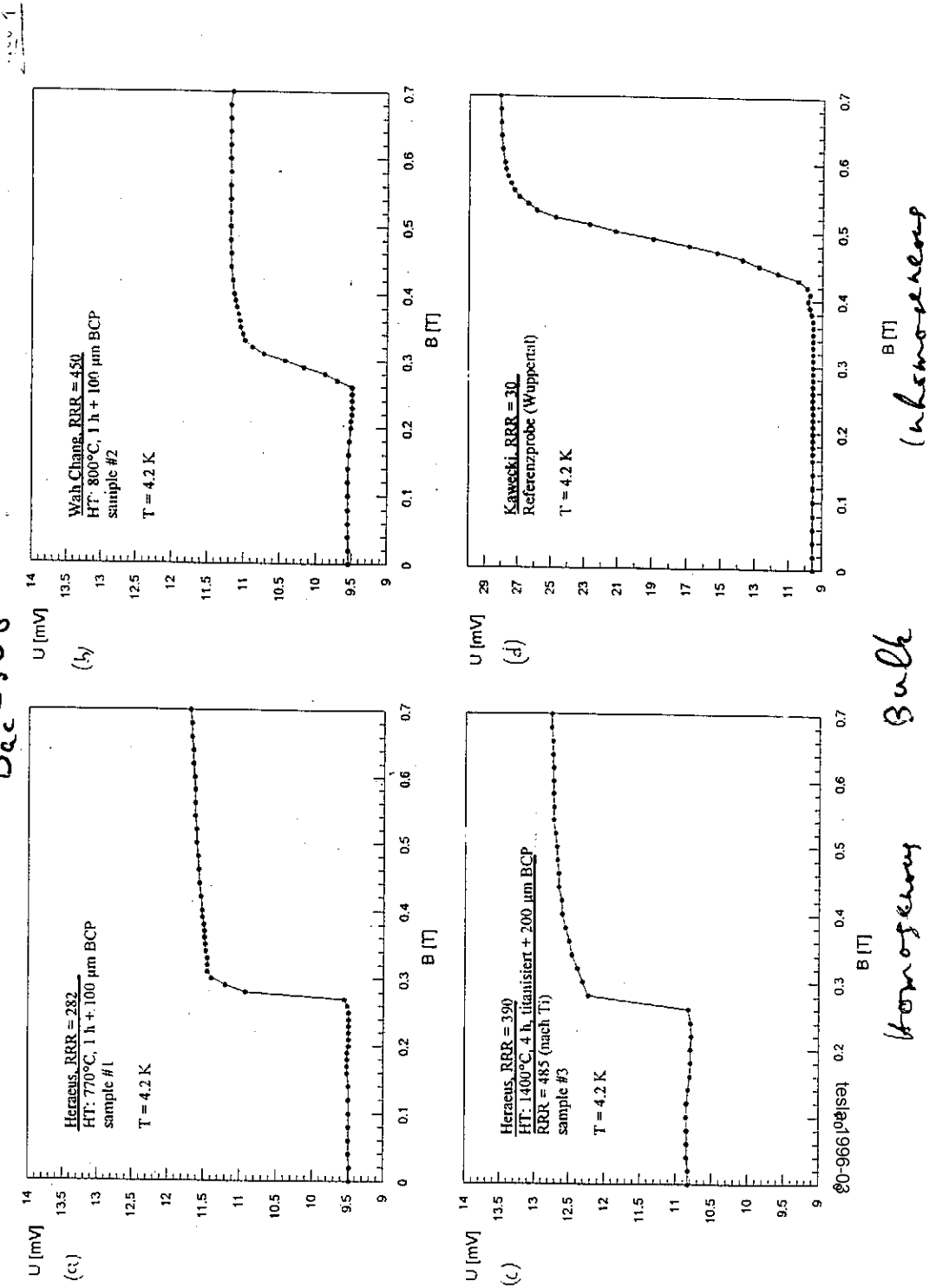

Bac = 50 G

Homogenes Bulk (Inhomogenes)

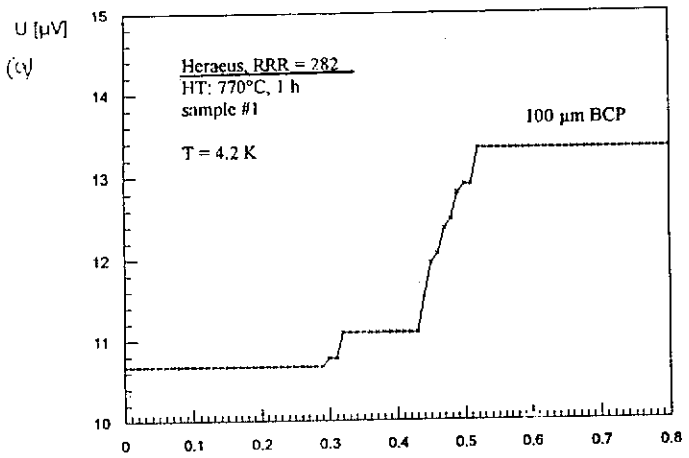

damaged surface

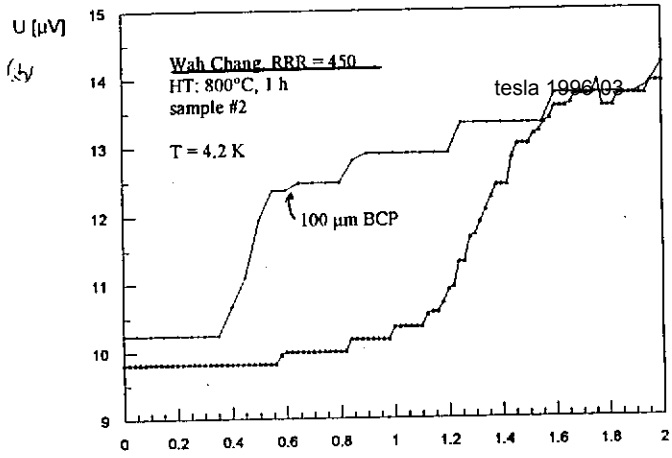

tesla 1996/03

damaged surface

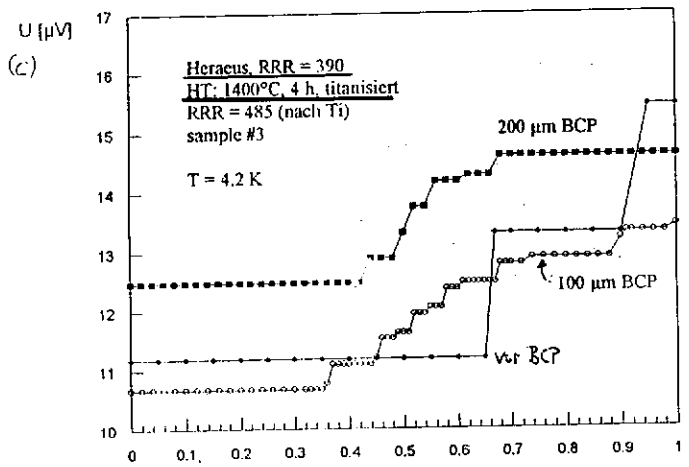

then after 200μm BCP not like Nb but rather Nb Ti

Surface

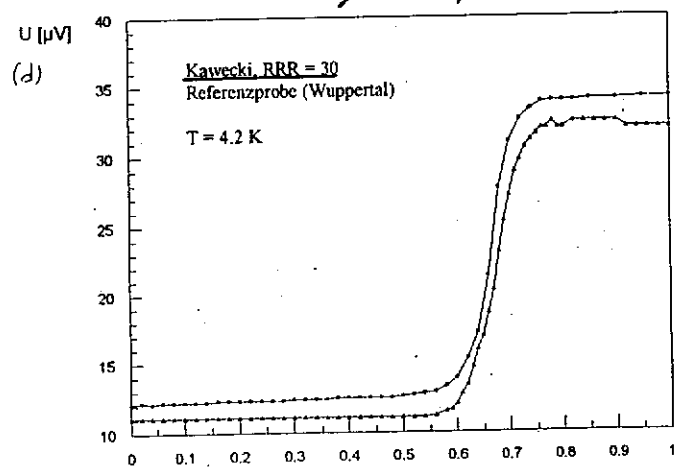

reduced RRR and inhomogeneous increased Hc2 compared to bulk

B_{ac} = 50mG

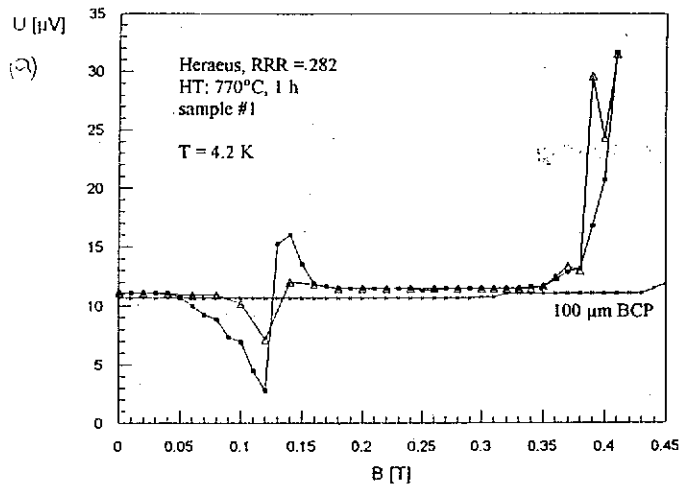

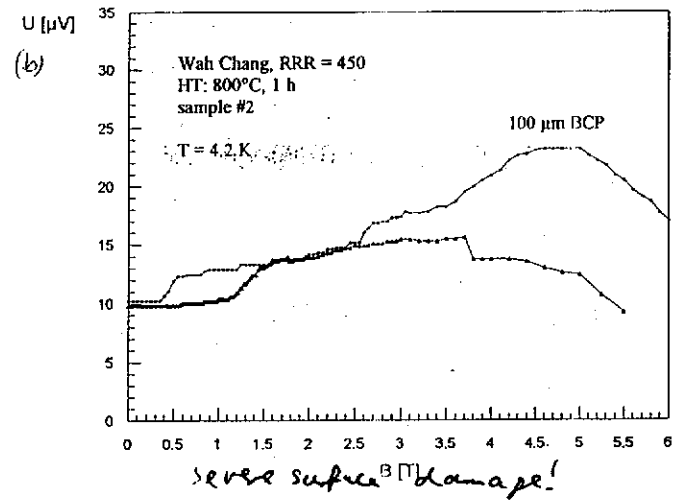

severe surface damage!

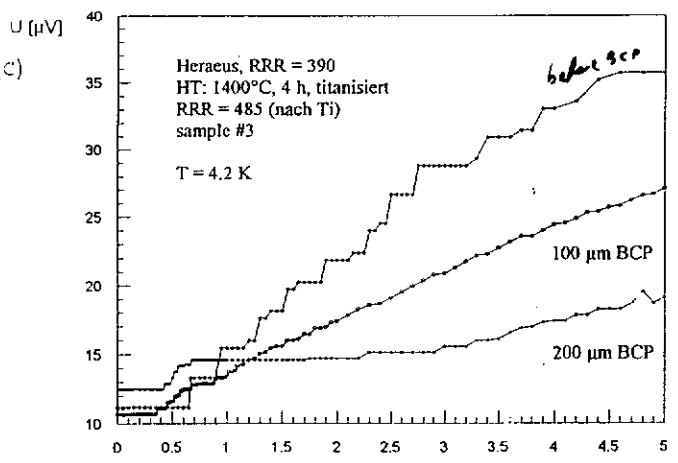

not saturated even at 5T!

(low RRR surface)

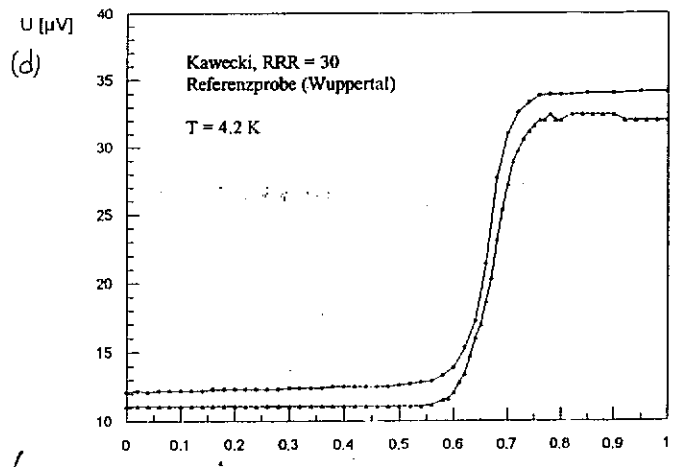

Ti- HT : 1400°C 1h, + 1250°C 3h no BCP

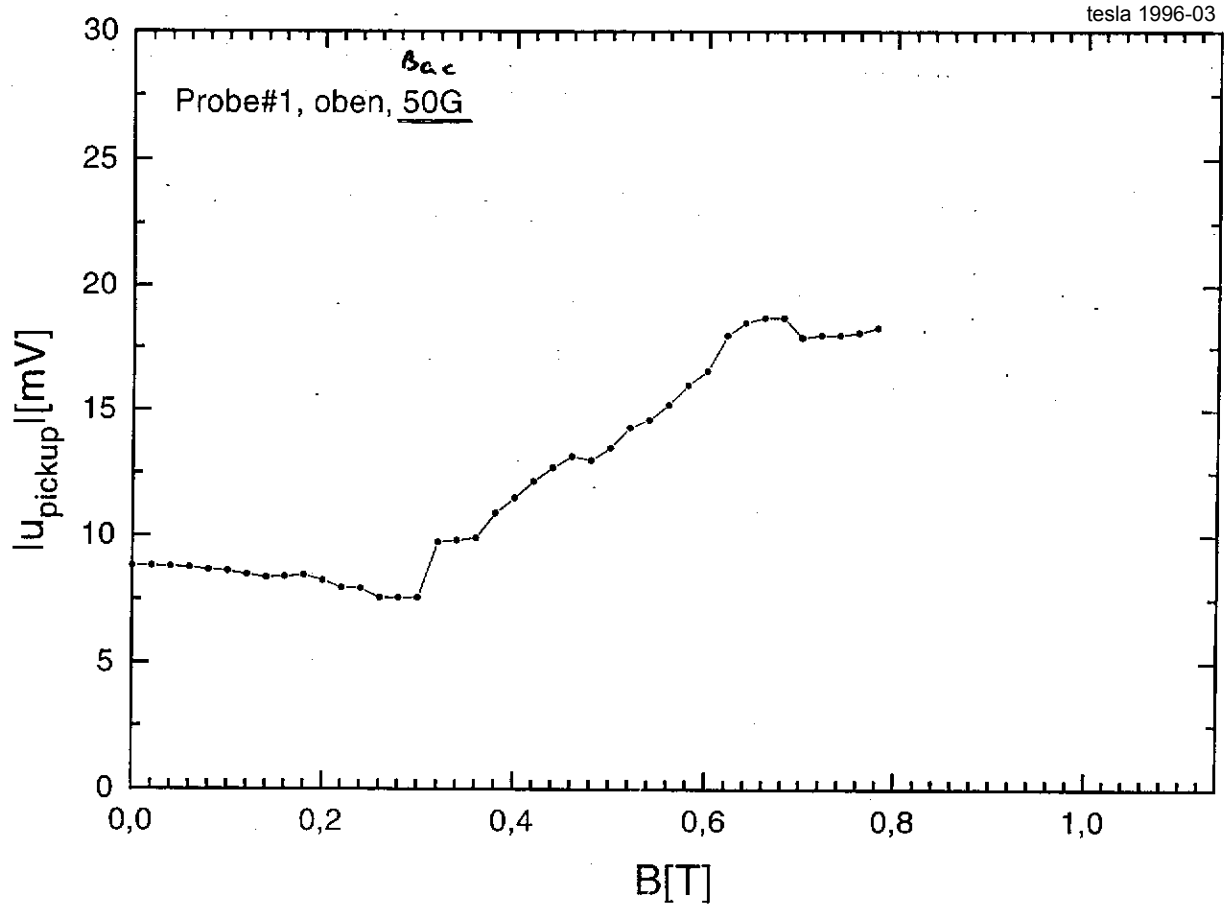

Ti- HT 1400°C 1h + 1100°C 3h no BCP

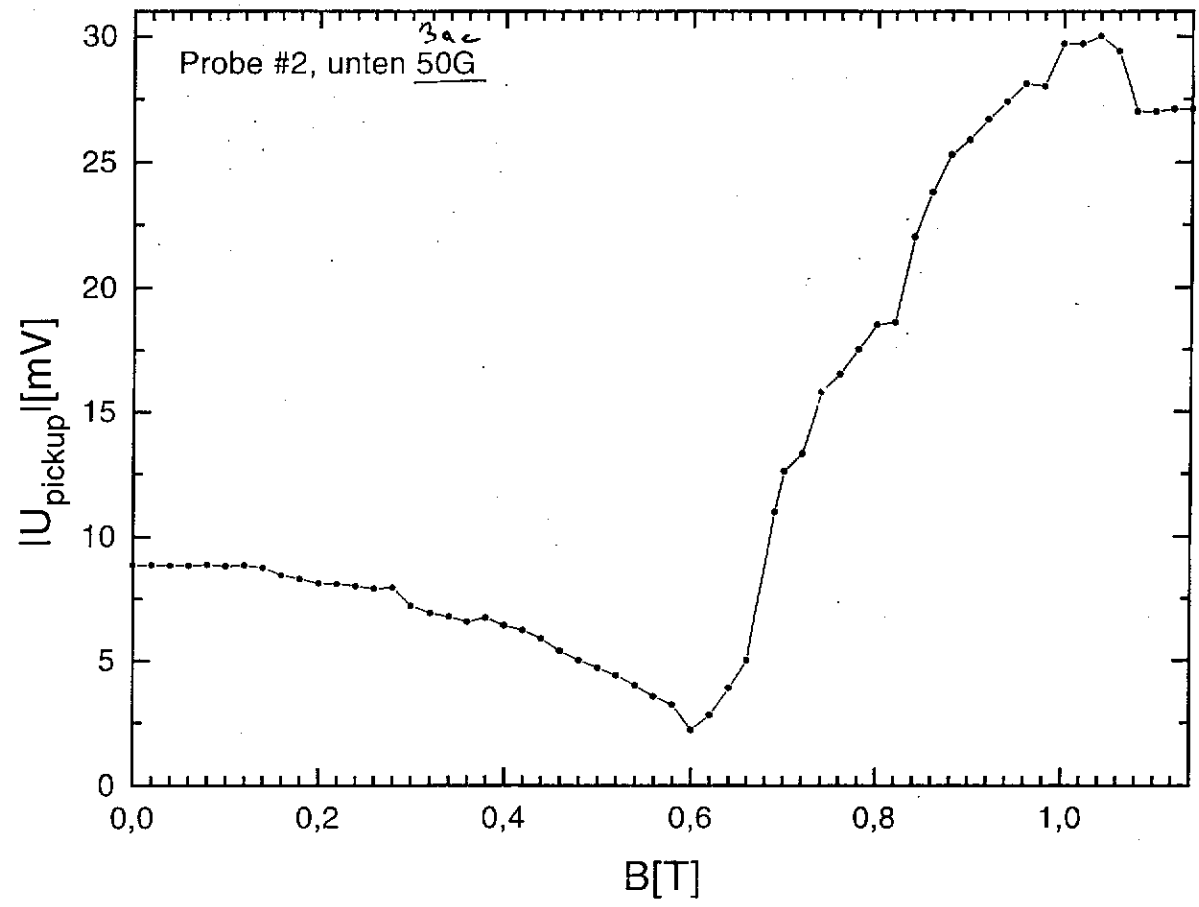

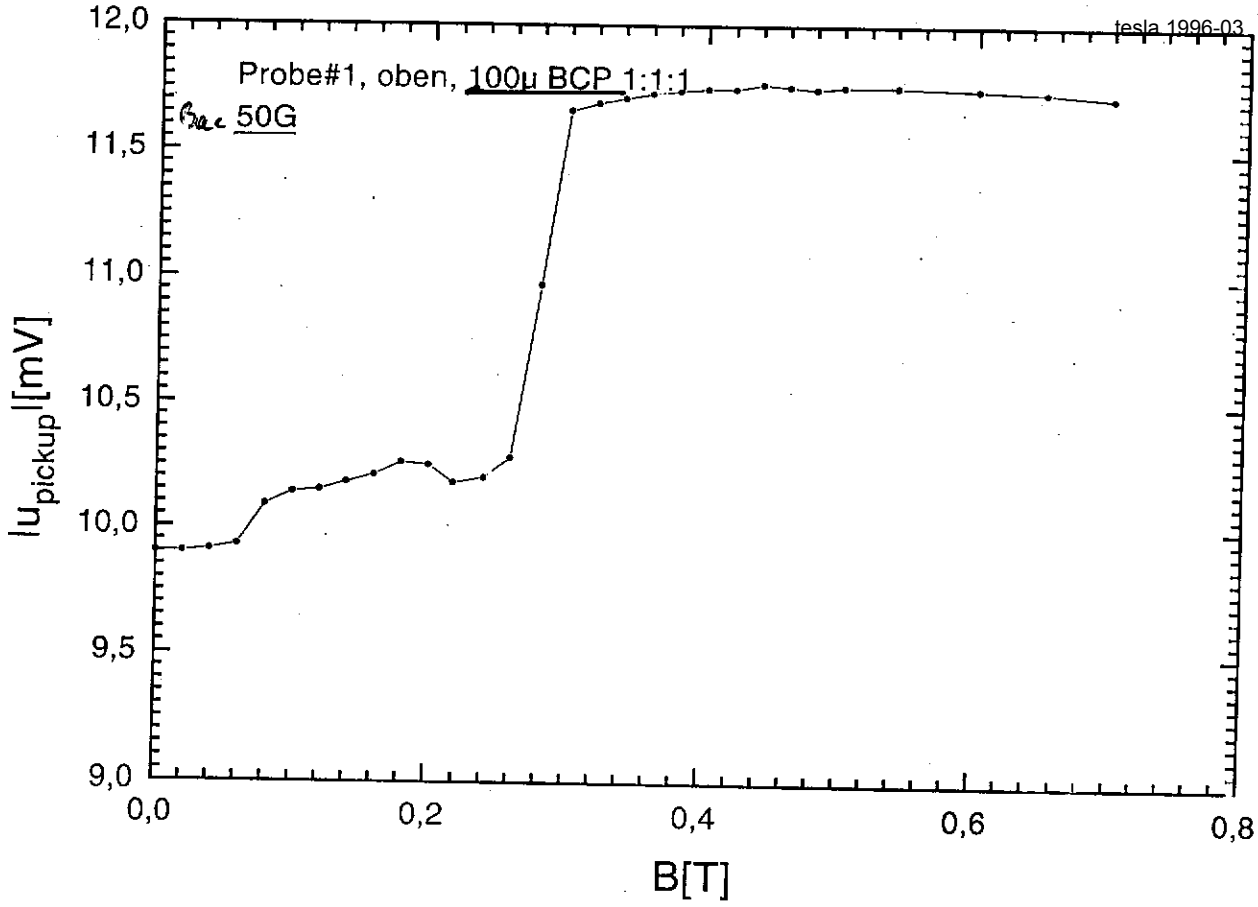
tesla 1996-03
Probe#1, oben, 100µ BCP 1:1:1
Bac 50G
12,0
11,5
11,0
10,5
10,0
9,5
9,0
0,0
0,2
0,4
0,6
0,8
B[T]
|u_pickup|[mV]

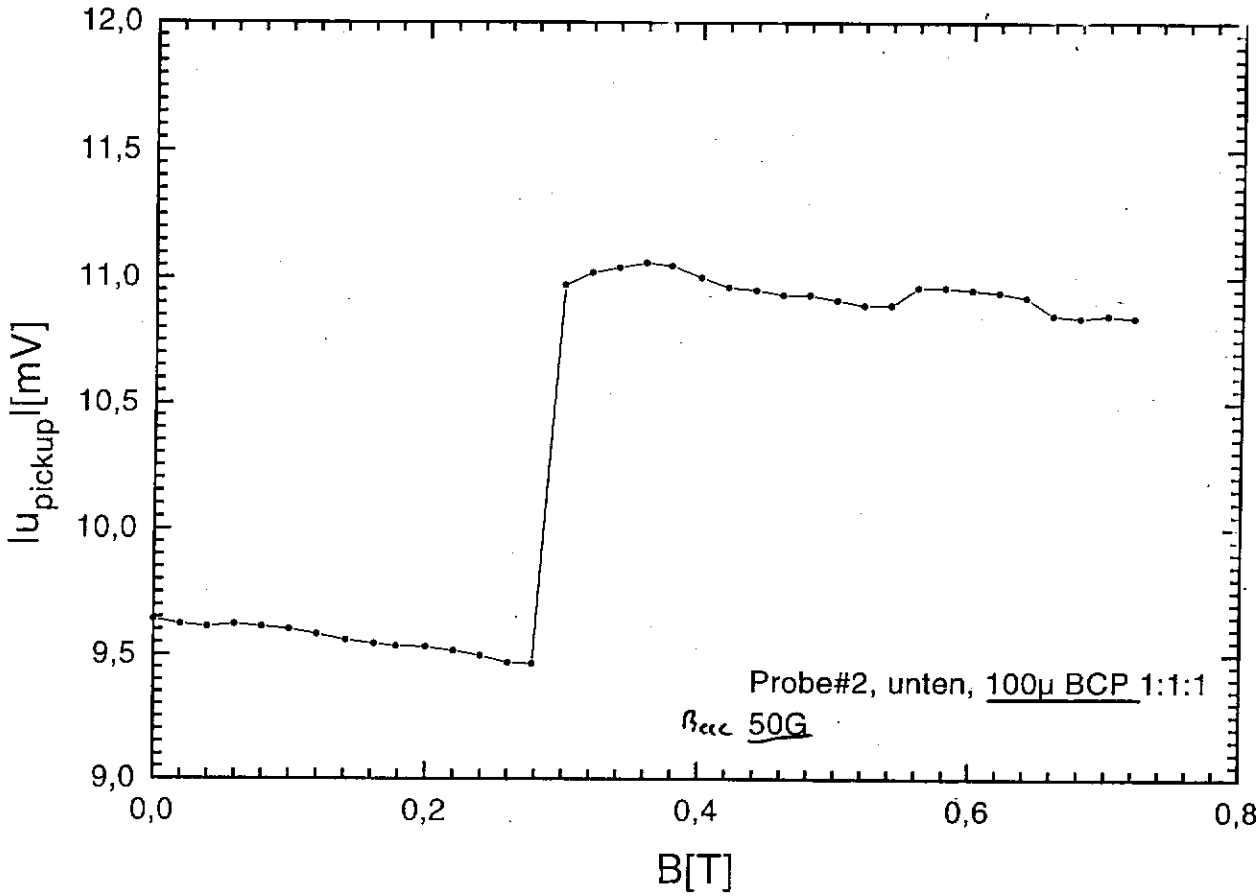
Probe#2, unten, 100µ BCP 1:1:1
Bac 50G
12,0
11,5
11,0
10,5
10,0
9,5
9,0
0,0
0,2
0,4
0,6
0,8
B[T]
|u_pickup|[mV]

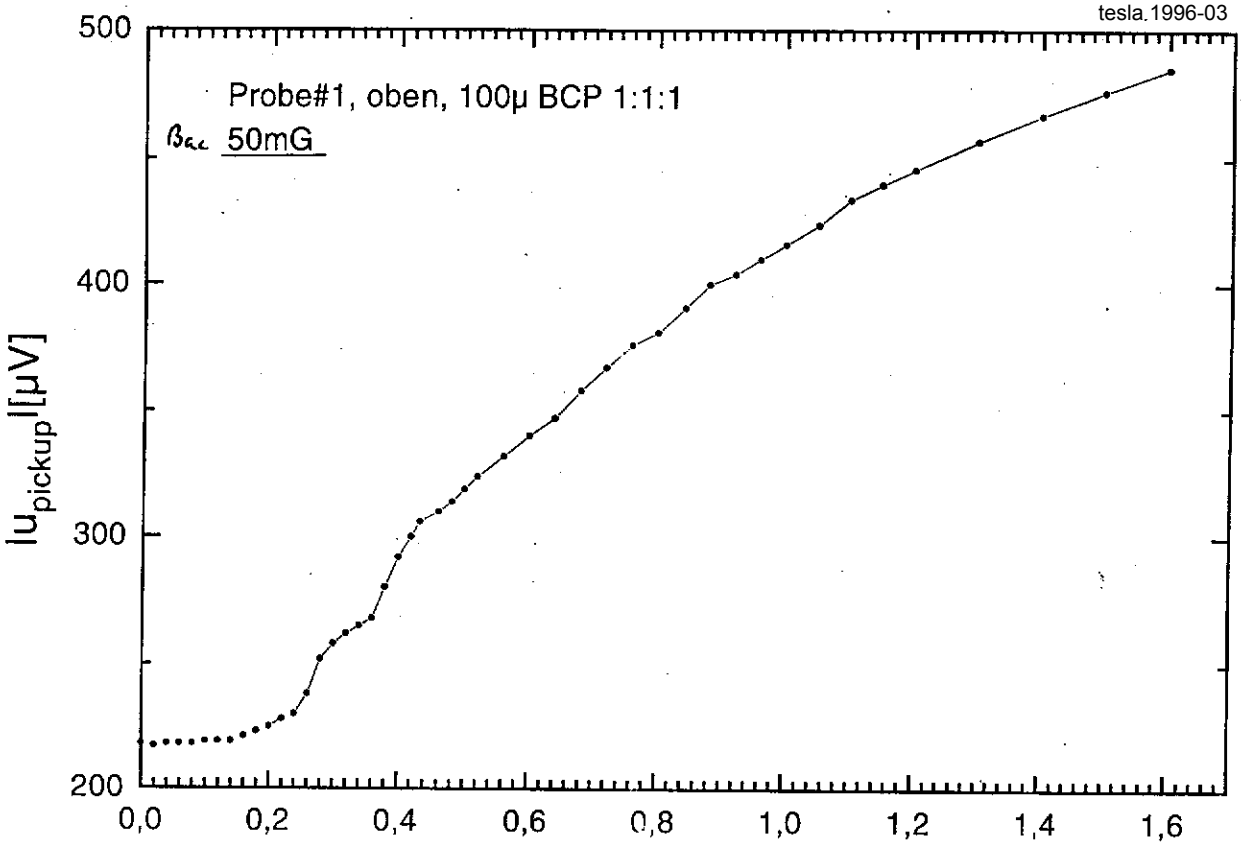
Probe#1, oben, 100µ BCP 1:1:1
B_{ac} 50mG
$|u_{pickup}|$[µV]
500
400
300
200
0,0
0,2
0,4
0,6
0,8
1,0
1,2
1,4
1,6
H_{c1}-onset ≙ bulk value B[T]
but rather in homogeneous, low conductivity surface

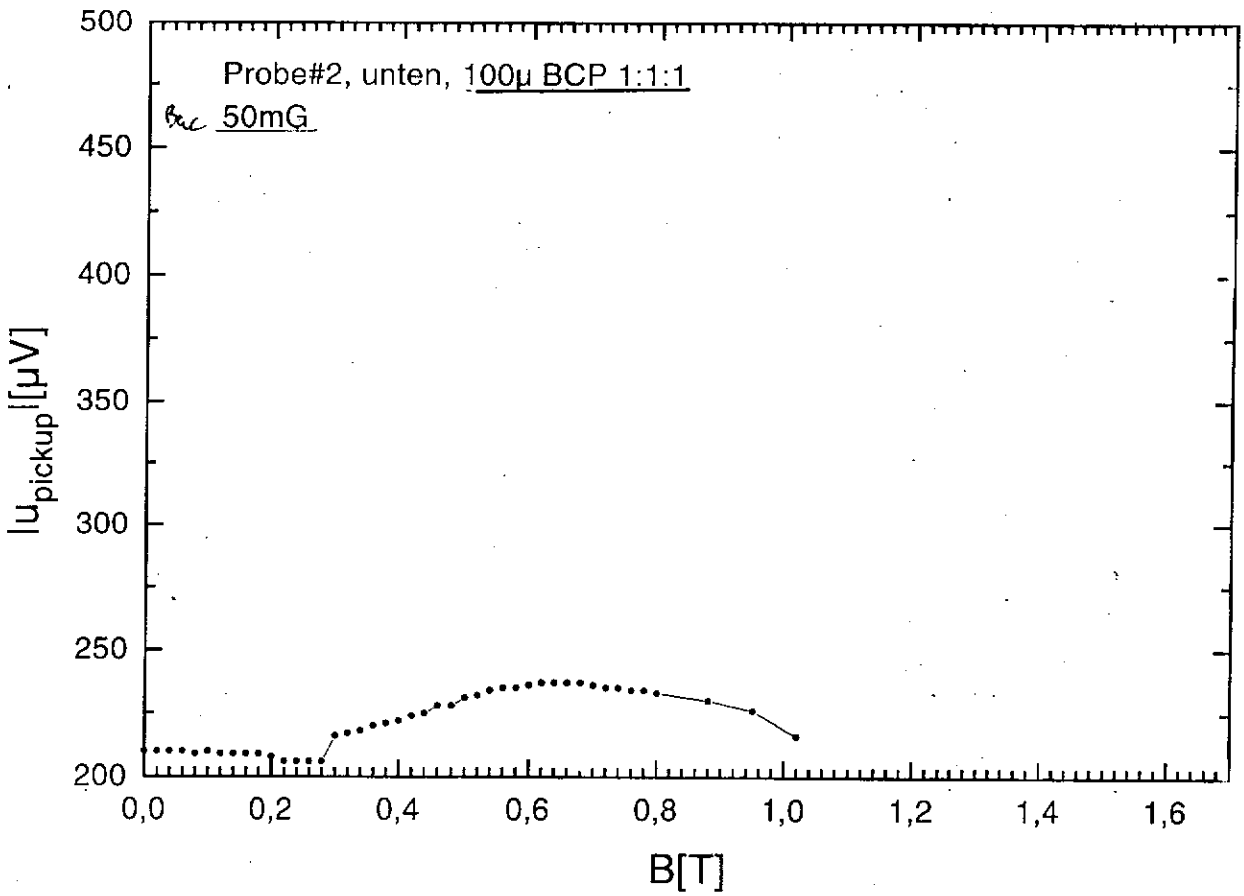
Probe#2, unten, 100µ BCP 1:1:1
B_{ac} 50mG
$|u_{pickup}|$[µV]
500
450
400
350
300
250
200
0,0
0,2
0,4
0,6
0,8
1,0
1,2
1,4
1,6
B[T]

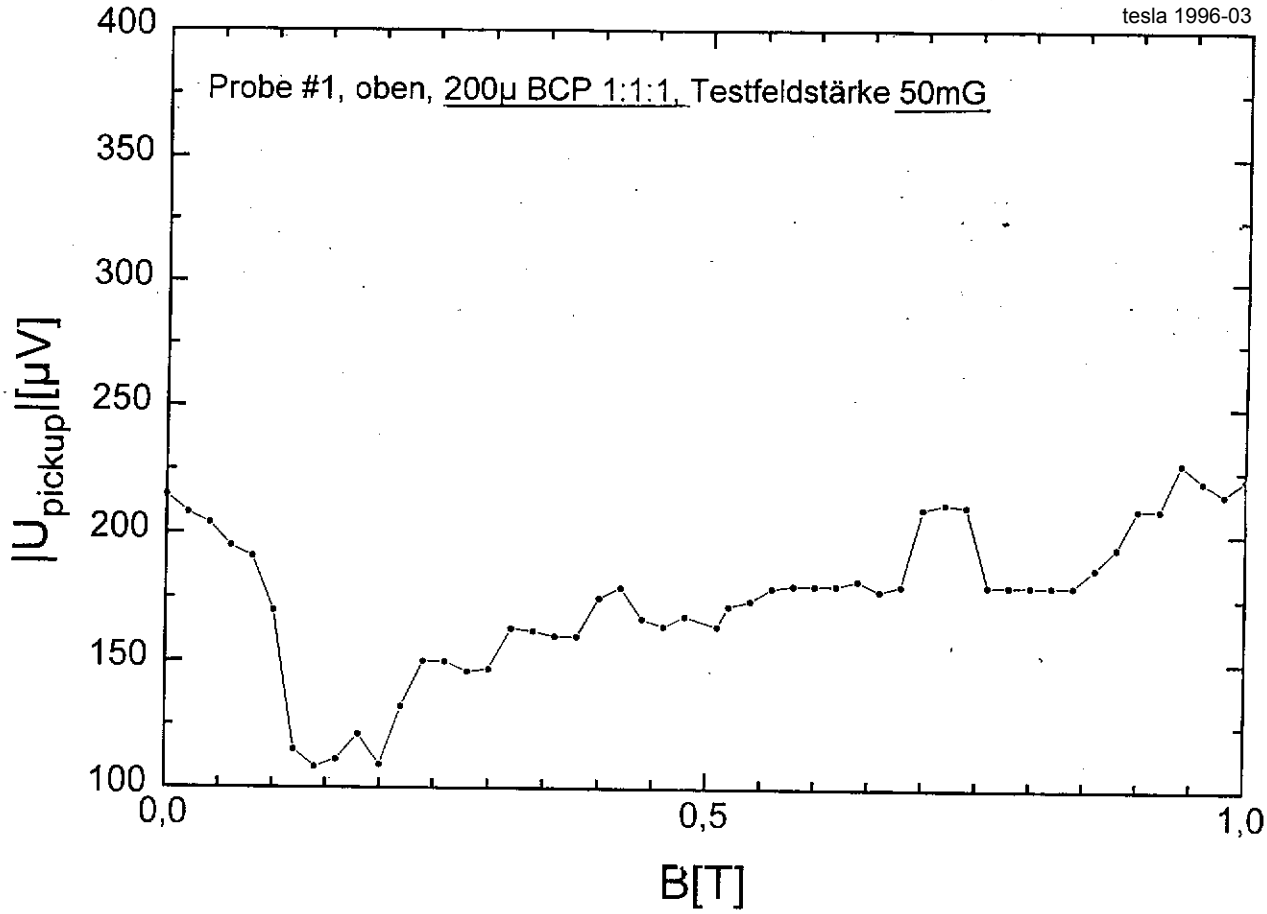
Probe #1, oben, 200µ BCP 1:1:1, Testfeldstärke 50mG
$|U_{pickup}|$[µV]
400
350
300
250
200
150
100
0,0
0,5
1,0
B[T]

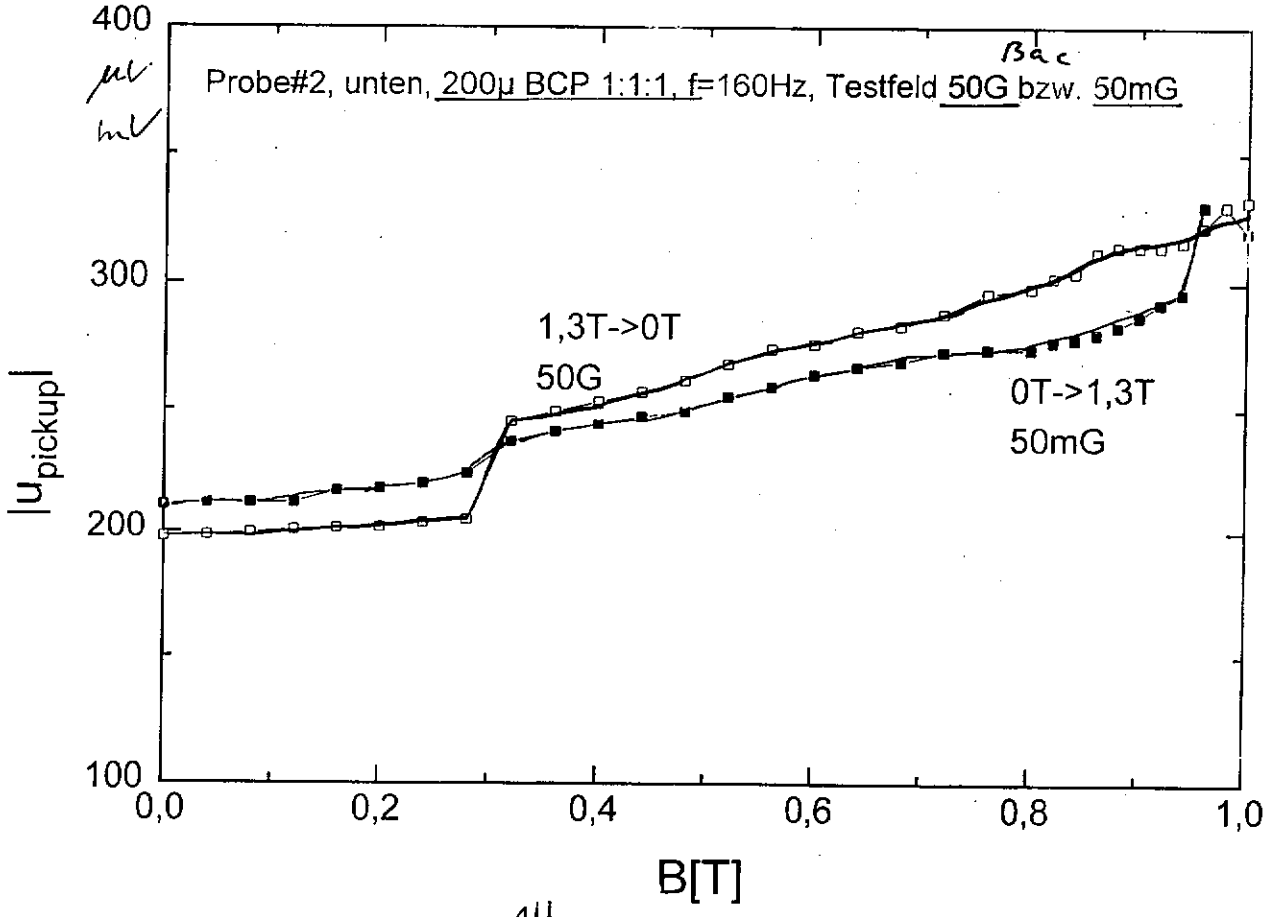
Probe#2, unten, 200µ BCP 1:1:1, f=160Hz, Testfeld 50G bzw. 50mG
Bac
µV
mV
$|u_{pickup}|$
400
300
200
100
1,3T->0T
50G
0T->1,3T
50mG
0,0
0,2
0,4
0,6
0,8
1,0
B[T]

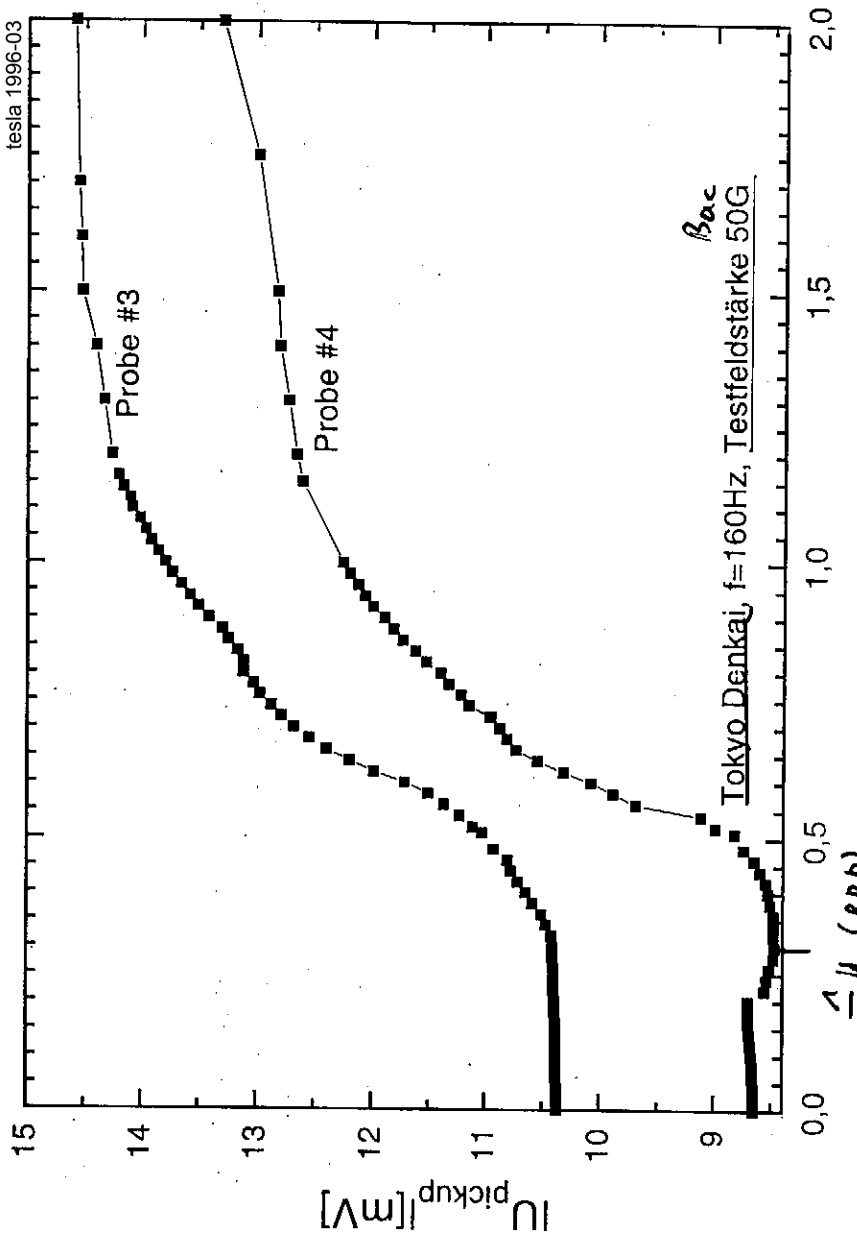

⇒ Very inhomogeneous Nb even in bulk

Conclusions

- The measurement technique is sensitive to surface damage, Ti-coatings/residues after polishing and HOMOGENEITY of H_{c1}
- Most raw Nb materials show severe surface damage and even some bulk inhomogeneity
- Ti-HTA homogenizes + purifies the bulk, but creates a NbTi-like coating at the surface which is at least 100μm – 200μm thick and inhomogeneous
- Reducing of the Ti-HTA Temperature is necessary to improve the surface quality
- The amount of Ti on the Nb samples depends on the position in the furnace, probably
- Systematic variation of Bac-testfield for given Bdc might be instructive for Depth-Profiles of the magnetic properties & homogeneity

Overall, H_{c1}-Measurements are a powerful tool to control the purity and homogeneity of Nb sheets, and to optimize the Ti-HTA process!

W. Singer
Application of Eddy-Current Method to Nb at BAM (Berlin)

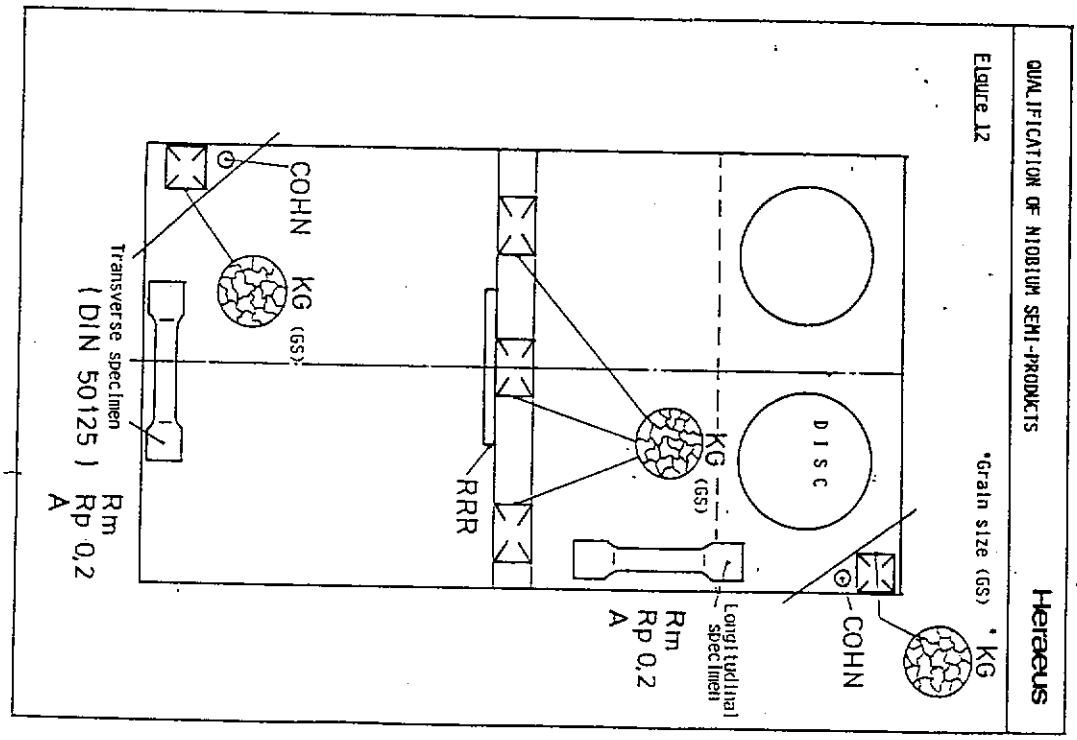

LEITZ 4734
Made in Germany

Nb sheet properties

Manufacturer	W.C.HERAEUS GmbH	W.C.HERAEUS GmbH	W.C.HERAEUS GmbH	TELEDYNE WAH CHANG
Properties	Cavity -2,-1	Cavity D1...D6	S7-S12,A13-A18	
RRR	407-433	300 -380	278-350	400
Impurities content, %				
Ta	0,037	0,036	0,012	0,02
W	<0,005	<0,005	<0,005	<0,003
Ti	<0,001		<0,002	<0,004
Fe	<0,002	0,002	<0,002	<0,003
Si	<0,002	<0,002	<0,002	<0,002
Mo	<0,002	<0,002	<0,002	<0,003
Ni		<0,003	<0,002	
Zr		<0,003	<0,002	
H	<0,0005	<0,0005	<0,0005	<0,0003
N	<0,001	<0,001	<0,001	<0,002
O	<0,001-0,03	<0,001	<0,001	<0,004
C		<0,001	<0,001	
Mechanical properties				
Tensile strength, Rm, (N/mm2)	175	150 -180	152 - 160	157,6 - 161
Yield strength, Rp 0,2 (N/mm2)	53	60 -97	79 - 81	90,8 - 94,9
Elongation,%	54	38 -70	48 - 68	51 - 52
Hardness, HV10		38 -45	40 - 46	49
Grain size, ASTM	6,5-8,5	6 - 8.	5 -8,5	7
Recristallisation heating.				
Temperature, °C	770	770	770 -800	
Time, h	1	1	1 -1,25	
Thickness, mm		2,69.....2,88	2,45.....2,85	2,67.... 2,90
Number of the sheet (2,8*262*262)	40	150	275	120
Delivery data		Feb 94	Jul 94	Jan 95

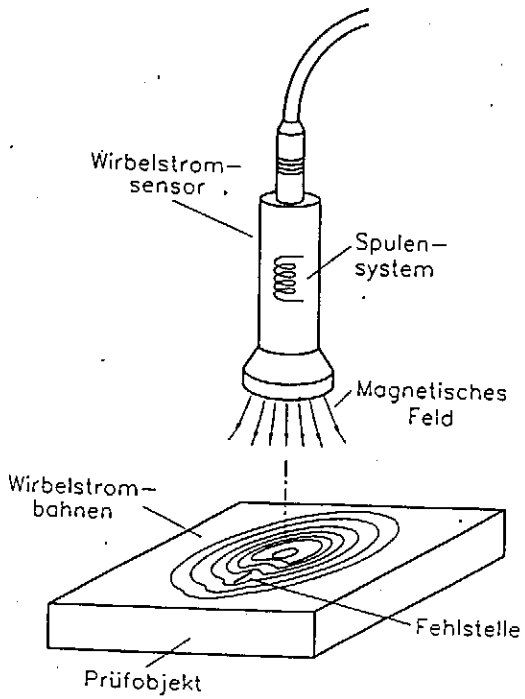

Abb. 1. Prinzip der Wirbelstromprüfung
Fig. 1. Principle of the eddy current test method

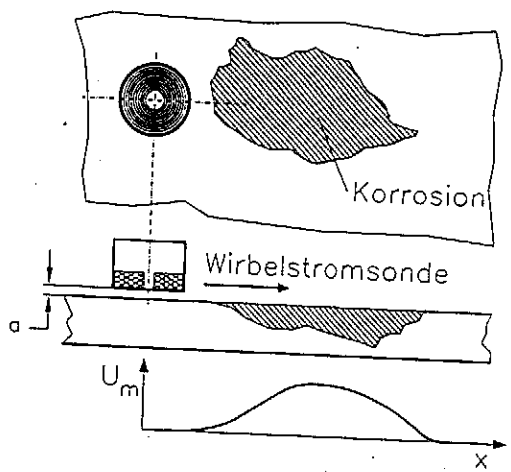

Abb. 3. Schematische Darstellung der Prüfaufgabe
Fig. 3. Schematic display of the test task

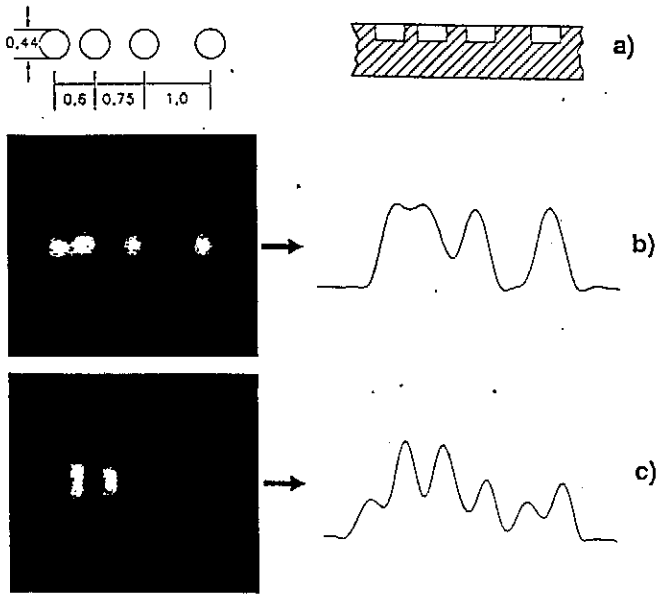

Abb. 8. Überprüfung des lateralen Auflösungsvermögens, a) Anordnung und Abmessungen der Testfehler, b) Prüfergebnis mit der Spezialsonde für Abbildungszwecke, c) handelsübliche Sonde mit sehr hohem lateralem Auflösungsvermögen, Rechts jeweils Amplituden/Ortsverlauf als Schnitt durch die Mitte der Anzeigen in waagrechter Richtung

Fig. 8. Examination of the local resolution power, a) layout and dimensions of the test defects, b) test result with the special probe for imaging purpose, c) customary probe with a very high local resolution power. On the right respectively amplitude versus displacement as a sectional view through the maximum of the indications in horizontal direction

LEITZ 4734
Made in Germany

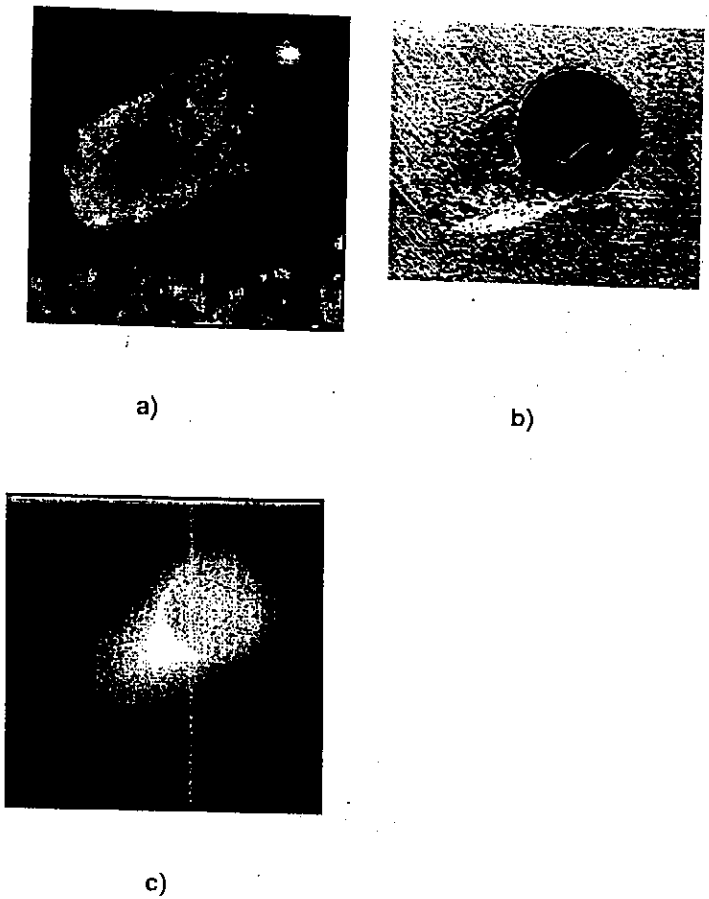

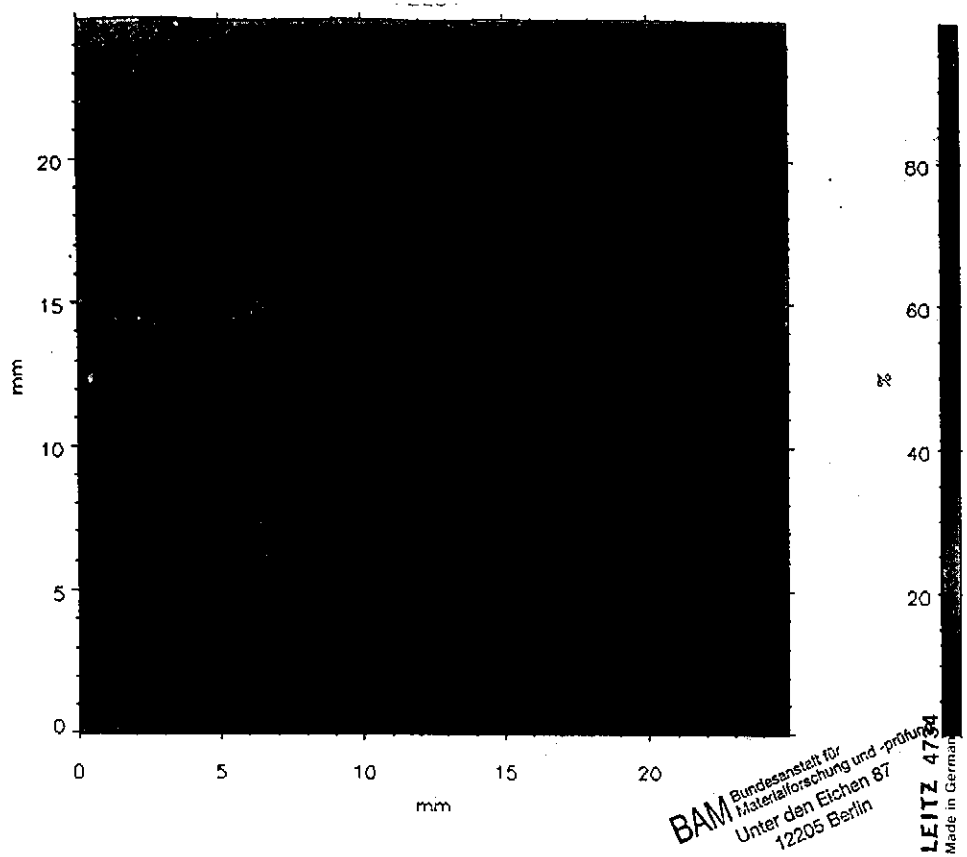

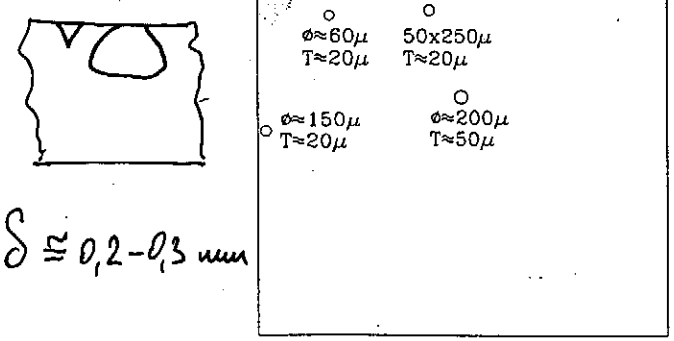

$\delta \approx 0{,}2-0{,}3$ mm

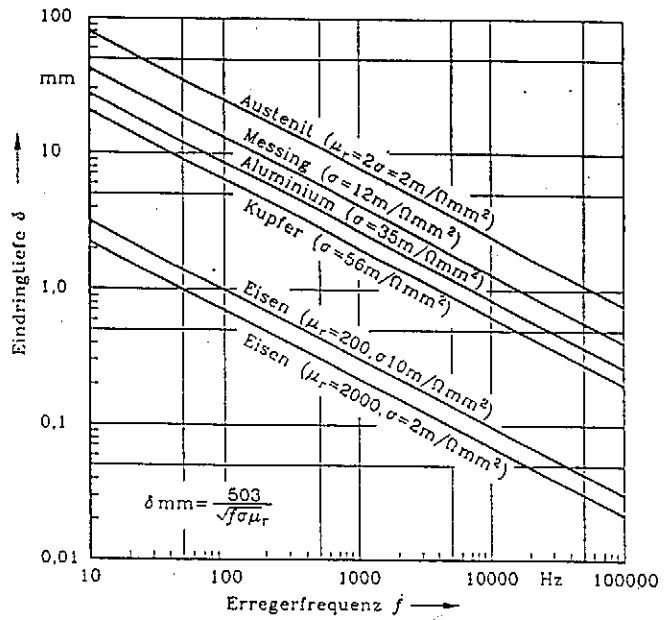

Abb. 2. Nomogramm zur Abschätzung der Eindringtiefe von Wirbelströmen als Funktion der Prüffrequenz für einige ausgesuchte Werkstoffe

Fig. 2. Nomogramm for the estimation of the eddy-current penetration depth as a function of the test frequency for some materials

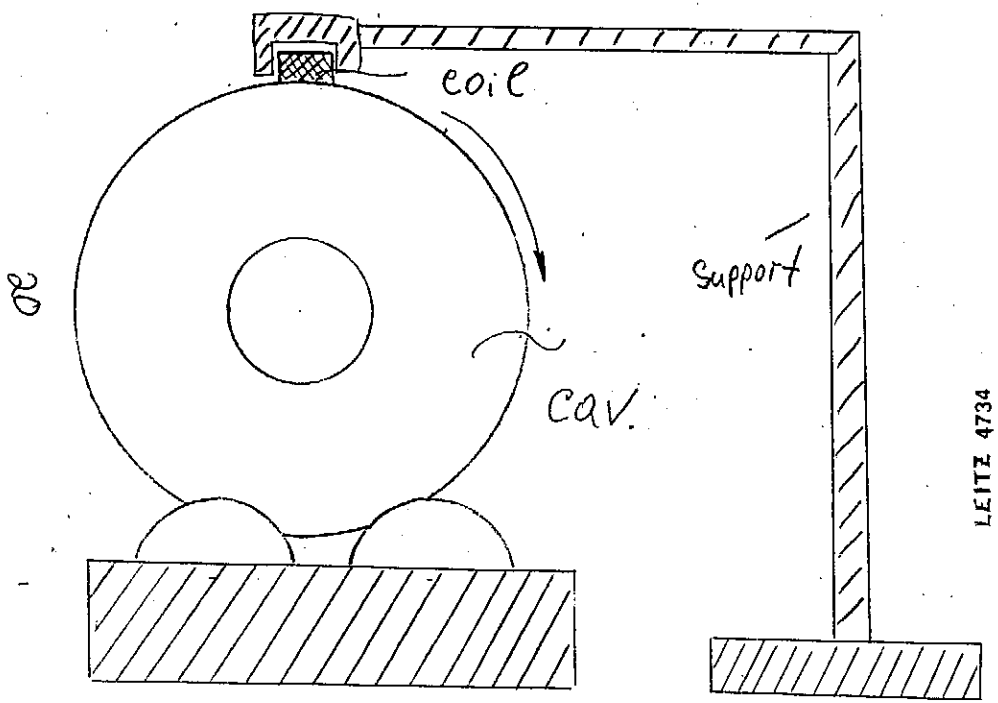

$\delta \cong 2-3$ mm

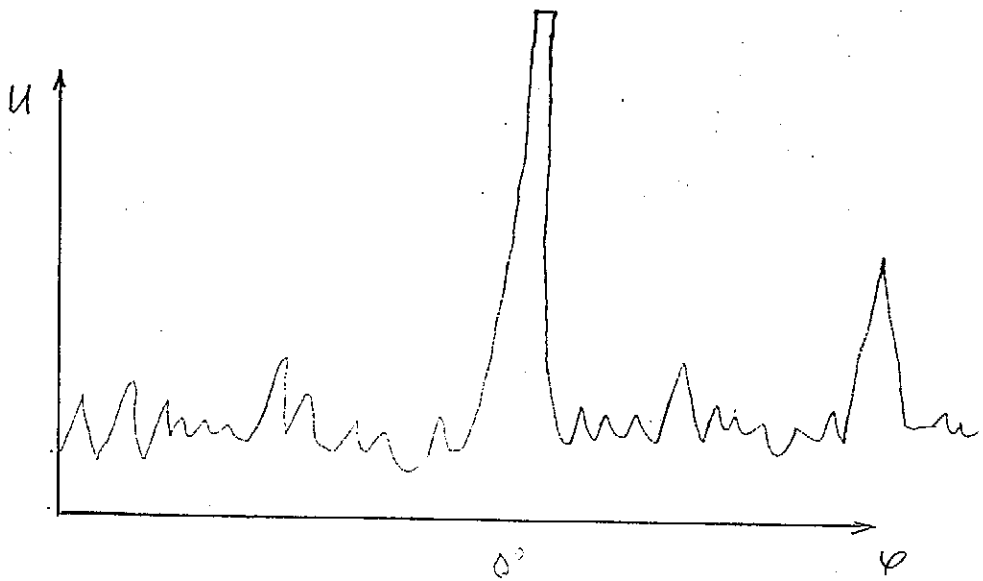

DC, cell 5

Conclusions

Eddy current inspection of Nb can be used:

1. to detect voids and scratches with minimal size of 100 µm on the surface and inside of the material (depth 0 - 300 µm).

2. to detect cracks and inclusions with minimal size of 500 µm inside of the material (depth 0 - 3 mm)

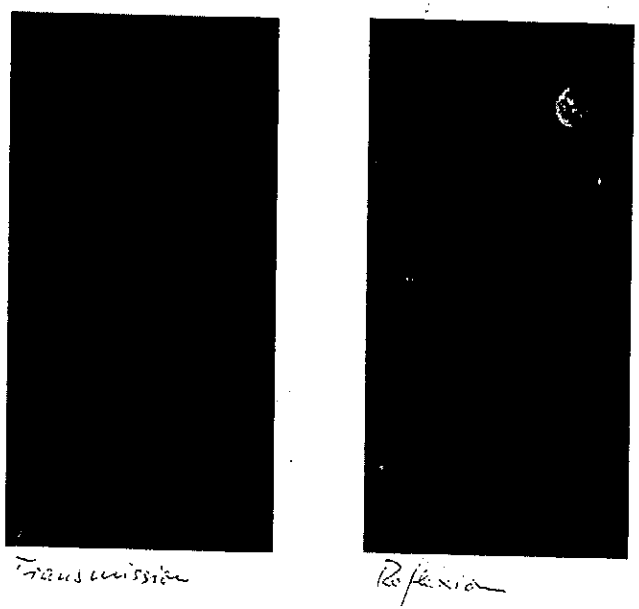

10 x 20 mm², 10 MHz

Sacklochfeld

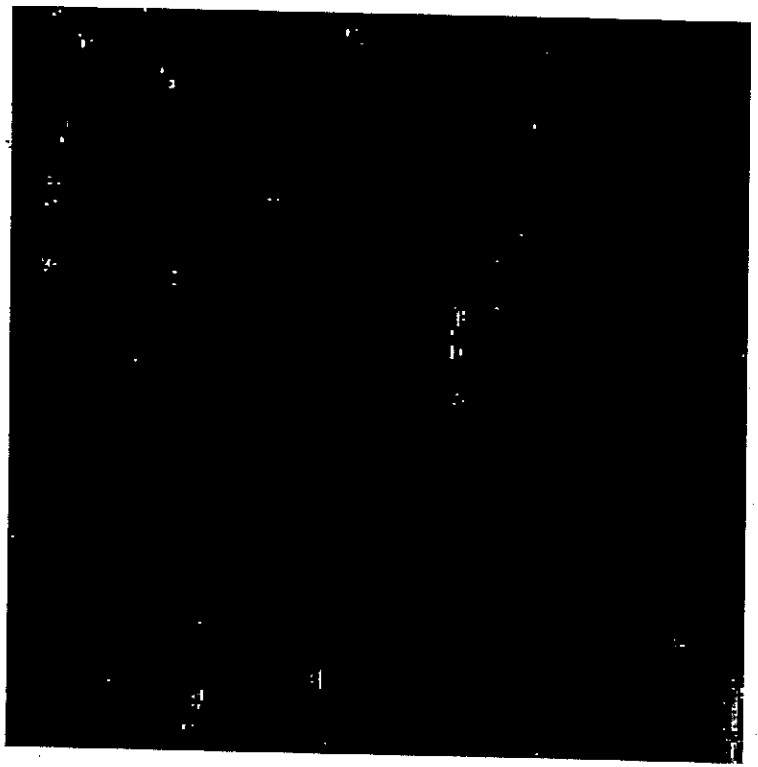

Ultraschall 10 MHz, Feldgröße 25 x 25 mm², ,
Schrittweite 100 µm

Offensichtlich werden bei dieser Schichtdicke bereits Details übersehen!

First results on Nb magnetization hysteresis measurements.

Peter Schmüser

Idea and first experiments:
M. Wake, K. Saito KEK

DESY setup:
mechanics: O. Peters + group
coils: B. Hentschel
electronics
and program: H. Brück, M. Stolper
design: PS.

Basic idea:
an ideal type II superconductor should exhibit <u>reversible</u> magnetization curve
hysteresis occurs when flux pinning centers are present:
dislocations, foreign material

⇒ possible source for increased surface resistance

Particular concern: formation of NbTi during Ti-gettered heat treatment

Niobium is a type II superconductor

flux tube lattice in pure Nb

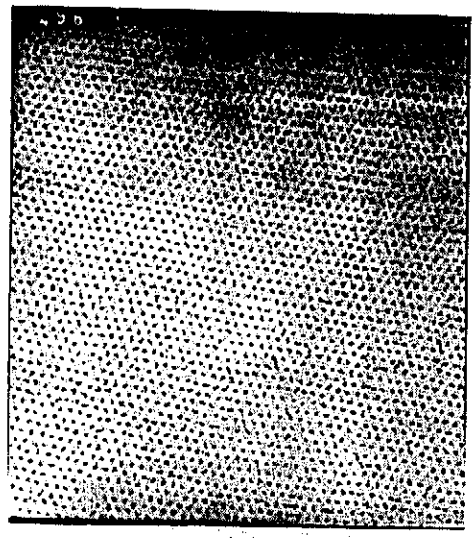

U. Essmann
Stuttgart

Niob
15400 x

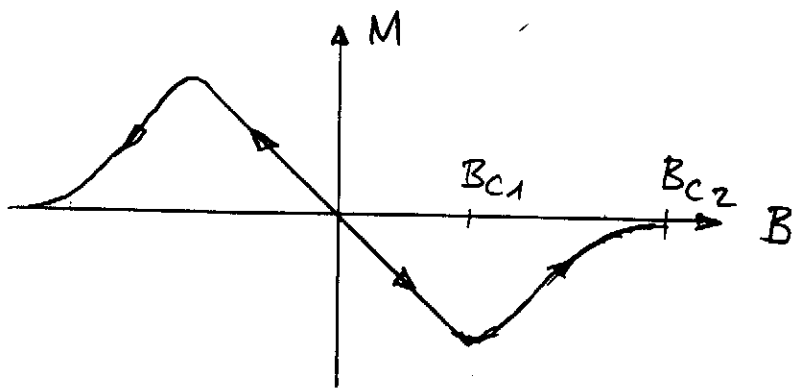

expected magnetization curve for Nb without flux pinning

KEK National Laboratory for High Energy Physics

from M. Wake

Magnetization Curves

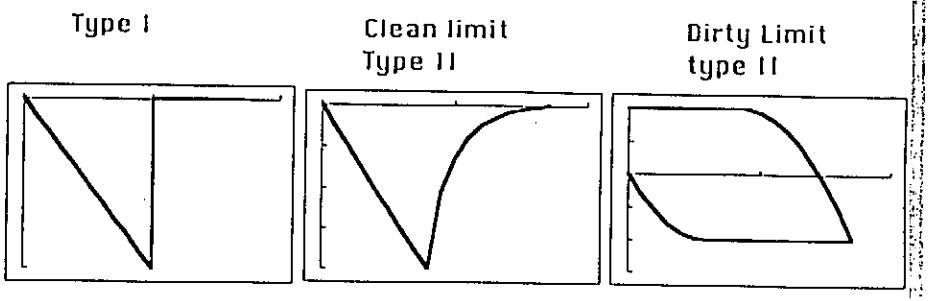

Cryogenics Center — Masayoshi Wake

KEK National Laboratory for High Energy Physics

Magnetization Measurement

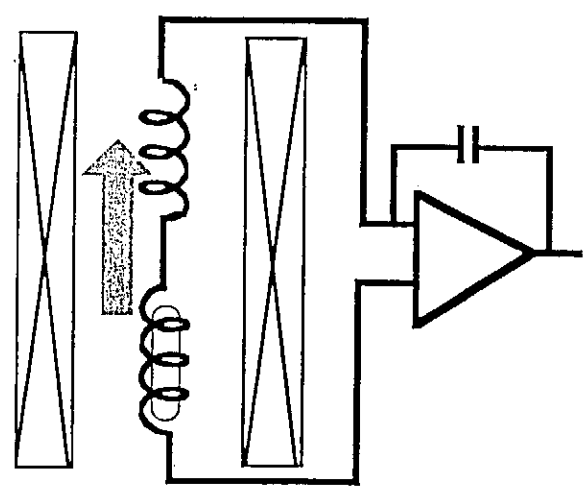

Cryogenics Center — Masayoshi Wake

Wake, Saito

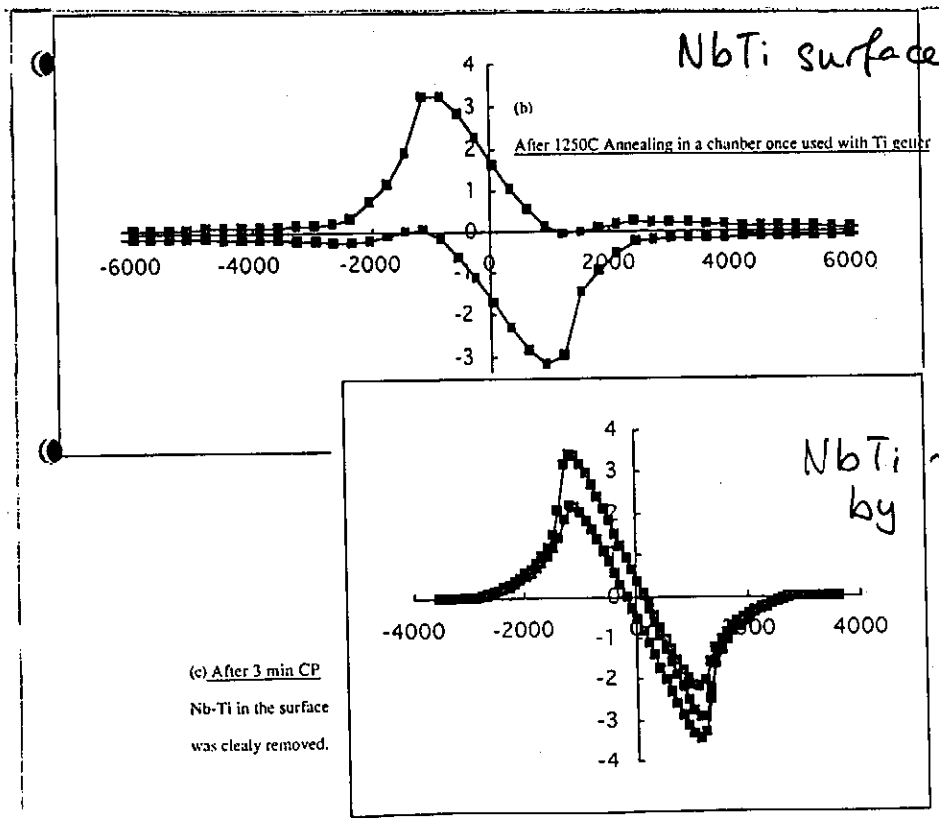

(c) After 3 min CP
Nb-Ti in the surface
was clealy removed.

Fig. 2 Titanium Migration

7

tesla 1996-03

Mon 26/Feb/1996 12:27:36 PST

raw material (Heraeus)

READ & ANALYSE mag mess data

Start

n:\mag_mess\data\NB_1.T01

Timestamp: 15/Nov/1995 16:08:18

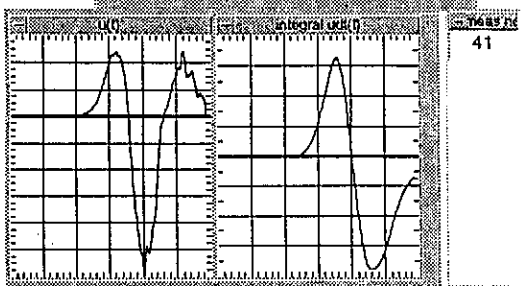

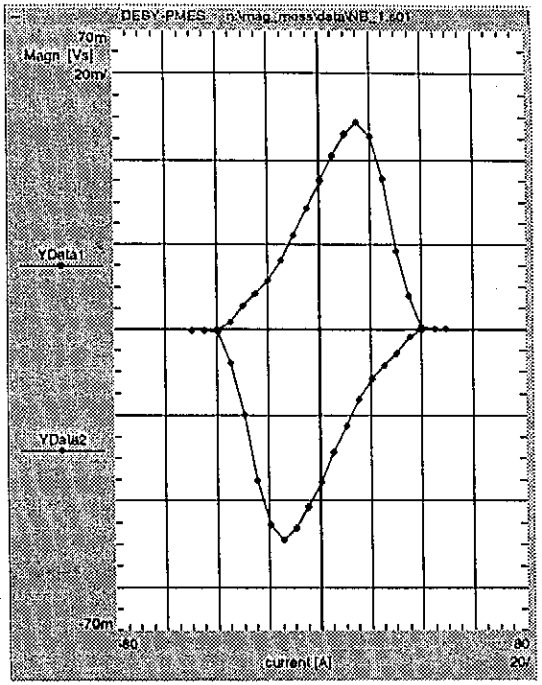

meas nr	integer	shaNume	alphaNumeri	first peak	second peak
41	130	298	1000	32.694m	-37.697m
	drift	shaNume	alphaNumeri	peak difference	
	179.58	71	179.58	35.196m	

peri	magnetization
0: -49.83	0: -0.1904m
1: 14.86	1: 48.855m
2: -14.86	2: -48.786m
3: 49.24	3: 0.19558m

hysteresis area: 3.7505

upper crossing: 35.39m

left crossing	right crossing
-40.246	41.01

down crossing: -35.653m

Mon 26/Feb/1996 14:11:01 PST

after heat treatment (1h 1400°, 3h 1250°C)

READ & ANALYSE mag mess data

Start

n:\mag_mess\data\NB_9.T01

Timestamp: 25/Jan/1996 11:30:07

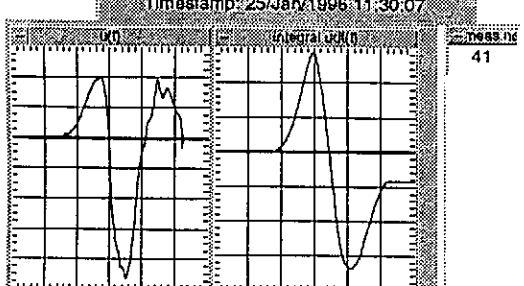

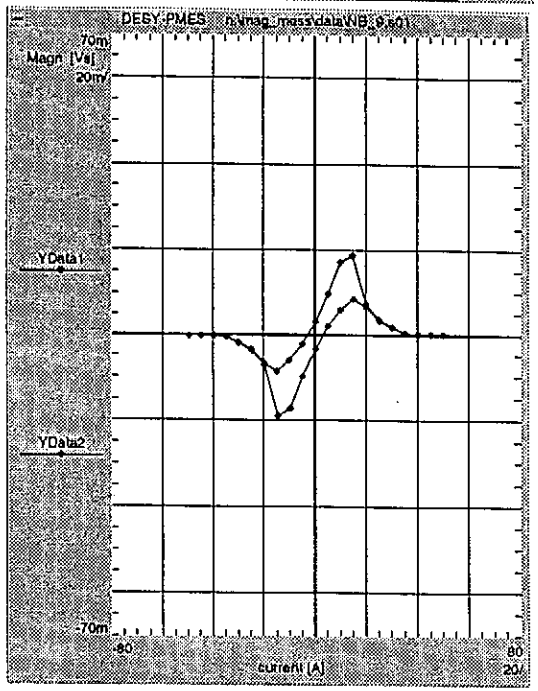

meas nr	integer	shaNume	alphaNumeri	first peak	second peak
41	130	298	-25	2.8716m	-3.3622m
	drift	shaNume	alphaNumeri	peak difference	
	32.778	45	32.778	3.1169m	

peri	magnetization
0: -15.16	0: -8.6309m
1: 14.86	1: 18.72m
2: -14.91	2: -18.971m
3: 15.11	3: 8.6171m

hysteresis area: 0.33744

upper crossing: 3.2m

left crossing	right crossing
-2.8894	2.9648

down crossing: -3.3849m

Mon 26/Feb/1996 12:32:18 PST

READ & ANALYSE mag mess data

Start

n:\mag_mess\data\NB_1.T02

Timestamp: 23/Jan/1996 08:55:29

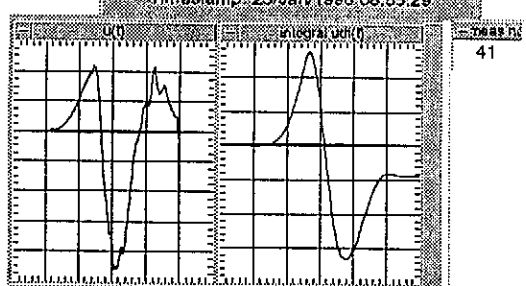

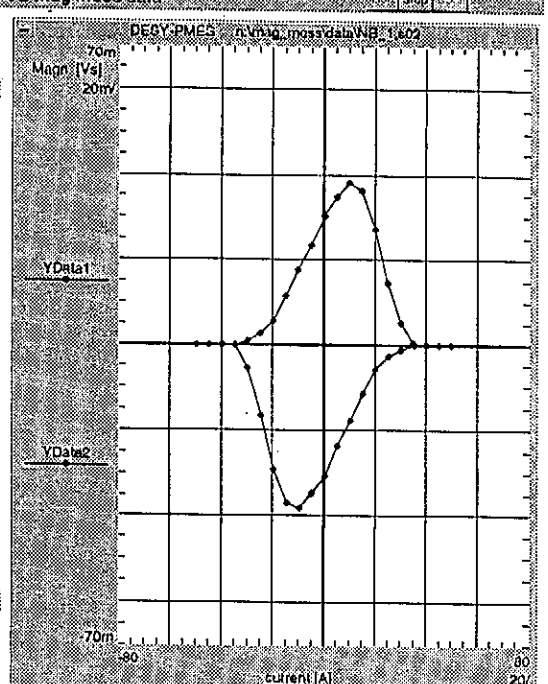

meas nr	integer	shaNume	alphaNumeri	first peak	second peak
41	130	290	27.778	27.39m	-32.988m
	drift	shaNume	alphaNumeri	peak difference	
	625	30	625	30.189m	

peri	magnetization
0: -35.06	0: -94.35u
1: 9.92	1: 38.373m
2: -9.97	2: -38.091m
3: 35.11	3: 0.10465m

hysteresis area: 2.5162

upper crossing: 30.544m

left crossing	right crossing
-34.503	34.362

down crossing: -30.587m

Mon 26/Feb/1996 12:36:58 PST

(no chemistry)

READ & ANALYSE mag mess data

Start

n:\mag_mess\data\NB_10.T01

Timestamp: 25/Jan/1996 14:53:23

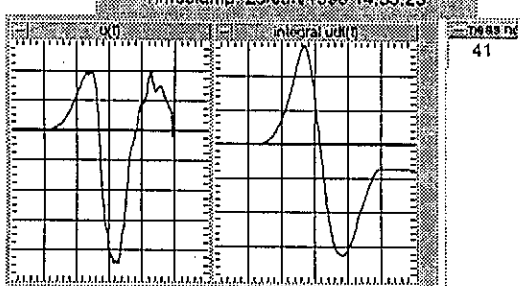

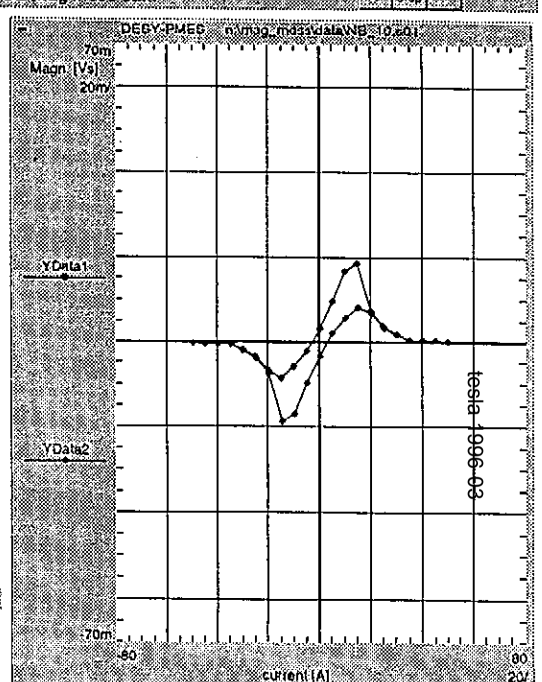

meas nr	integer	shaNume	alphaNumeri	first peak	second peak
41	130	292	1.4286	2.8997m	-3.2465m
	drift	shaNume	alphaNumeri	peak difference	
	3.4375	32	3.4375	3.0731m	

peri	magnetization
0: -15.16	0: -8.2825m
1: 14.86	1: 18.803m
2: -14.91	2: -18.642m
3: 15.11	3: 8.2437m

hysteresis area: 0.33942

upper crossing: 3.2722m

left crossing	right crossing
-2.9397	2.9648

down crossing: -3.34m

Yuki Denkai raw material

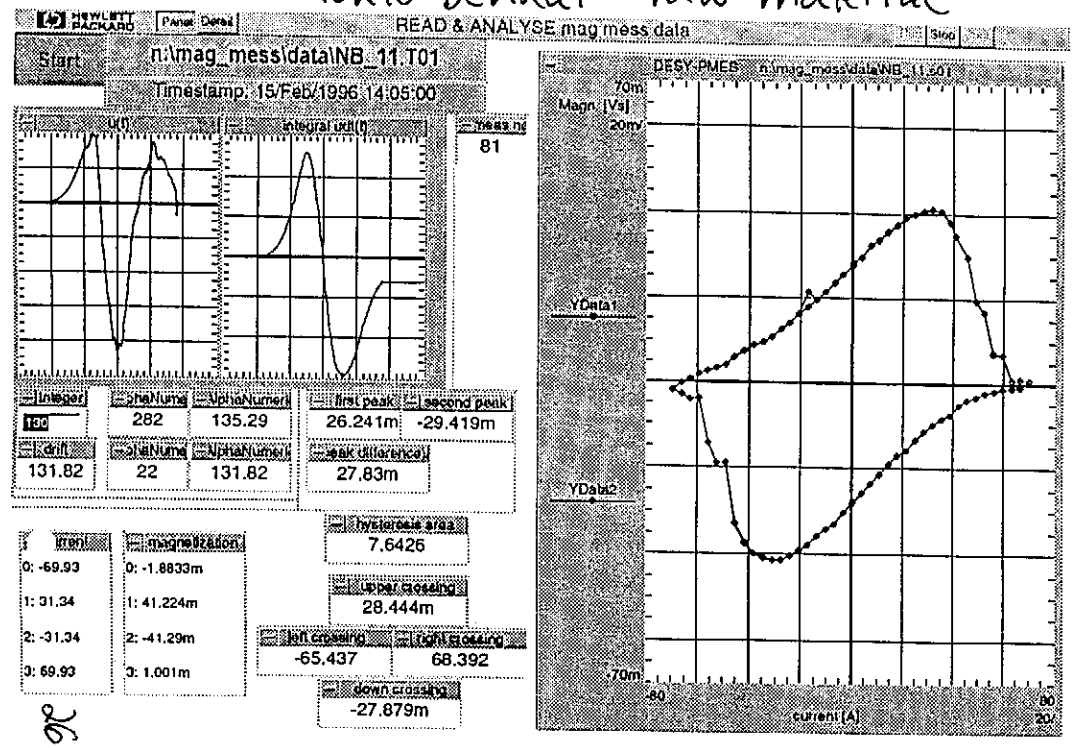

Mon 26/Feb/1996 13:18:20 PST

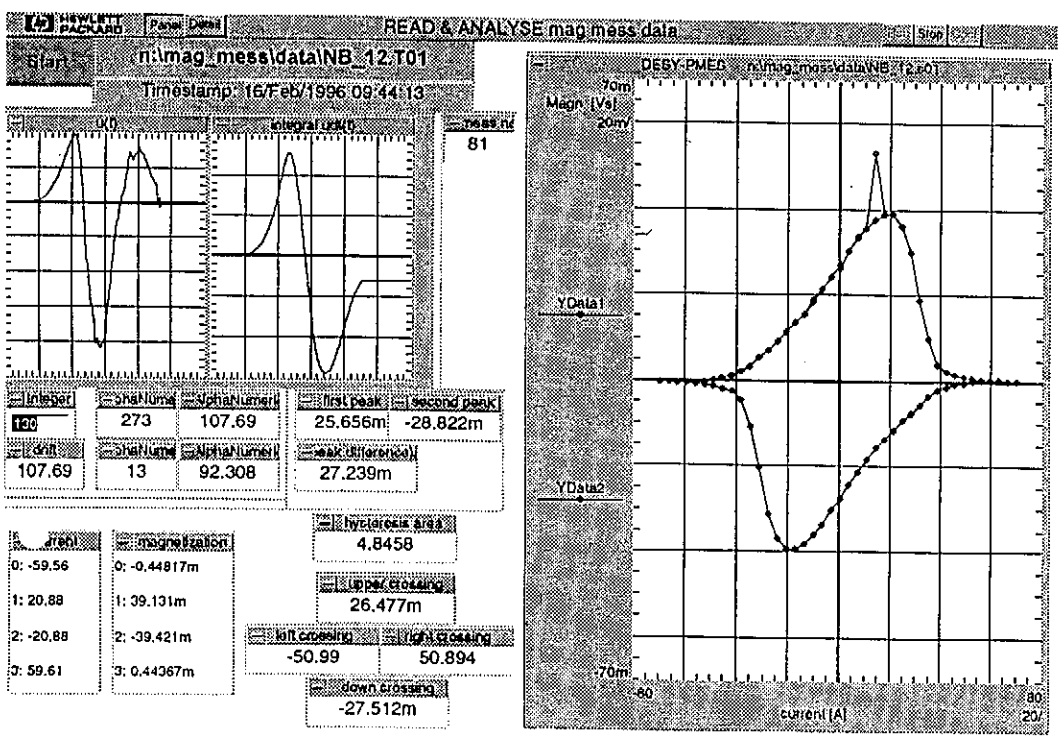

tesla 1996-03

Thermal model calculations

29.2.96 / Detlef Reschke

Hartmut Elias
Günter Müller

Hans-Gerd Kürschner
Ralf W. Röth
Detlef Reschke

Ansatz

- Equation for the thermal conductance on a lattice:

$$\Delta T(x) + \lambda(x,T)^{-1} \cdot \frac{dq(x,T)}{dt} = 0$$

- Steady state for $\frac{dQ}{dt}$:

$$-\dot{Q}_i = \dot{Q}_1 + \dot{Q}_2 + \dot{Q}_3 + \dot{Q}_4$$

$\Rightarrow$ Power and temperature distribution without time dependance

- Cylinder symmetrical disk with or without defect in the center

$\rightarrow$ two-dimensional problem

Lattice and boundary conditions

- Lattice of variable size
  → Narrow spacing near the defect
- Boundary conditions:

RF-side ($z = 0$):

$$\frac{dQ}{dt} = \frac{dP}{dA} = \frac{1}{2} R_s(x,T) \cdot H_s^2$$

i) $R_s(\omega, T) = R_{BCS}(\omega, T) + R_{res}^{hom} \rightarrow r \neq 0$

ii) $R_s\{(T)\} = R_{Def}\{(T)\} \rightarrow r = 0$

Helium bath ($z = z_{max}$):

$$\frac{dQ}{dt} = R_K(T_B, \Delta T) \cdot (T_{Nb} - T_B)^{-1}$$

$T_B = const$

Outer boundary ($r = r_{max}$):

$$\frac{dQ}{dt} = 0$$

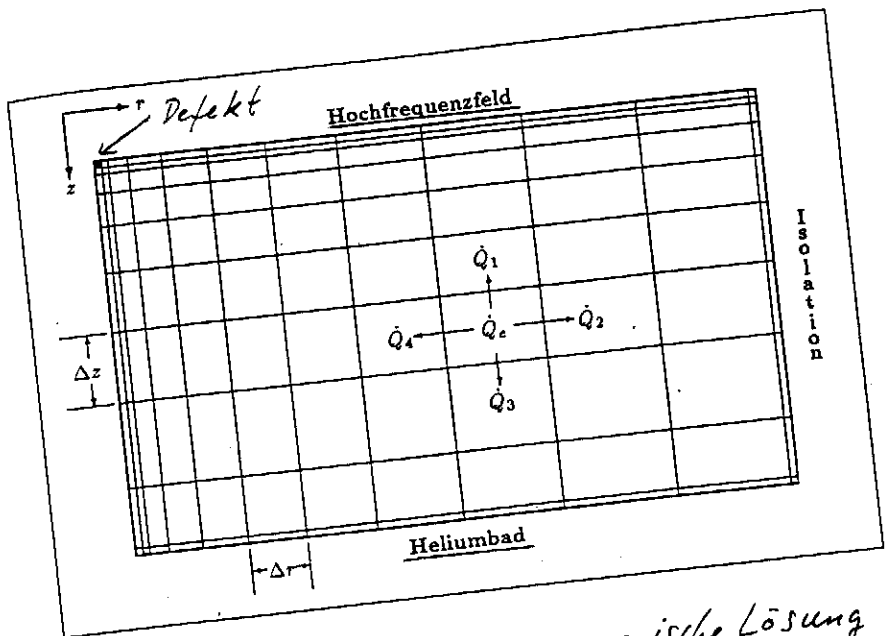

Gitteraufteilung für numerische Lösung

Parameter

- Defect size r_D — fixed
- Defect surface resistance R_D — fixed/calc.
- Homogeneous surface resistance $R_{s,hom}$ — fixed
- Thermal conductivity $\lambda(T)$ — calculated
  (parametrized measurements)
  not only the RRR
- Kapitza resistance $R_K(T, \Delta T)$ — calculated

$$R_K(T, \Delta T) = 200 \cdot F \cdot T_B^{-4,65} \left[\frac{Km^2}{W}\right]$$

$$F = 1 + \frac{3}{2}\frac{\Delta T}{T_B} + \left(\frac{\Delta T}{T_B}\right)^2 + \frac{1}{4}\left(\frac{\Delta T}{T_B}\right)^3$$

for fired niobium (Mittag, 1973)

- Bath temperature T_B (1,4 K → 4,2 K) fixed
- Frequency ω (3 GHz) fixed
- Thickness of the disk (cavity wall) (2 mm) fixed
- R_s of normalconducting niobium (8 mΩ) fixed
- + some more (numerical, $H_{c,Nb}(0)$, T_c ...)

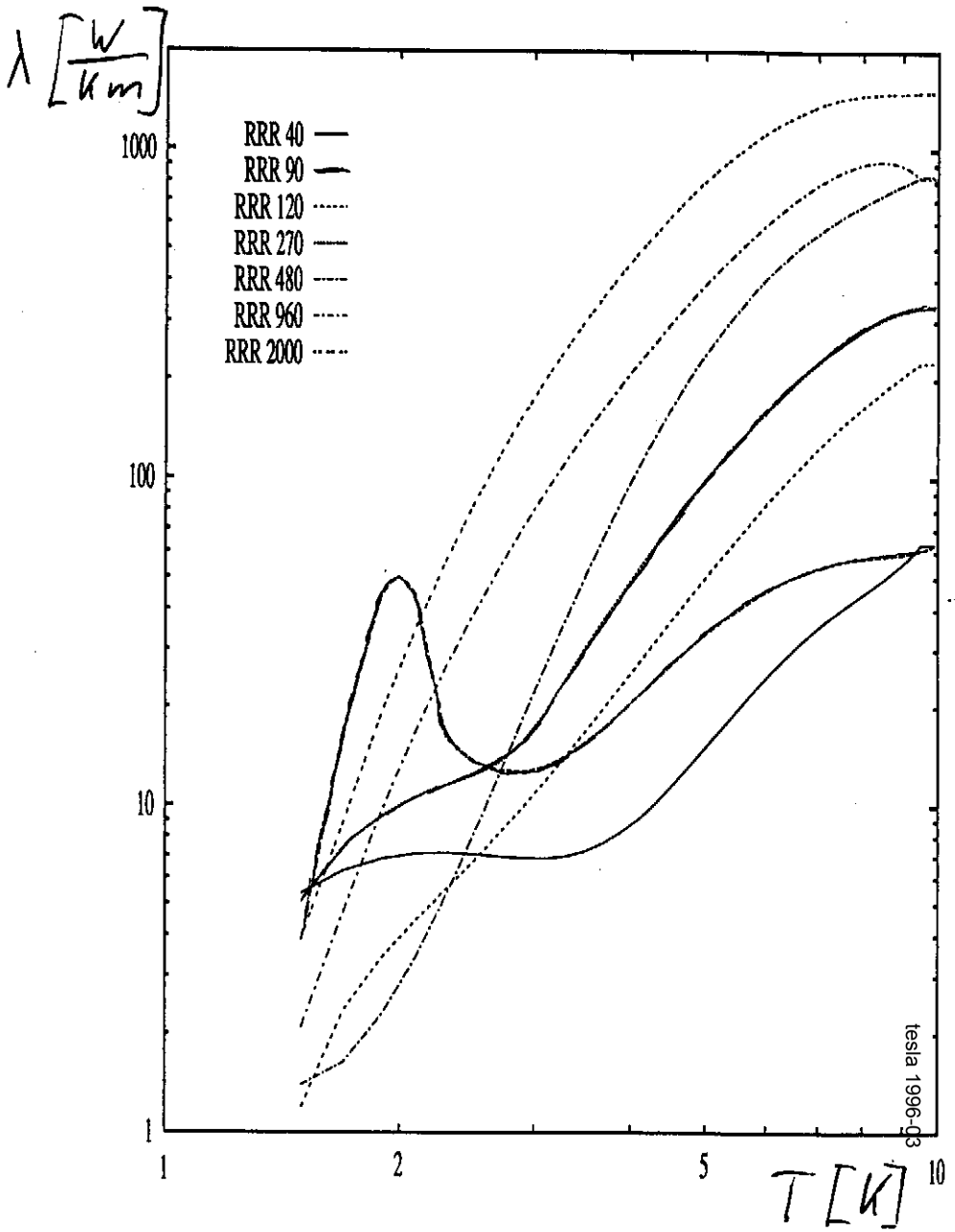

Two Remarks:

- $\lambda(T) \leftrightarrow RRR$

Normal conducting, electric conductivity related to superconducting thermal conductivity (Kadanoff-Martin; Wiedemann-Franz)

$\Rightarrow RRR = c \cdot \lambda(4,2K)$ ← One point of $\lambda(T)$!

with $c \simeq 4\,(-7)$

- Kapitza resistance

- Material and preparation dependance

→ Mittag and Orsay fit within 30%
(RRR 40, Nred) (RRR 200-300, BCP) ($T = 1,5K - 2,1K$)

but:

Saclay data factor of 2 higher!

What is a "calculated" Quench?

- Quench independent of the temperature of the defect

- i) No stable power distribution in the lattice can be achieved

→ (ii) "High" temperatures in the neighbourhood of the defect)

Results

- For a given set of parameters:
  i) quench field
  ii) temperature distribution for each step of the RF-field

- Most calculations up to now:
  $f_0 = 3\,GHz$ ○
  $d = 2\,mm$ ○

- One set of calculations for 1.3 GHz by H.G. Kürschner
  but:
  "wrong" thermal conductivity ○!

RRR 270 : Wah-Chang / non-fired
RRR 480 : Cired met / non-fired
RRR 960 : Protvino / non-fired
RRR 2000 : Cired met / fired with Ti

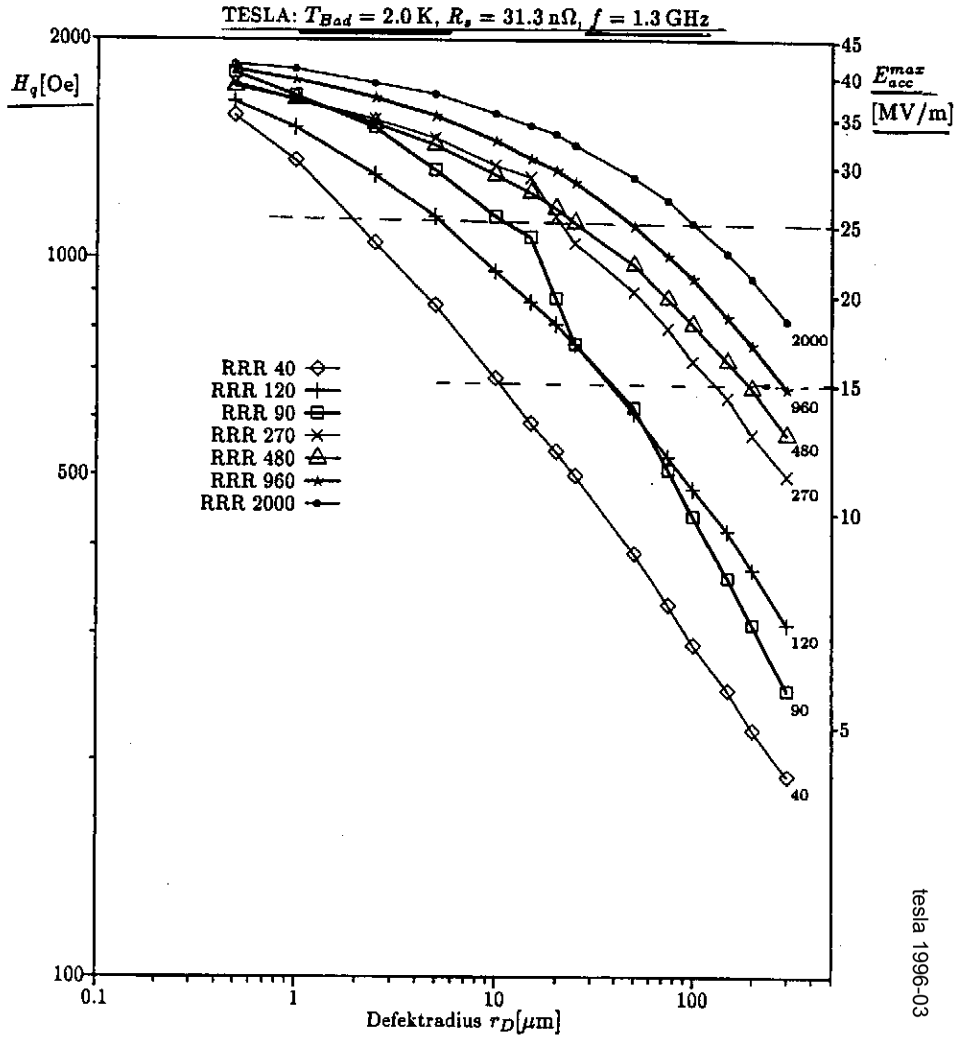

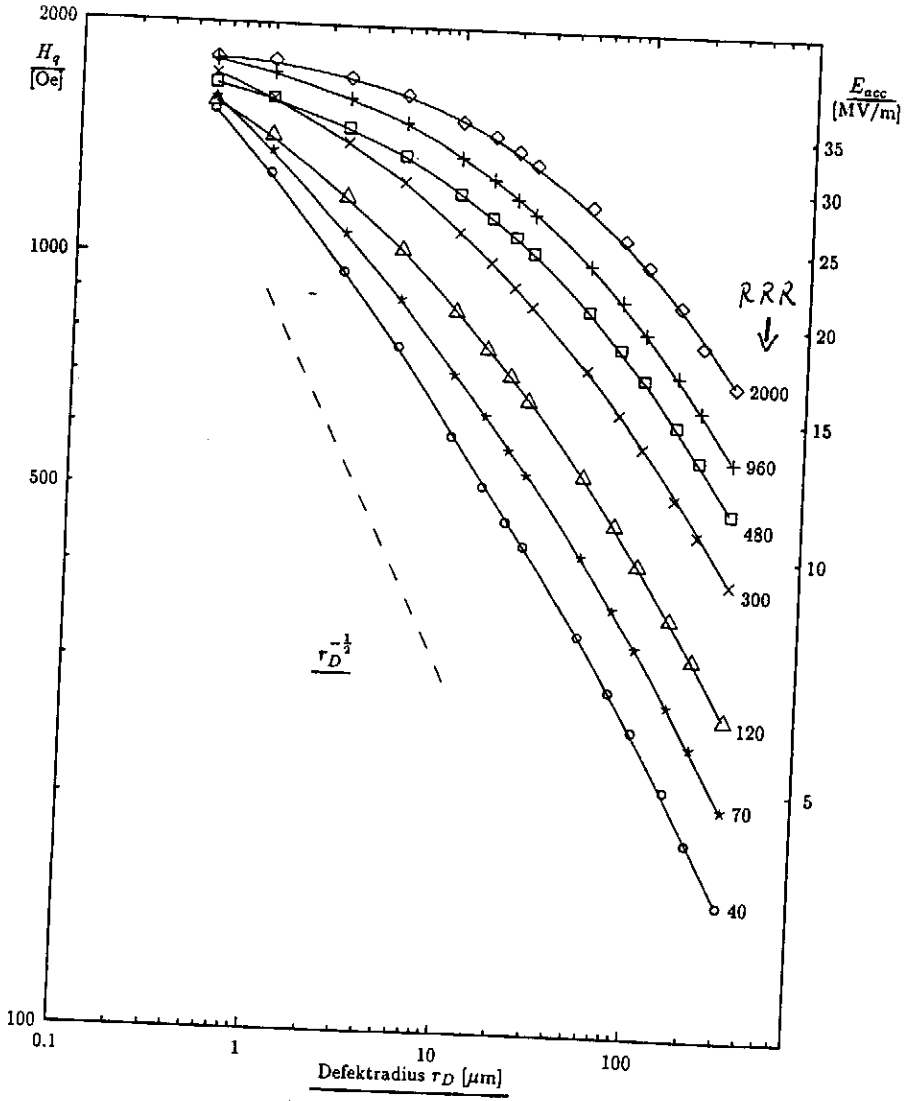

32

Parameter:

$T_B = 1{,}4\,K$; $D = 2{,}0\,mm$; $R_{hom} = 0\,\Omega$; $R_{Pf} = 8\,m\Omega$

$f = 3\,GHz$

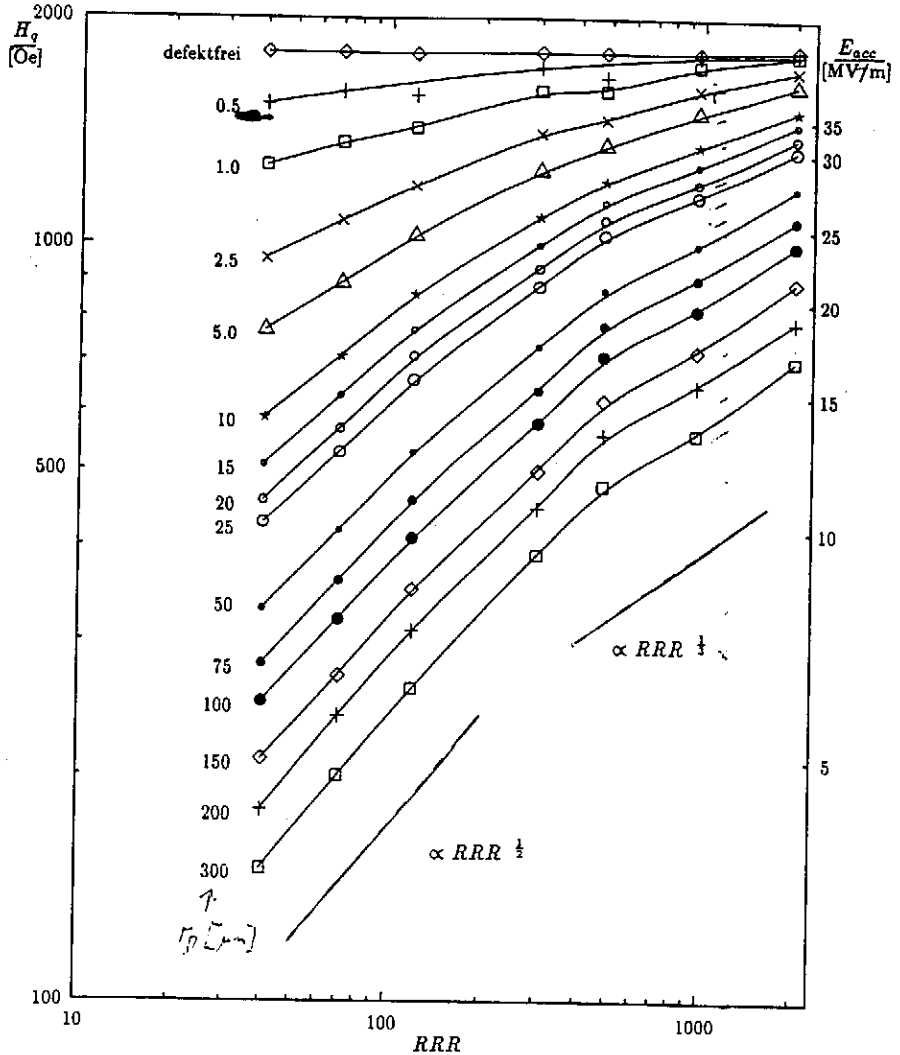

Parameter:

$T_B = 1.4\,K$; $D = 2\,mm$; $R_{hom} = 0\,\Omega$; $R_{Pf} = 8\,m\Omega$

$f = 3\,GHz$

tesla 1996-03

Summary for quench fields

- The calculated quench fields are in agreement with the experiments.
- Calculations for TESLA-parameters are no problem:
  e.g. dependence of the wall thickness

→ but have to be done!

- The higher the ~~RRR~~ $\lambda(T)$ and the smaller the defects the benefit of increasing the thermal conductivity becomes less.
  (less than $\sim \sqrt{\lambda}$)

- Final remark:
  A closer look shows, that the simple model of a n.c. defect and surrounding homogeneous material cannot explain the experiments of $\Delta T(H_s)$, $\Delta R_s(H_s)$!

M. FOUAIDY IPN_Orsay

TESLA/TTF R&D Meeting
DESY - HAMBURG Feb. 29, 1996

High Heat Flux Kapitza Conductance at Cu-HeII Interface and critical Heat Flux in Saturated HeII

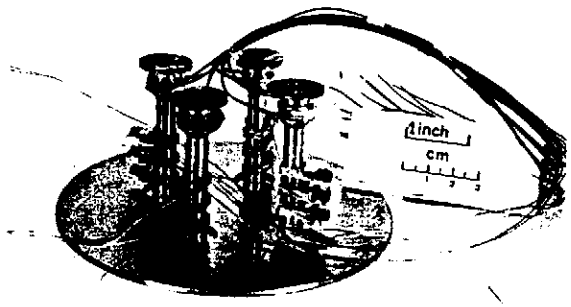

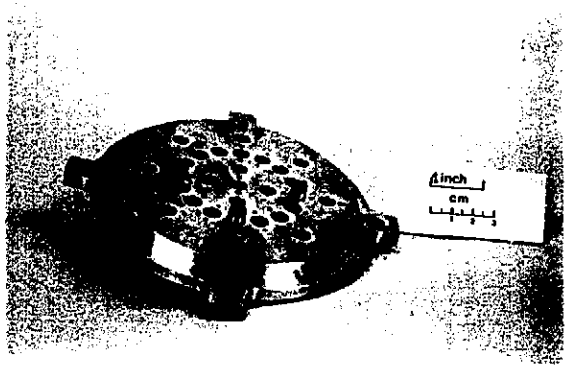

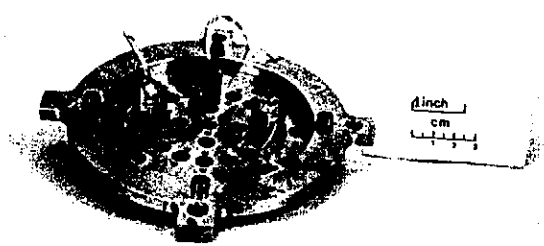

(3)

COPPER ROD TEMPERATURE VARIATIONS
VERSUS THE APPLIED HEAT FLUX
Th#1 z=23.3mm, Th#2 z=15.3mm, Th#3 z=7.3mm, Th#4 z=0
Run of November 1995

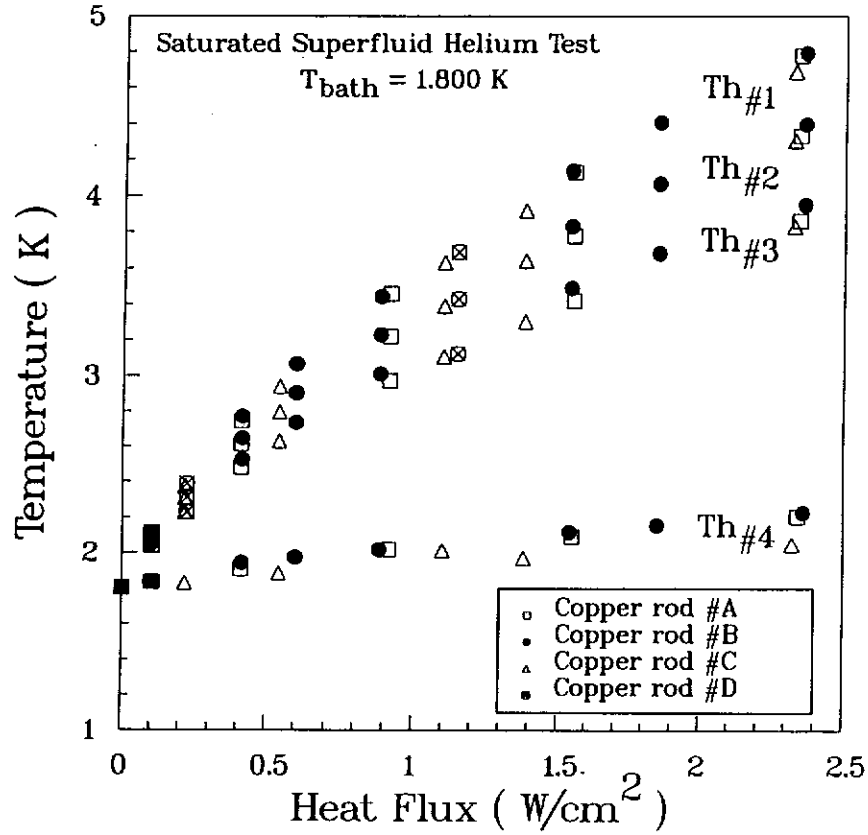

(4)

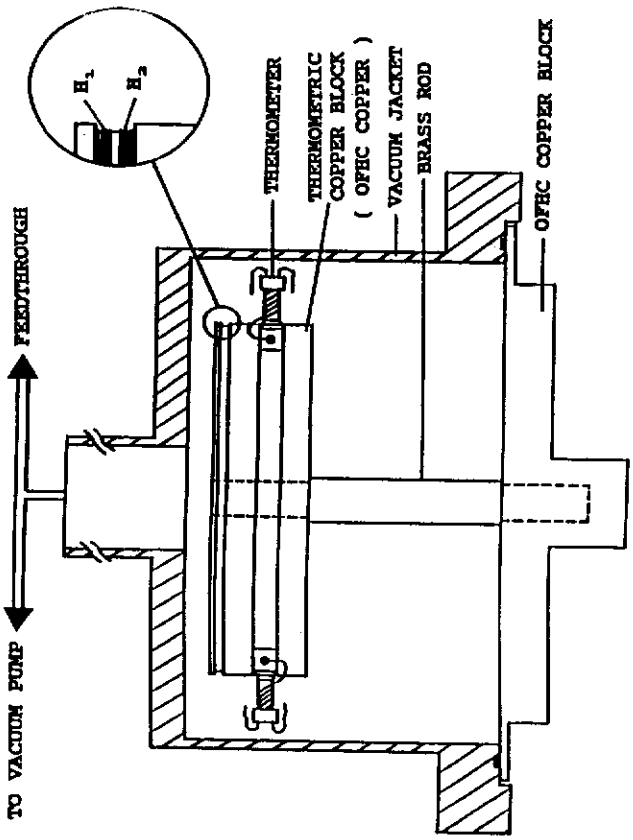

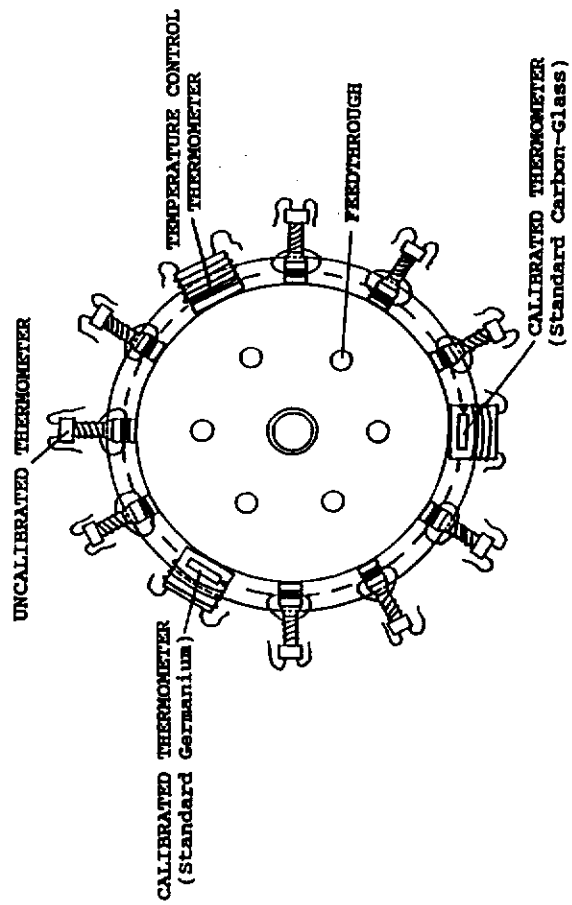

CALIBRATION CELL (4.2 K - 20 K)

(5)

COMPARISON OF THE SURFACE SCANNING THERMOMETER THERMAL REPONSE WITH THE SURFACE TEMPERATURE EXTRAPOLED FROM THE TEMPERATURE PROFILE ALONG THE COPPER ROD

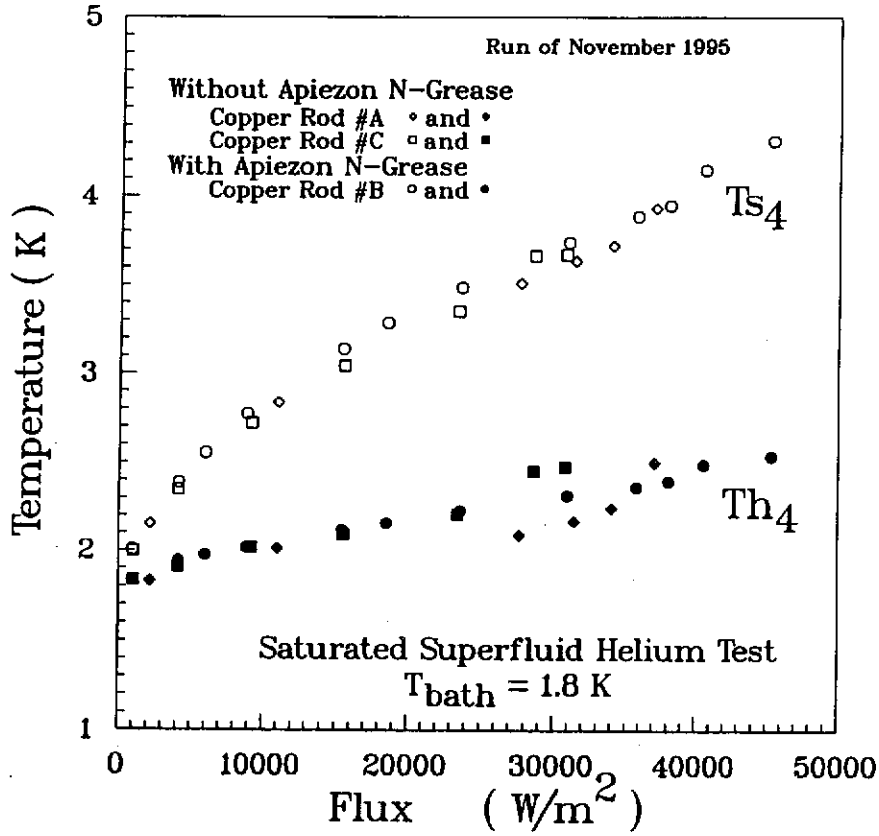

(4)

OFHC COPPER RODS
THERMAL CONDUCTIVITY
Experimental cell with four heater-posts
Run of November 1995

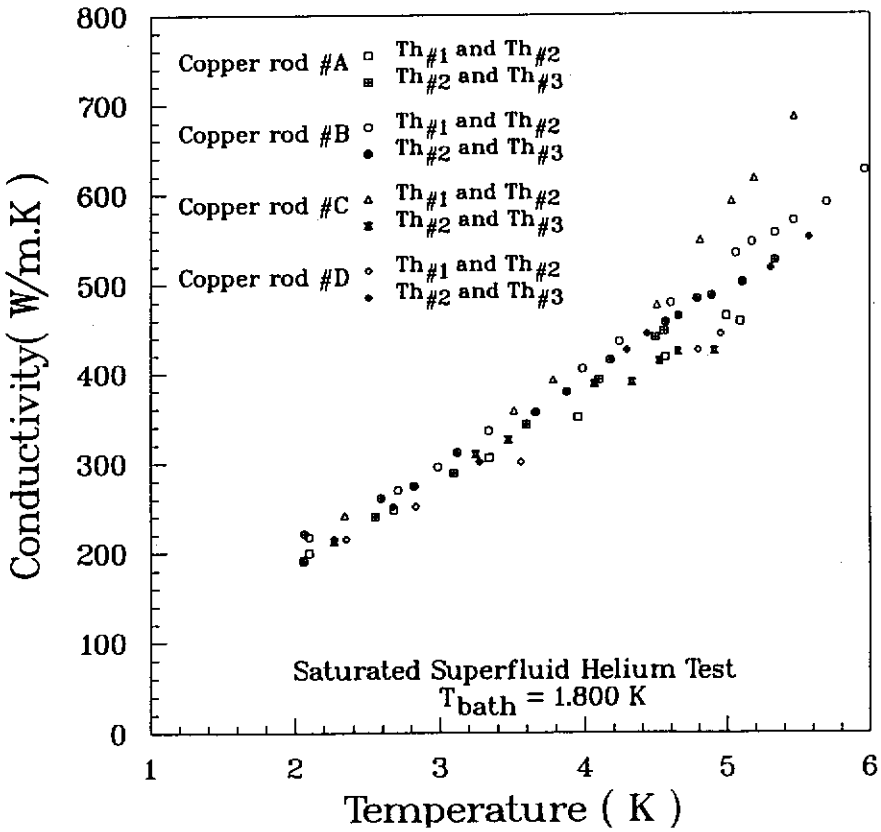

(7)

LOW HEAT FLUX KAPITZA CONDUCTANCE
AT Cu – HeII INTERFACE FOR THE 4 COPPER RODS
(A, B, C and D)
Run of November 1995

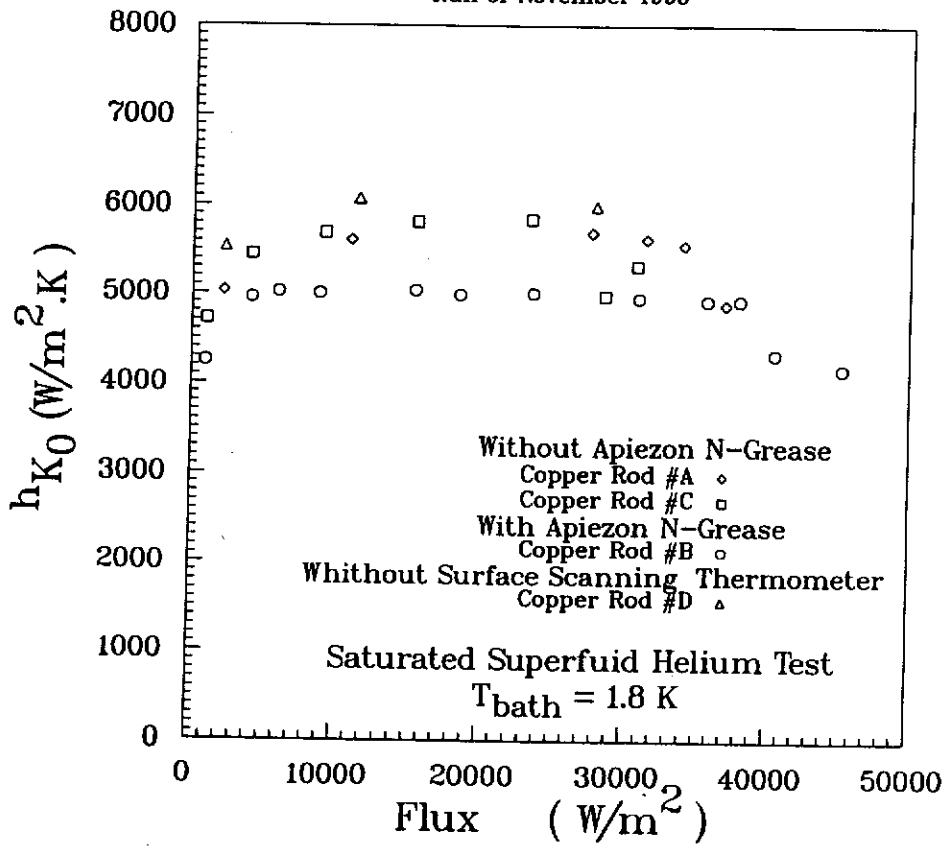

(8)

GLOBAL KAPITZA CONDUCTANCE
AT Cu – HeII INTERFACE FOR THE 4 COPPER RODS
(A, B, C and D)
Run of November 1995

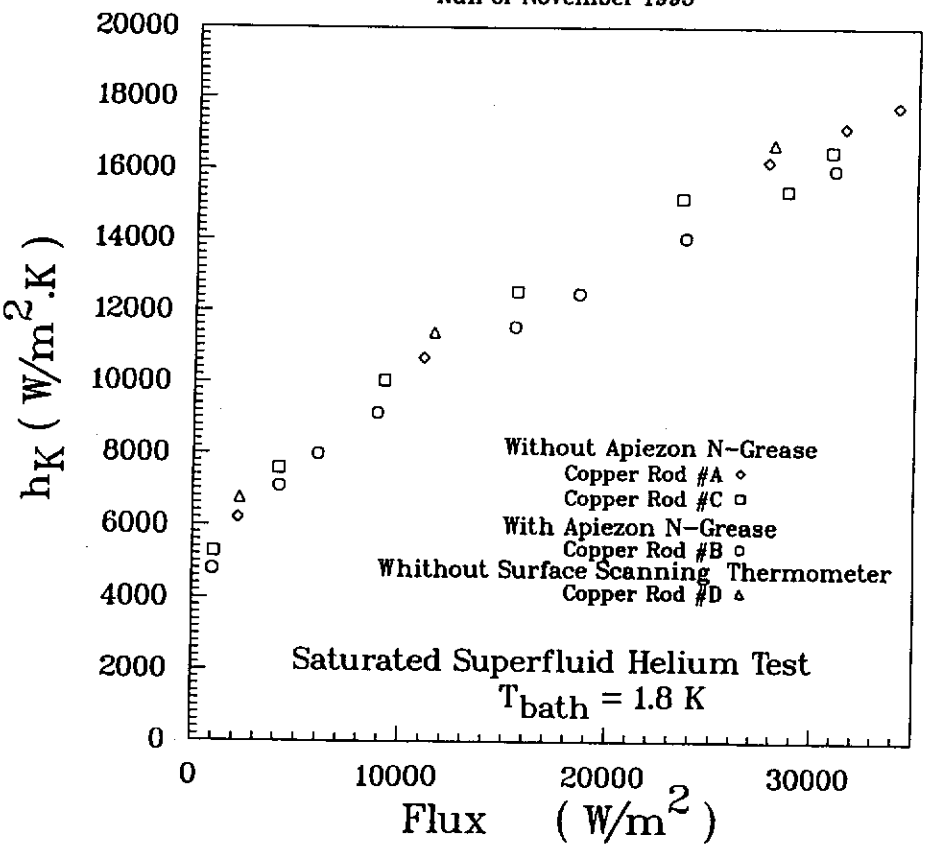

COPPER ROD TEMPERATURE VARIATIONS
VERSUS THE APPLIED HEAT
For the THERMOMETER #3 located at z = 7.3 mm from the Hell Cooled surface.
Run of November 1995

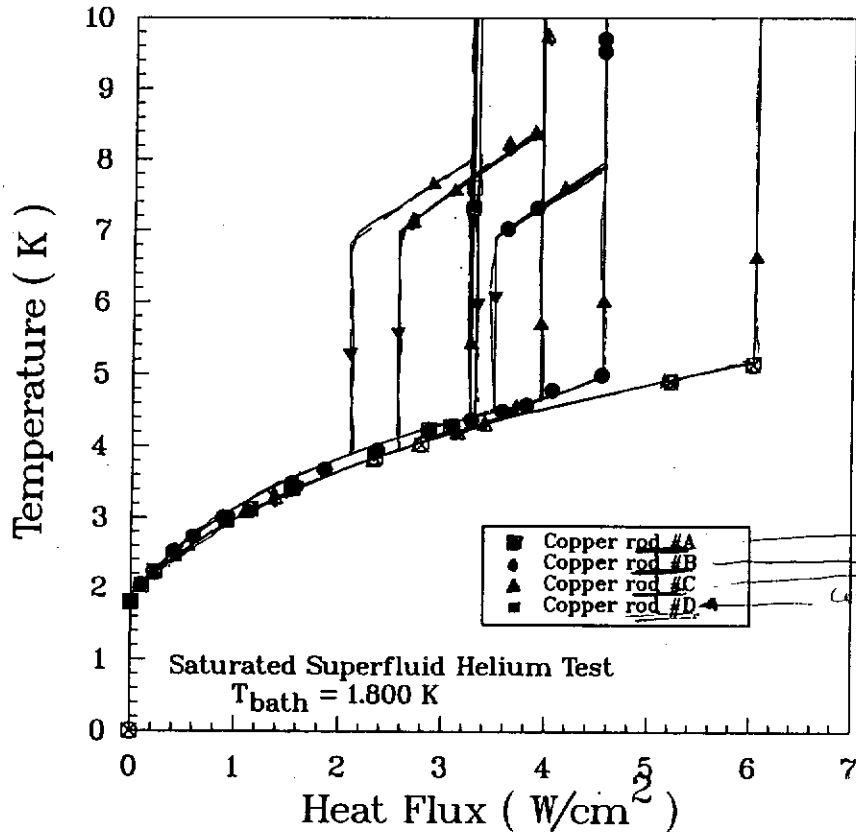

Authors	h_o	n	H_K@1.8 K	Runs
Mittag(1973)	0.0170	3.62	0.143	
Mittag(1973)	0.020	4.65	0.308	
Wilkes(1978)	0.0136	3.99	0.142	
Wilkes(1978)	0.0252	3.90	0.242	
Wilkes(1978)	0.0072	4.41	0.096	
Wilkes(1978)	0.0145	3.96	0.149	
Wilkes(1978)	0.0240	4.30	0.310	
IPN-GECS	0.0883	3.25	0.596	Oct.90 (*)
IPN-GECS	0.0774	3.44	0.585	Dec.90 (*)
IPN-GECS	0.0359	4.28	0.444	Oct.91 (**)
$H_K = h_O T_{bath}^n (W/cm^2.K)$				

(*) Standard SRF Surface Chemical Treatment and **Long Term** (≈ 9 months) **stay** of the sample under **Ambiant Atmosphere** (Air)

(**) The same sample underwent a new Chemical Treatment in standard way as for item (*) but was kept under helium atmosphere before experimental runs

Table 1 : Experimental Kapitza conductance HK for niobium samples of different surface treatments

11

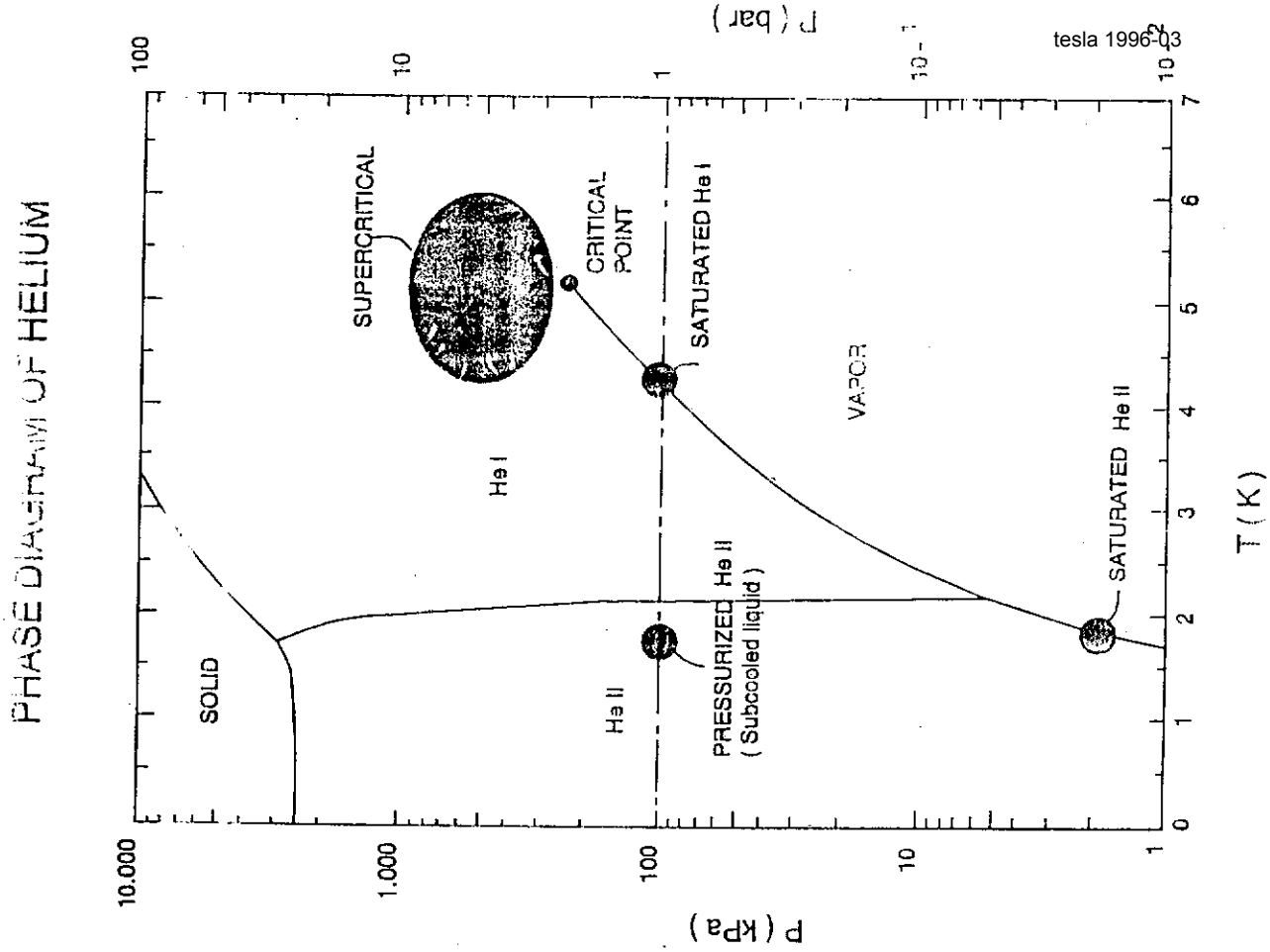

10

CRITICAL HEAT FLUX AT THE TRANSITION TO FILM BOILING

Horizontal heated surface facing downward

Run of November 1995

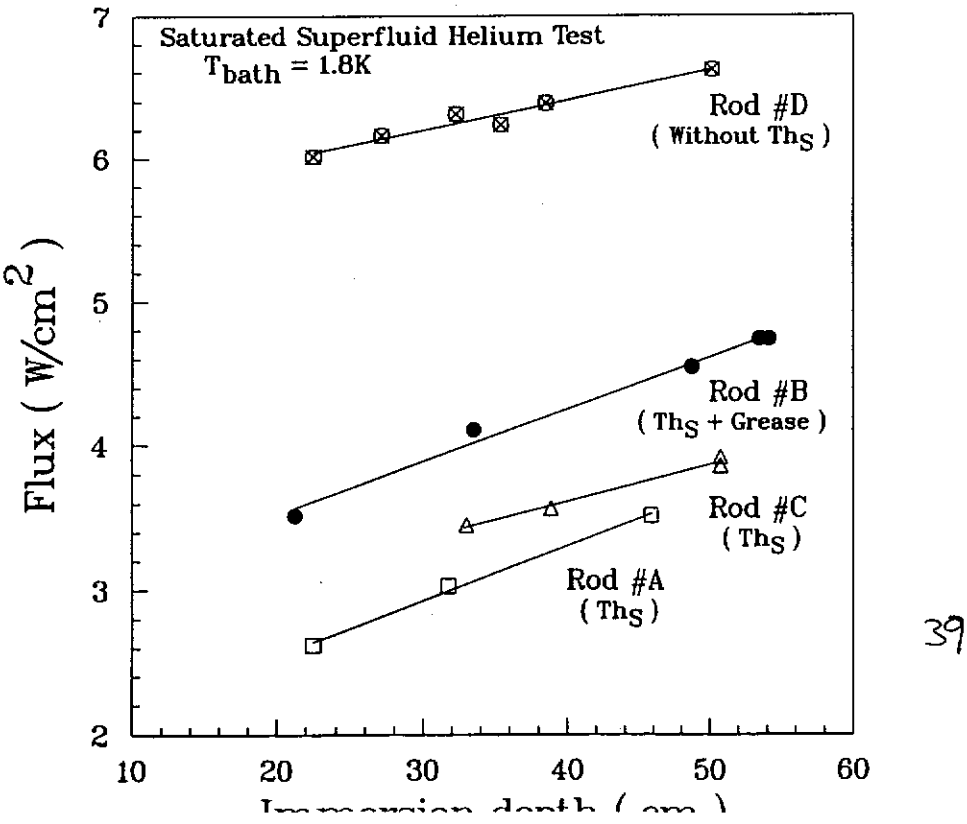

39

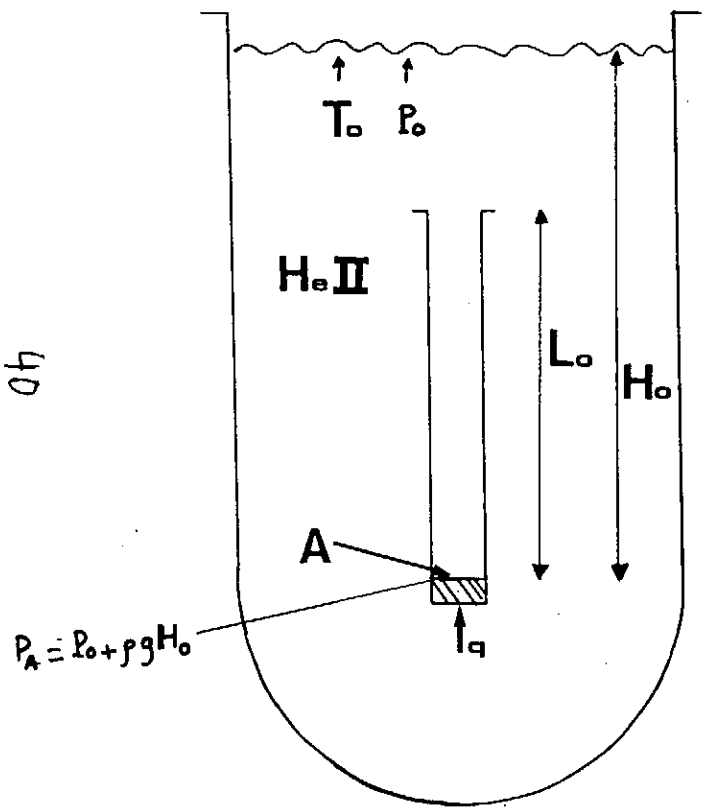

Fig. 2.16a : Transport de chaleur solide-conduit He II - Thermostat : schéma de la configuration expérimentale

Heat transport in He II confined to a channel.

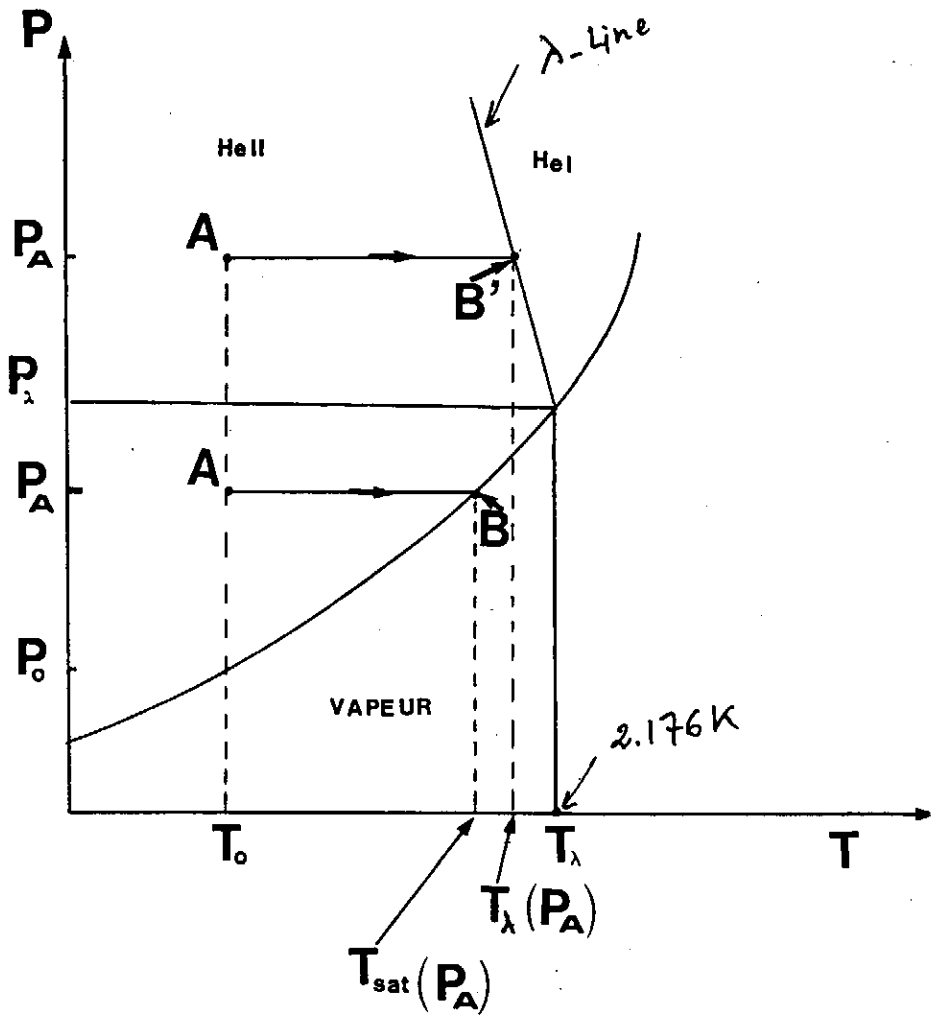

Fig. 2.16.b : Schéma des états thermodynamiques suivis par le "fluide A" adjacent à la paroi chauffée.

Thermodynamic path of the He II layer adjacent to the heat source.

LIMITING HEAT FLUX (INDUCING PHASE CHANGE) IN HE II CONFINED TO A CHANNEL

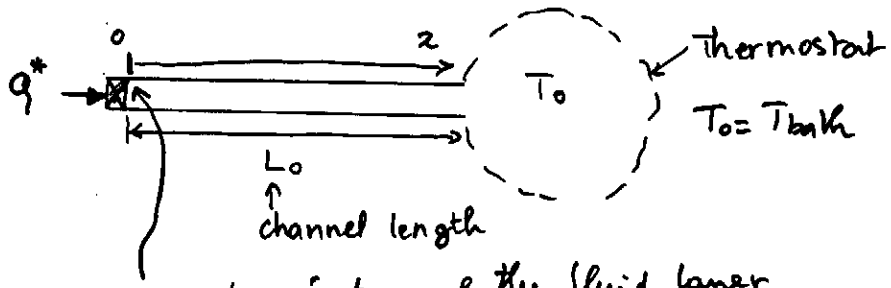

T_L = temperature of the fluid layer adjacent to the cooled solid.

The limiting heat flux is determined by the limiting temperature on the Helium phase diagram:

$T_L = T_{sat}(P_A)$ if $P_A < P_\lambda$

$T_L = T_\lambda(P_A) \simeq T_\lambda^{SVP}$ if $P_A > P_\lambda$

P_A is the local pressure of the liquid in front of the cooled solid

$$P_A = P_{sat}(T_{bath}) + \rho \cdot g \cdot H$$

(H: immersion depth; $\rho \cdot g \cdot H$: Hydrostatic pressure head)

Limiting heat flux

Eq (GHI) $$q_L = q^* = \left(\frac{1}{L_0} \int_0^{T_L} \frac{dT}{P(T)} \right)^{1/m}$$ (Gorter-Mellink relation)

with $m = 3$

$P(T)$: heat conductivity function see the curve.

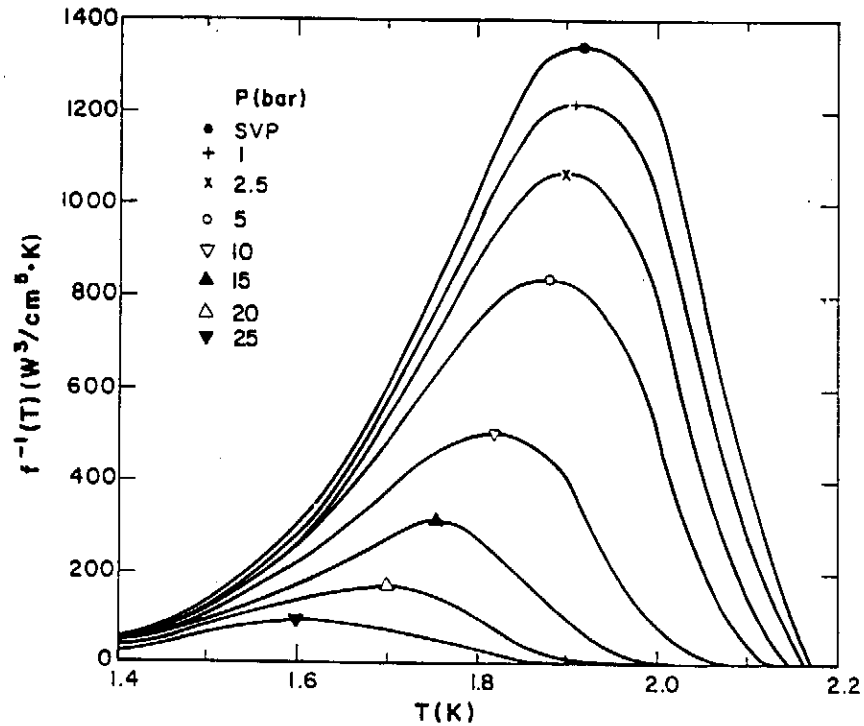

Fig. 5.3. Heat conductivity function for turbulent He II. Symbols indicate the location of the peak value.

H. FOUAIDY
PhD Thesis Paris VI
Univ., January 1989

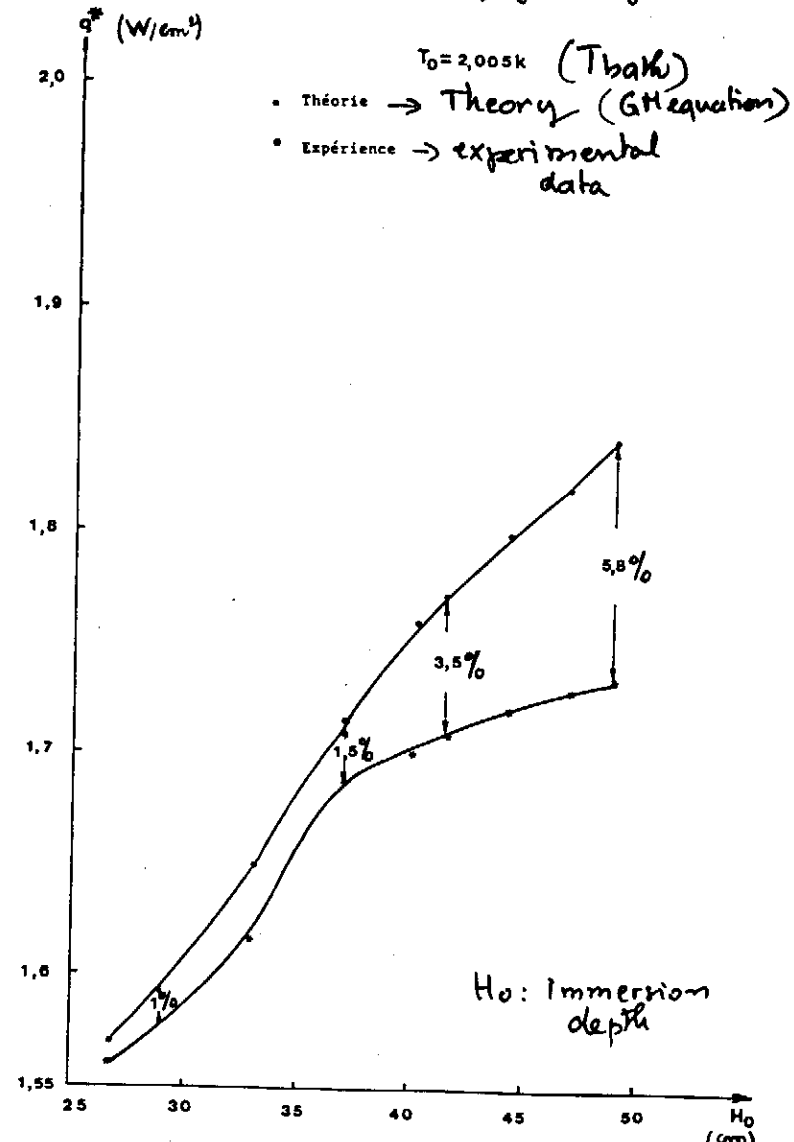

Fig. 5.44 : Flux limite q^* à la transition He II ⟶ vapeur en fonction de la profondeur d'immersion H_0 de la paroi chauffée par rapport à la surface libre du bain.

Critical Heat Flux in He II confined to a vertical channel (diameter: 10mm Length = 150mm)

H. FOUAIDY
PhD Thesis Paris VI Univ
January 1989

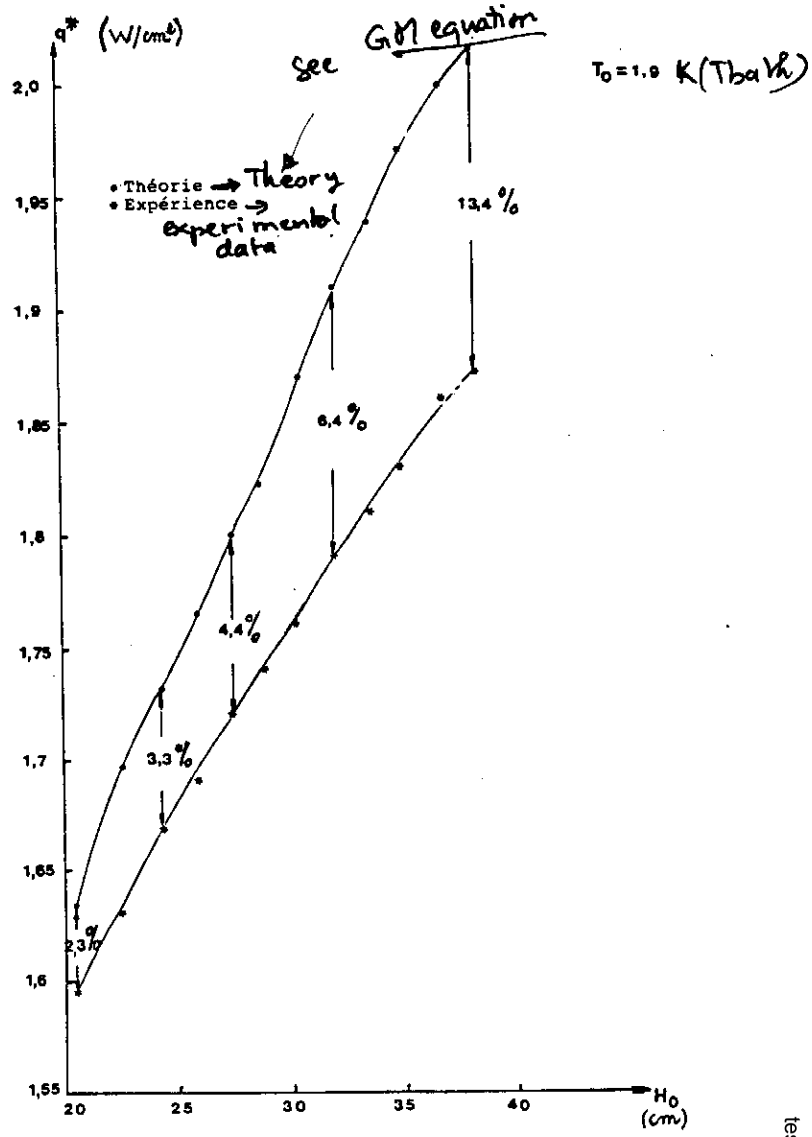

Fig. 5.43 : Flux limite q^* à la transition He II ⟶ vapeur en fonction de la profondeur d'immersion H_0 de la paroi chauffée par rapport à la surface libre du bain.

Critical Heat Flux in He II confined to a vertical channel (diameter: 10mm, length = 150mm)

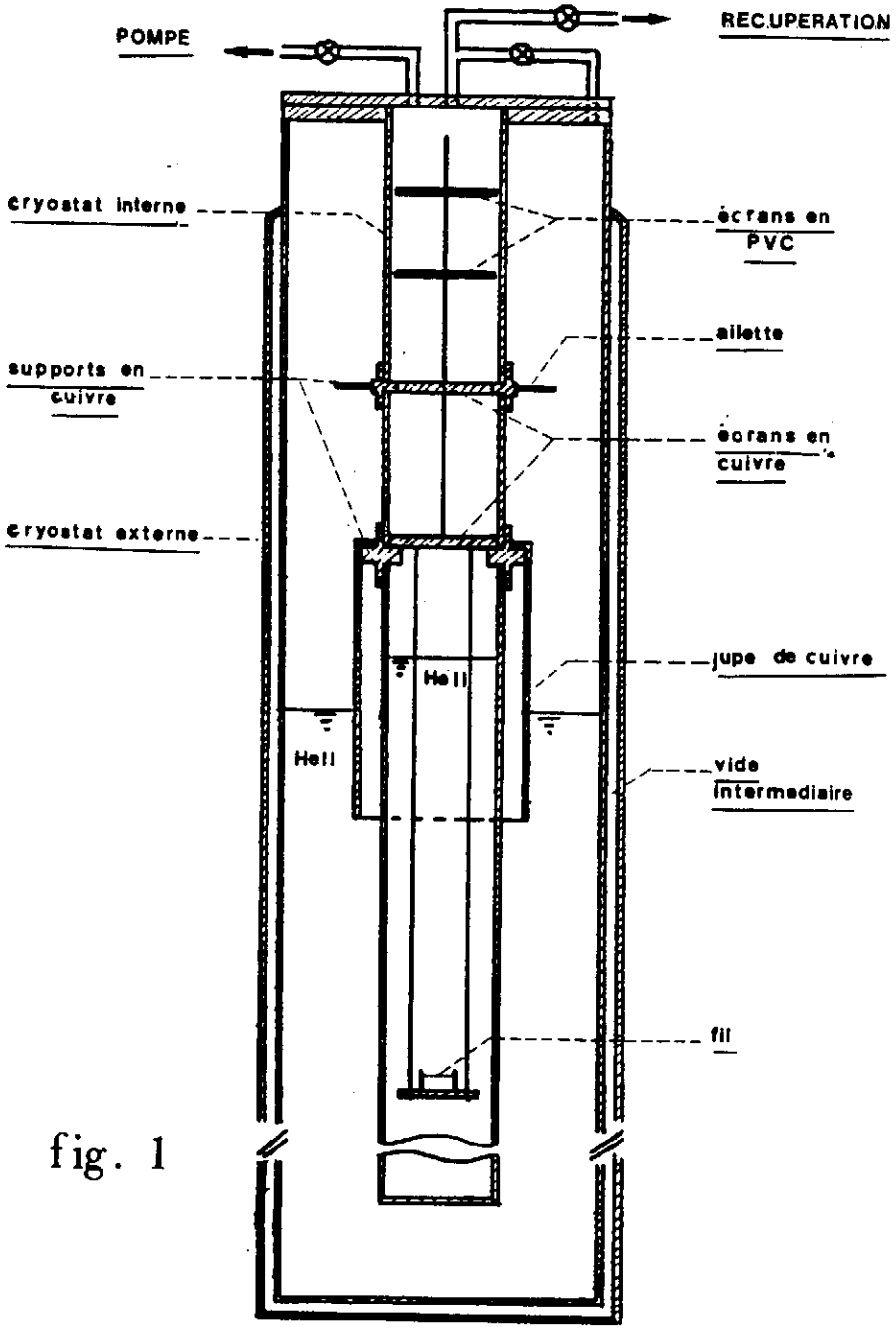

fig. 1

c- Régime III | b- Régime II | a- Régime I

FIL HORIZONTAL

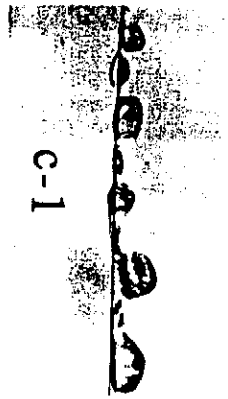

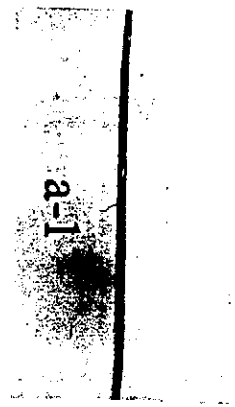

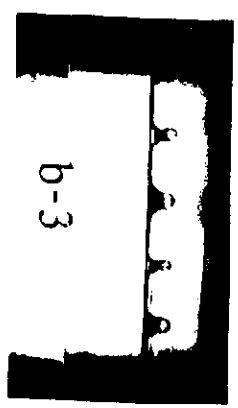

(1)

W.-D. Möller
29.2.96

Quench limitations vs. RRR

Measured Results

Does higher RRR lead to higher fields ?

th

(2) Hasan Padamsee

28 tests

37 tests

56 tests

40 tests

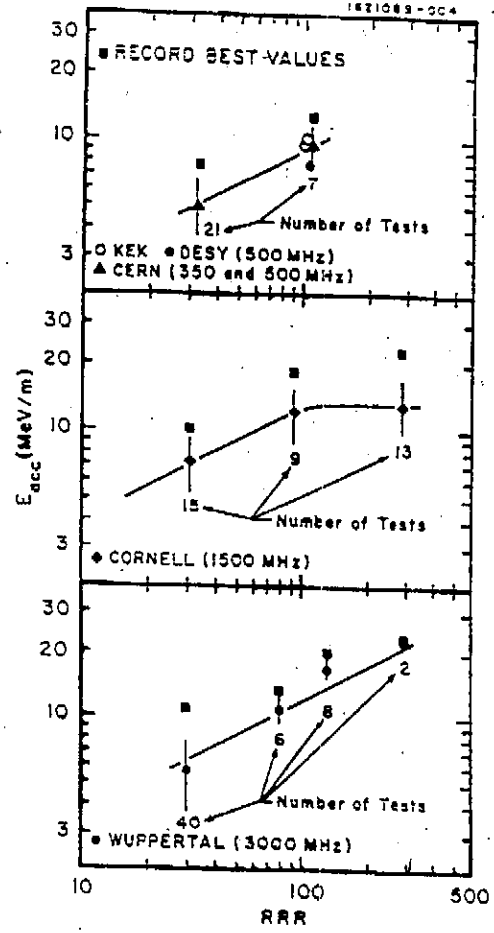

plotted: maximum and standard deviation

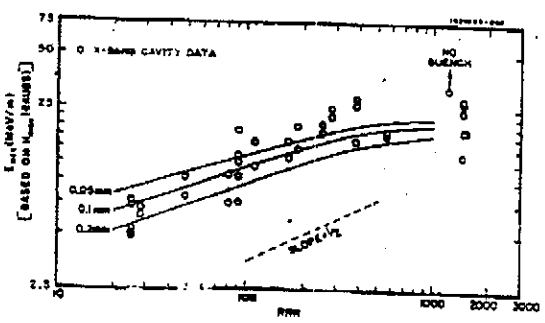

tesla 1996-03

quench fields of 1-cell cavities

⇒ thus E_a is a correlation between quench field and RRR

5h

Quench fields of multicell cavities

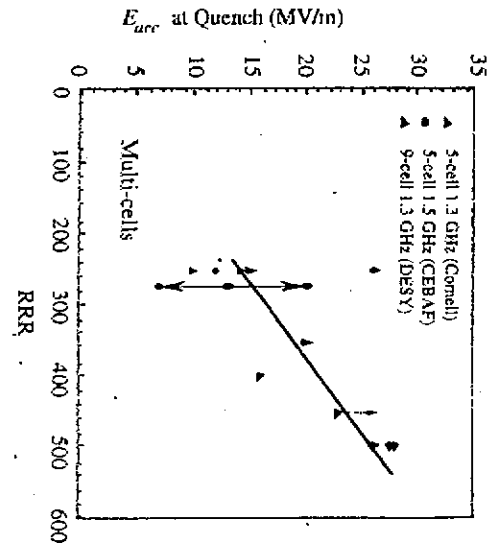

B. Bonin
1995

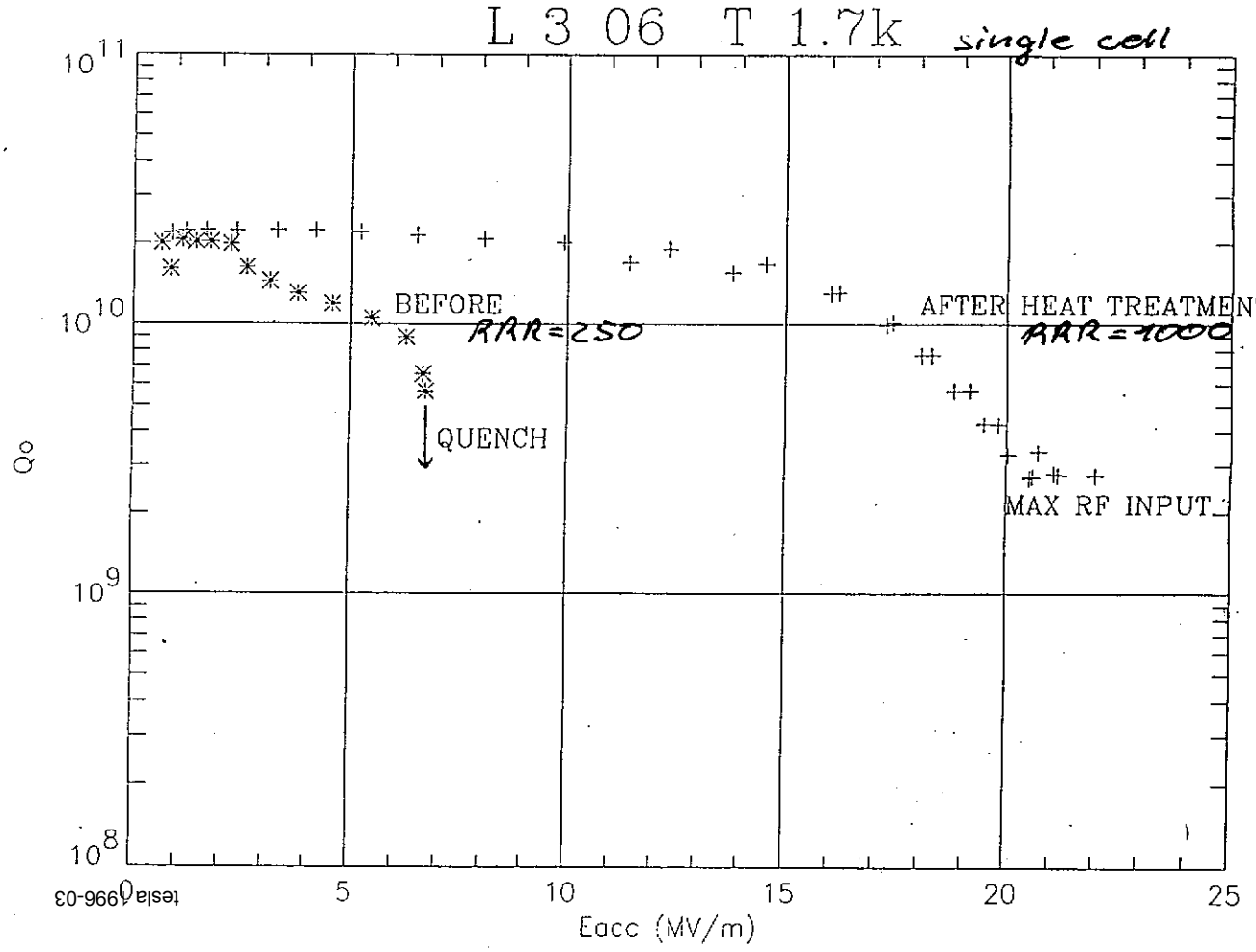

1995

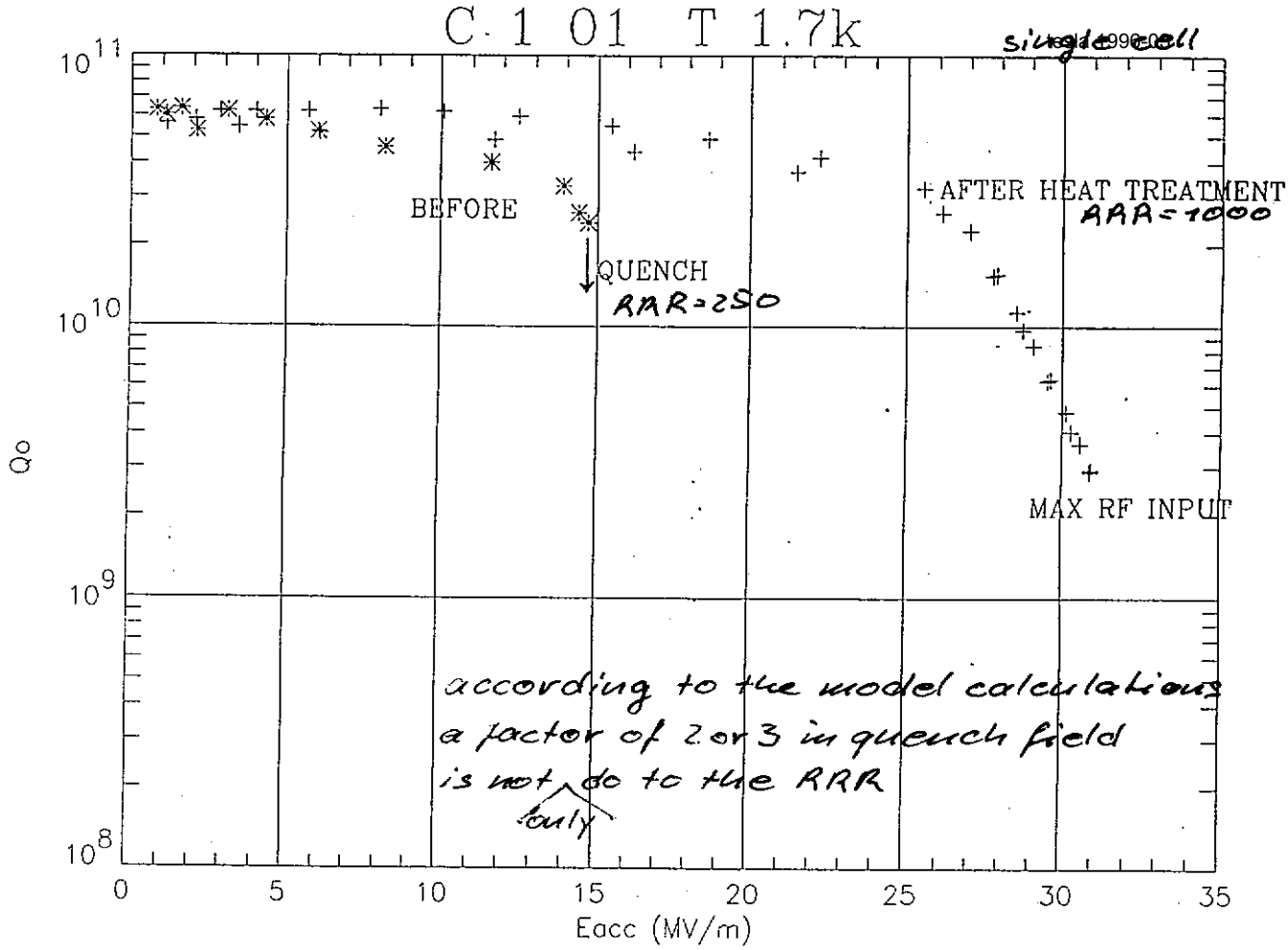

E. Kako
1995

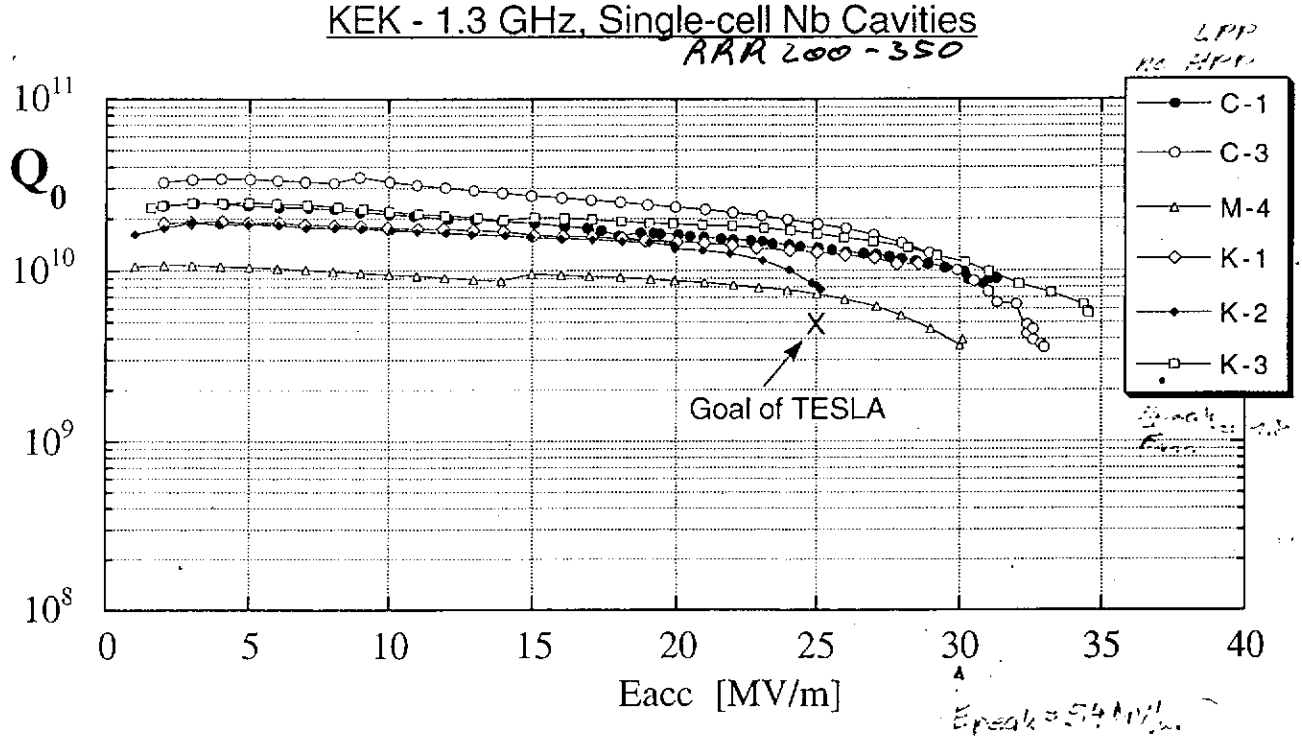

Also relatively low RRR gives very high quench fields

for RRR > 200 – no increase of field limit

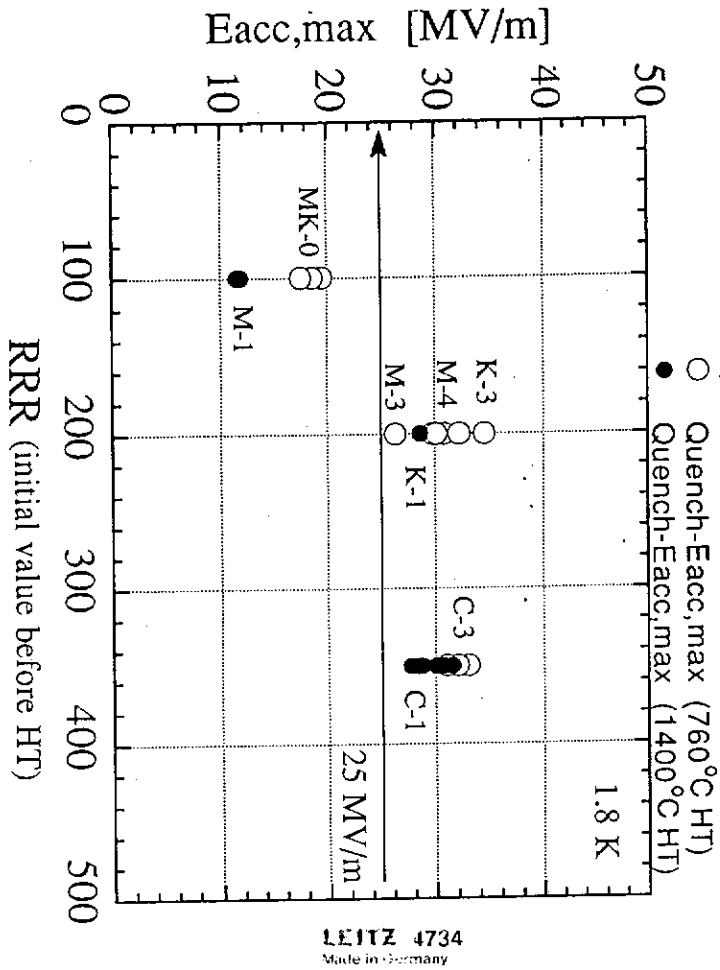

KEK single cell cavities

E. Kako 1995

E. Kako 1995

History of Cavity Tests

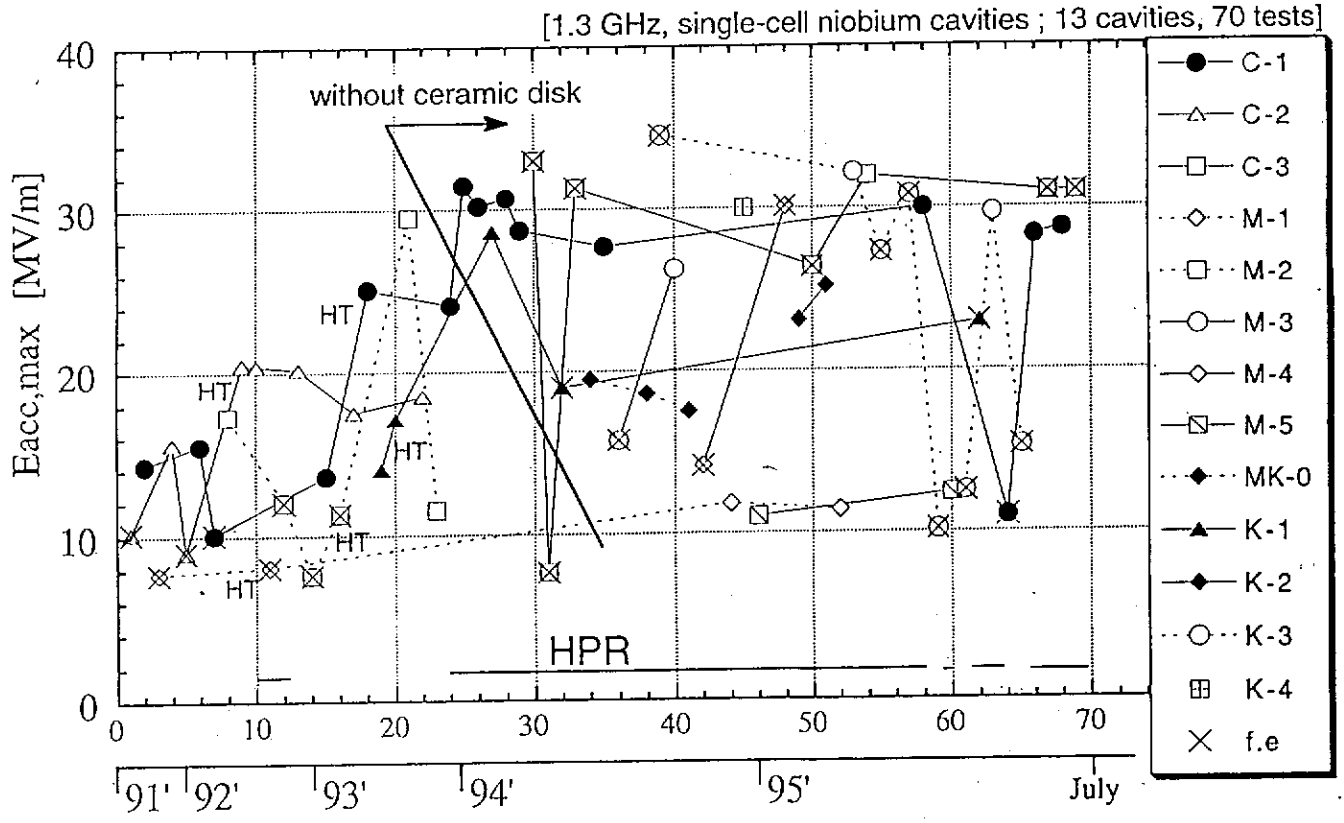

Summery

① there is a strong evidence for an improvement of quenchfield with RRR at least for RRR < 300 (multicells < 500)

② also low RRR cavities can show high fields > 30 MV/m

③ cavities made out of high RRR Russian Nb showed not a great field improvement (not enough data jet)

④ model calculations show:
big defects → big improvement by RRR
small defects → small " "

data improved - Nb material
- fabrication methodes
- clean treatment,
we have smaller defects
↘ less influence of RRR

⑤ Ti heat treatment improves RRR
+ cures quench limitations by more than calculations can explain.
↘ evidence for material homogenisation?

for TTF

W. Singer
DESY – MHF

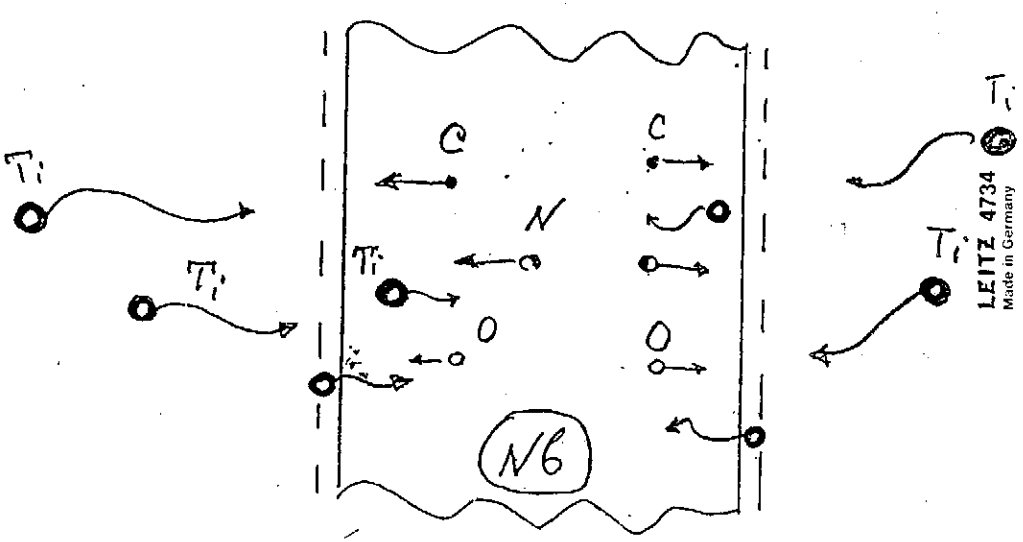

Fig. 1

Scheme of the Nb-refining by high temperature treatments

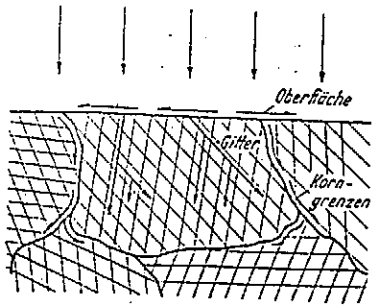

Abb. 144. Diffusion auf der Oberfläche, entlang der Korngrenzen und im Kristallgitter, schematisch. (Nach MEHL.)

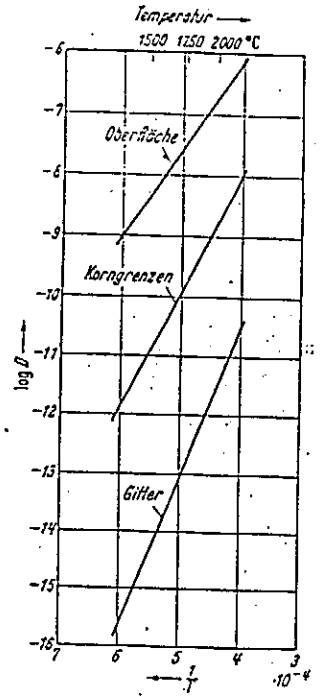

Abb. 145. Diffusion von Th in W.

Plane sheet

O, N, C in Nb

$$\frac{\partial C}{\partial t} = D \frac{\partial^2 C}{\partial x^2} \quad (1)$$

$$t=0 \begin{cases} C = 0 & x < -l \\ C = 0 & x > l \\ C = C_0 & -l \leq x \leq l \end{cases}$$

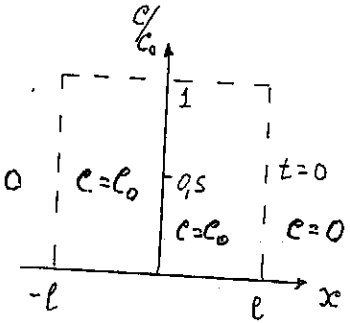

Solution

$$C/C_0 = 4/\pi \sum_{n=0}^{\infty} \frac{(-1)^n}{2n+1} \cdot e^{-\frac{D(2n+1)^2\pi^2 t}{4l^2}} \cdot \cos\frac{(2n+1)\pi x}{2l} \quad (2)$$

$$M/M_0 = 1 - \sum_{n=0}^{\infty} \frac{8}{(2n+1)^2\pi^2} \cdot e^{-\frac{D(2n+1)^2\pi^2 t}{4l^2}} \quad (3)$$

sheet thickness: $2l = 2{,}8$ mm

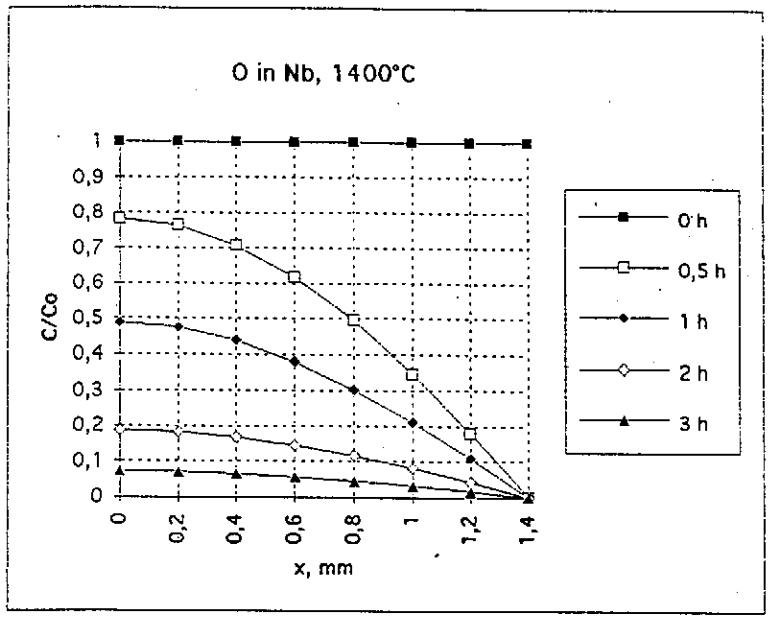

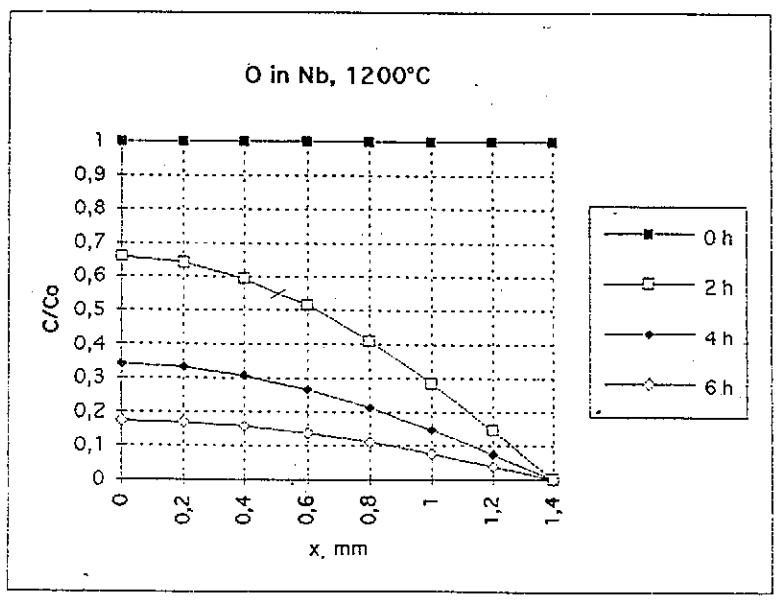

Fig. 2 The oxigen distribution in Nb sheet after refining

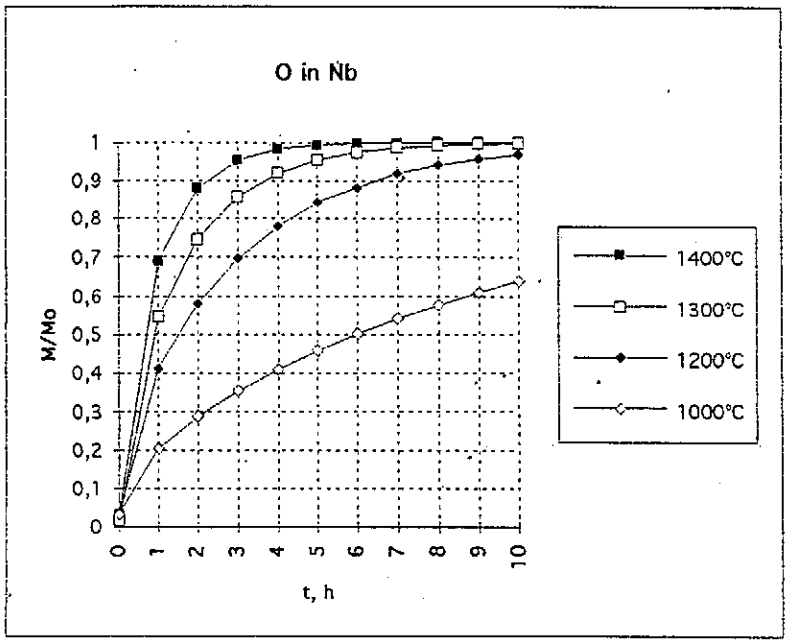

Fig. 5 Amount of oxygen which has left the Nb sheet

M, C (N in Nb)

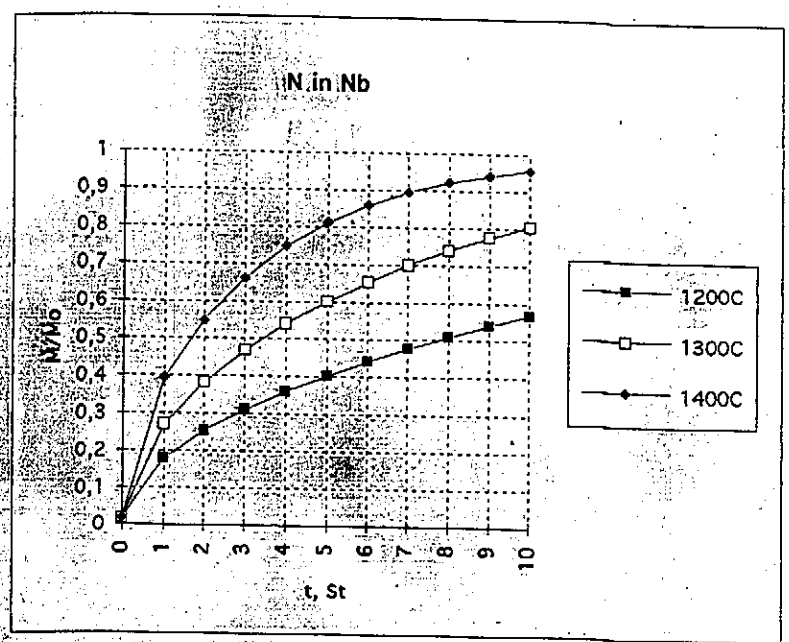

LEITZ 4734
Made in Germany

tesla 1996-03

25

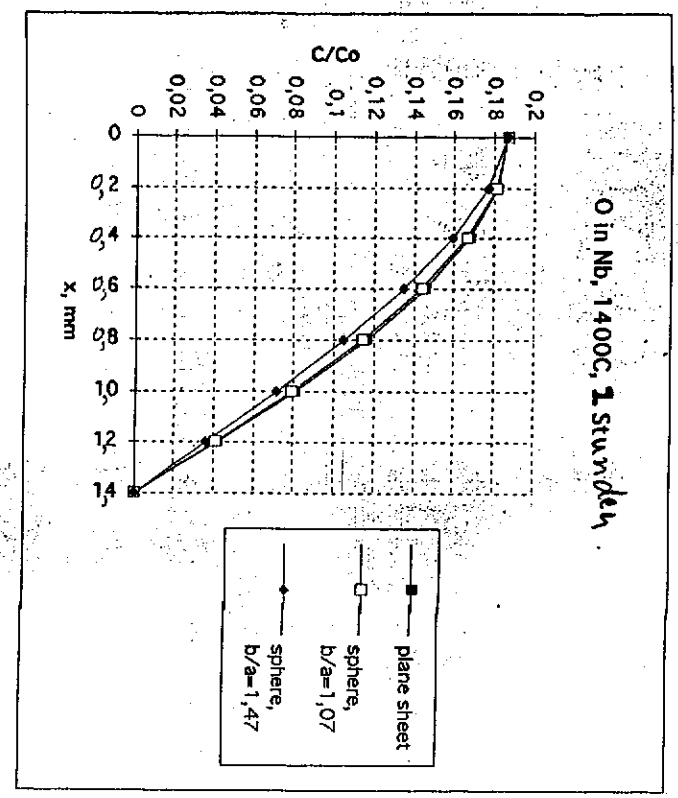

Calculation of RRR Increase by Solid State Gettering

DESY Furnace					Cornell Furnace				
Before Solid State Gettering sample with cav. D3					Before Solid State Gettering				
O, µg/g	N, µg/g	C, µg/g	RRR(cal.)	RRR(exp.)	O, µg/g	N, µg/g	C, µg/g	RRR(cal.)	RRR(exp.)
4	6	3	285	288	3	2	2	460	450
After Solid State Gettering sample with cav. D3					After Solid State Gettering				
O, µg/g	N, µg/g	C, µg/g	RRR(cal.)	RRR(exp.)	O, µg/g	N, µg/g	C, µg/g	RRR(cal.)	RRR(exp.)
0,08	1,8	0,9	750	525	0,06	0,6	0,6	1030	1070

$$RRR = \rho_i(300K)\left[\rho_i(10K) + \left(\frac{\Delta\rho}{\Delta C}\right)_O C_O + \left(\frac{\Delta\rho}{\Delta C}\right)_N C_N + \left(\frac{\Delta\rho}{\Delta C}\right)_C C_{e+\Delta}\right]^{-1}$$

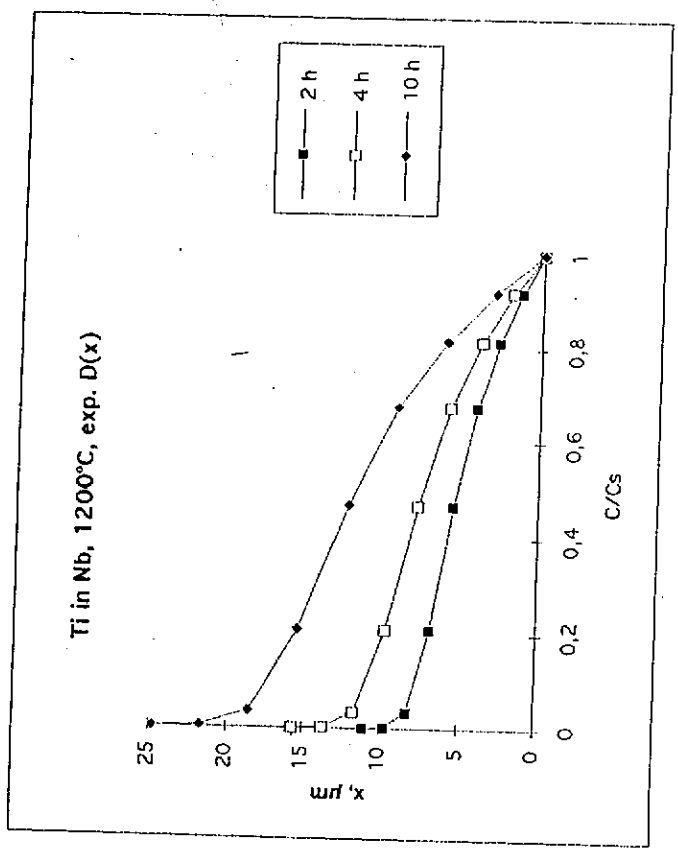

Fig 13-14 Penetration`s depth of Ti in Nb

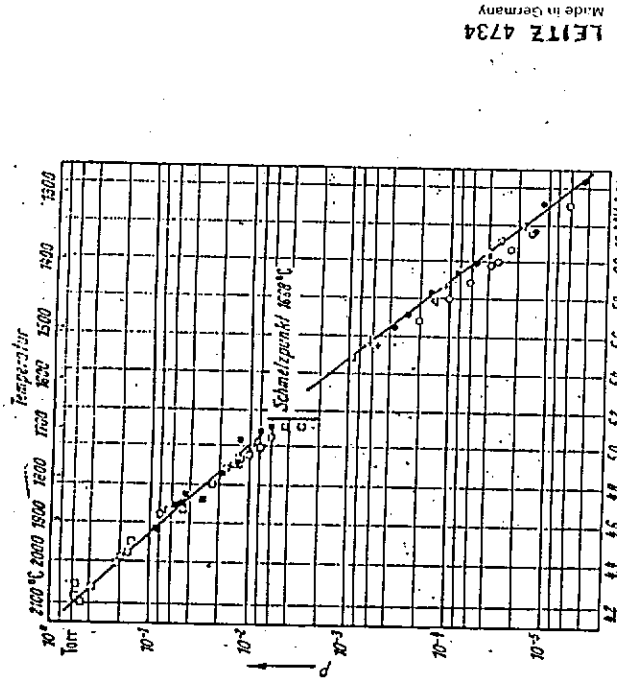

Abb. 4.22 Dampfdruck des Titans. △ [B 46]; + [C 33]; ○ [E 1]; ● [S 143a]; □ [K 49]; ■ [K 49a].

Concentration dependent diffusion

$$D = D(x)$$

$$\frac{\partial c}{\partial t} = \frac{\partial}{\partial x}\left(D \frac{\partial c}{\partial x}\right)$$

$$\begin{cases} c = c_s, & x = 0,\ t > 0 \\ c = 0, & x > 0,\ t = 0 \end{cases}$$

$$D = D_0 e^{\beta(c - c_0)}, \quad \exp D(x)$$

numerical solution

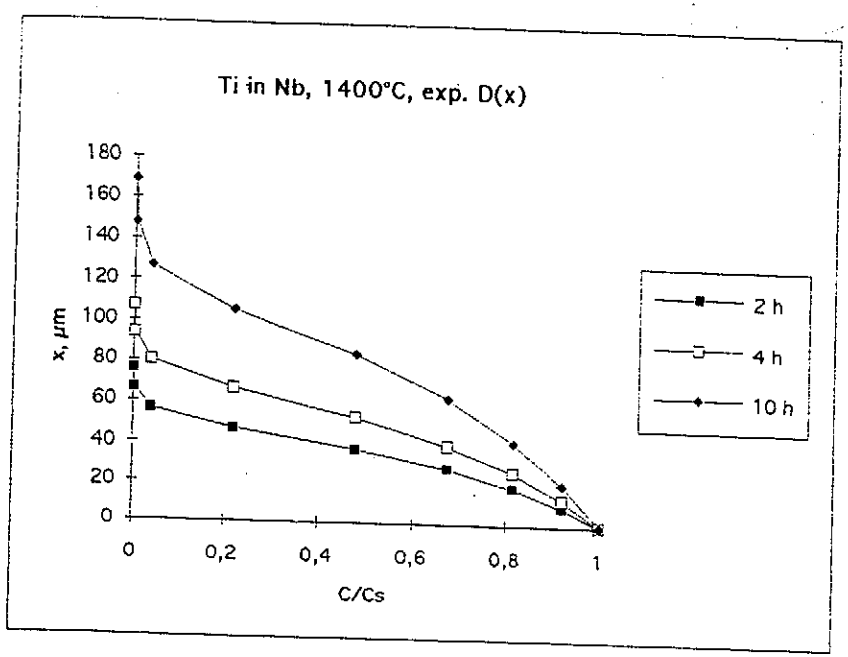

Cavities - Titanisation (DESY Furnace)

Sample	Note	RRR(dc,samp.)	RRR(ac,cav.)	treatment	tot. time
Nb	Ref. for P2, D2, D4, D6	265		as receiv.	
Nb -2Ti/1	Cav. P2	388		1400°C,4St,Ti	30 h
Nb -2Ti/2	Cav. P2	384		1400°C,4St,Ti	30 h
Nb 23/95/1	Cav. D2	348		1400°C,4St,Ti	82 h
Nb 27/95/2	Cav. D4	525		1400°C,4St,Ti	cycle
Nb 37/95/1	Cav. D6	521		1400°C,4St,Ti	cycle
Nb 37/95/2	Cav. D6	534		1400°C,4St,Ti	cycle
Nb	Ref. for D3	288		as received	
D3-II	Cav. D3	529 (520)		1400°C,4St,Ti	cycle
Nb	Ref. for D1	281		as received	
Nb	Ref. for D5	289		as received	
Nb 61/95	Cav. D1	535 (521)	575±50	1400°C,4St,Ti	cycle
	Cav. D5		200±20	without Ti treatment	
Nb 3/96	Cav. D5 (middle)	494		1400°C, 1St; 1250°C, 3St	
Nb 2/96	Cav. D5 (top)	498		1400°C, 1St; 1250°C, 3St	

55

LEITZ 4734
Made in Germany

T. Schilcher

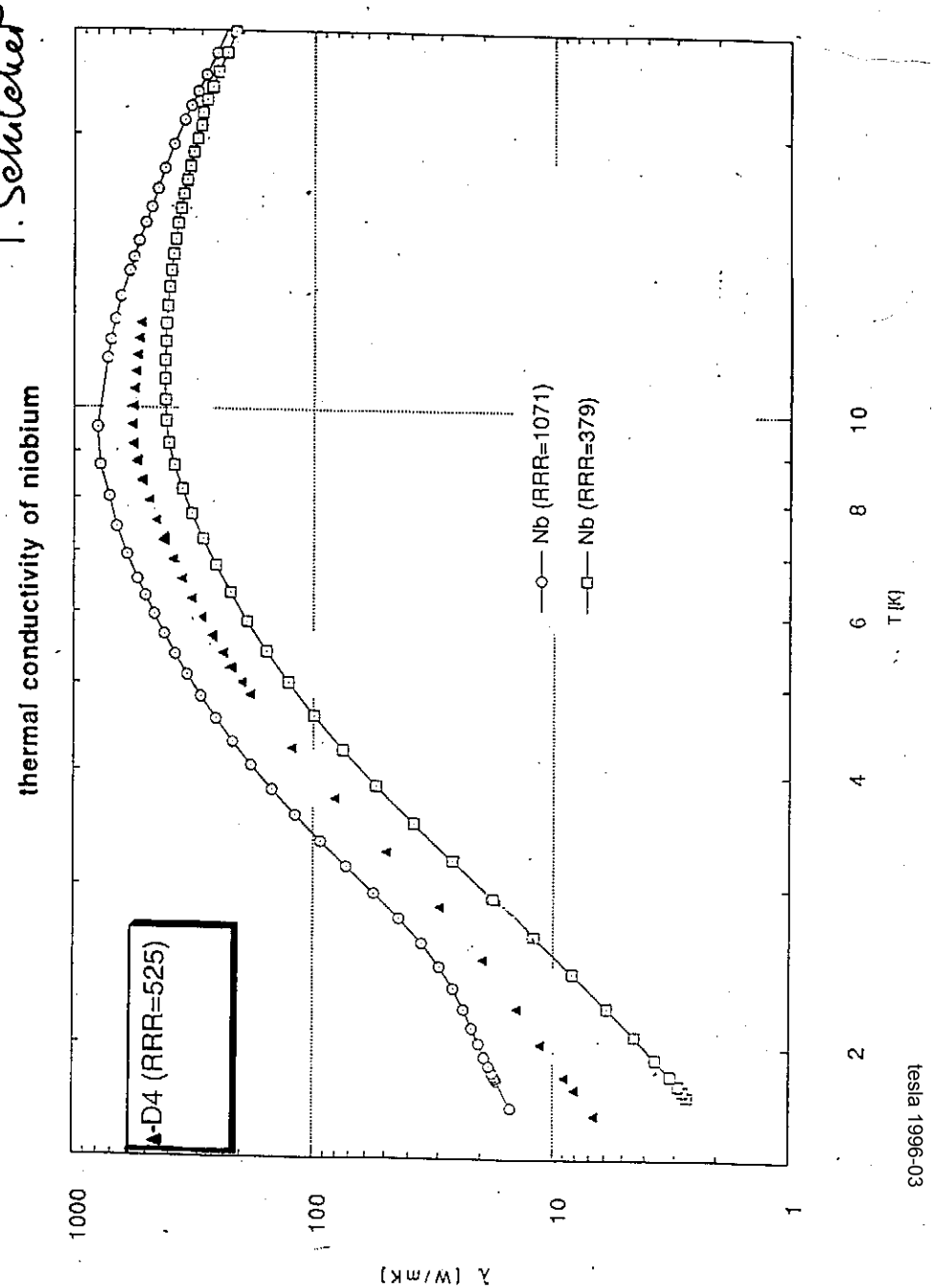

Kennzeichnung der Nb Proben

Nummer	RRR neu	RRR gemessen	Behandlung	Kommentar	Ort	Herst
0./0	300	114	1400 C 4 h ohne Zusatz Grundzustand des Ofens testen	Vorbehandlung Aceton + Ultraschall/BCP 1/1/1 20 µm Abtrag/Heizen 4h T=1400-1410 C Pfinal 2*10-7 mbar	27.1 Wtal 4.2 Hamburg Verkat 10.2 Singer	
2/1	300	382.5	Referenz zu 2/2 RRR Messung	Probe RRR gefräst	27.1 HAM 10.2 Singer	
2/2	300	236	1400 C 4 H mit Mantel Zeichnung Messstr 18	Vorbehandlung Entfetten 10 µm BCP US + Spülen T= 1400-1410 4 h	27.1 Ham 23.2 Wentstadt	
3/0	300	283,5(926) 282	as delivered by Heraeus Grundmaterial für 4.0 ff	gefräst aus Probe 3.0	10.3 Singer	
4/	300	530 (546)	Ti Behandlung mit 0.2mm Blech Aufbau wie in Ofen DESY Einsatz	Vorbehand. wie Probe 1 T = 1400 C Puz Zeit 4 ht		
5/	300	374	Ti Behandlung mit 0.2 mm Blech Aufbau wie in Ofen DESY Einsatz	Vorbehandlung wie Probe 1 T = 1300 C Zeit 4h		
6/	300	293	Ti Behandlung mit 0.2 mm Belch Desy Einsatz Aufbau wie in Ofen	Vorbehandlung wie Probe 1 T = 1100 C Zeit 6 h		
7/	300	661	—"— " —	T=1400°C, 4h		
8/	300	(343) 345	—" — " —	T=1300°C, 4h		
9/	300	523	—" — " —	T=1400°C, 4h		
10/						
11/						
12/						
13/						

LEITZ 4734 Made in Germany

95

Cavities - Titanisation (DESY Furnace)

Sample	Note	RRR(dc)	treatment
Nb 1/96	sample (top)	464	HT* - 1400°C, 1h; 1250°C, 3h
Nb 4/96	sample (bottom)	524	HT* - 1400°C, 1h; 1250°C, 3h
Nb 2/96	Cav. D5 (top)	500	HT* - 1400°C, 1h; 1250°C, 3h
Nb 3/96	Cav. D5 (middle)	494	HT* - 1400°C, 1h; 1250°C, 3h

Conclusions

1. The solid state gettering in the DESY furnace increase the RRR of Nb300 to RRR_{exp} >500, nevertheless RRR_{exp}<RRR_{calc} (RRR_{calc} ≈750)

2. Decreasing of the purification temperature to 1200-1300°C is not limited by the diffusion of the interstitial impurities

3. The purification at temperatures below 1200°C reduces the penetration depth of Ti in Nb significant but it is limited by Ti vapor pressure

4. Solid state gettering procedure which contains:
a) creating of sufficient Ti vapor pressure in initial stage of purification (for example 1400°C, 1h)
b) purification at reduced temperatures (for example 1250°C, 3h)
can be promising

Ti postpurification at DESY

start from RRR 250 - 280

D. Hubert + man power from PVAC

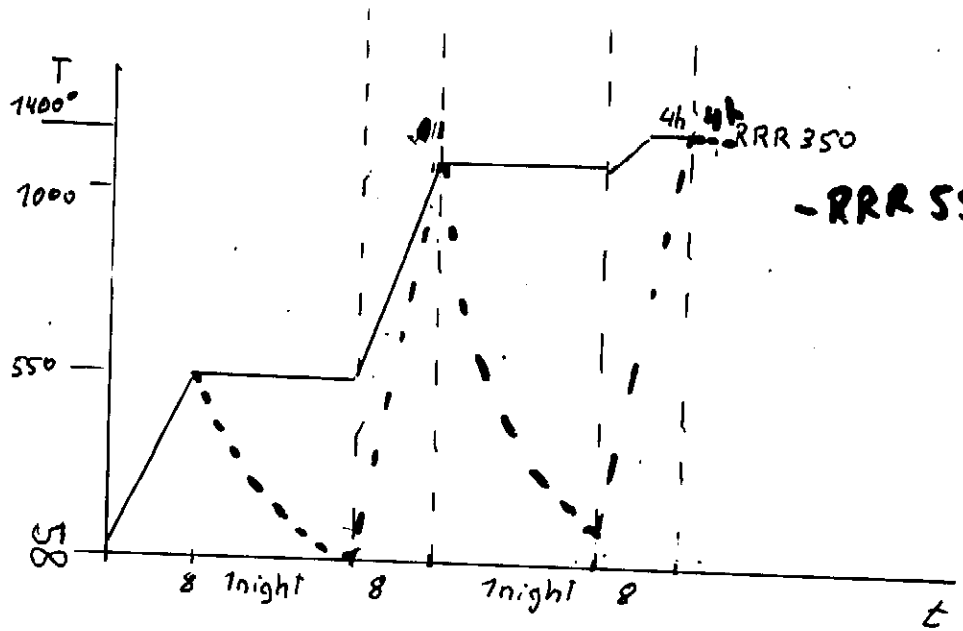

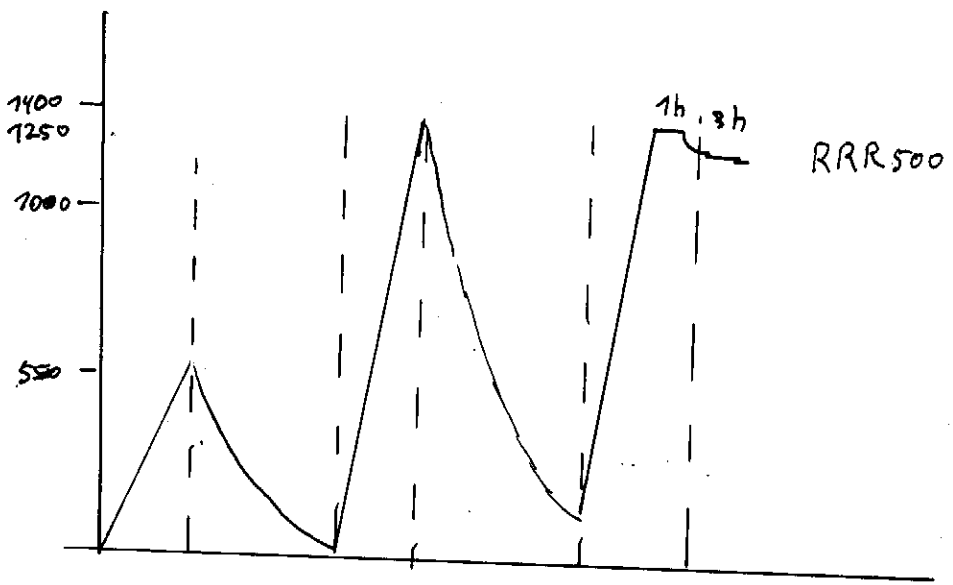

Time and slop depending on total vacuum pressure!!

$P_{tot} \leq 5 \cdot 10^{-6}$

Ti treatment

pre-cleaning of furnance + Ti carrier
two side Titanification
control of masses (masspectrum)
control of total pressure
control of temperature (heater + infrared on cavity)

temperature gradient ↑ C°/min

Sample and Analysis done at Cornell

H.Padamsee D.Moffat A.Matheisen

Sample geometry

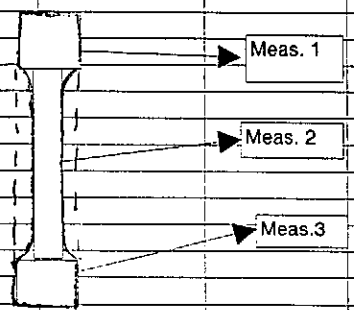

ANALYSIS

SIMs

Sequence:
remove 10 µm
Check with SIMs
Remove 10 µm
Check with SIMs
etc.

Grinding

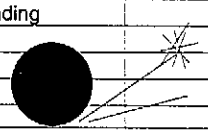

saclay 1.3 Ghz Temperature-Time

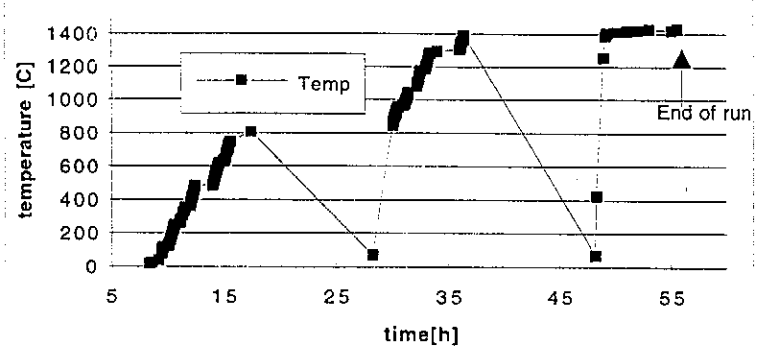

59

Results of Samples

Numbers are averages out of the 3 measurement points on each sample

RRR 1000

Sample No		Ti concent >10%	Ti local>1%	Ti concent<1%
1	"	<50µm	50-80	>=90
2	"	<40 µm	50-70	>=70
3	"	<50µm	50-75	>=80
4	"	<40	40-60	>=70
5	"	<40	40-65	>=70
6	"	<50	50-70	>=80
7	long "	<30	30-50	>=60
8	long "	<30	30-50	>=60
9	long "	<30	30-50	>=60
10	long "	<40	40-60	>=70
11	"	<50	50-70	>=80
12	"	<40	40-60	>=80
13	"	<50	50-80	>=90

MAN B&W

Untersuchungsbericht

Nr. 95/0225
Blatt 3/6
Datum: 09.02.95

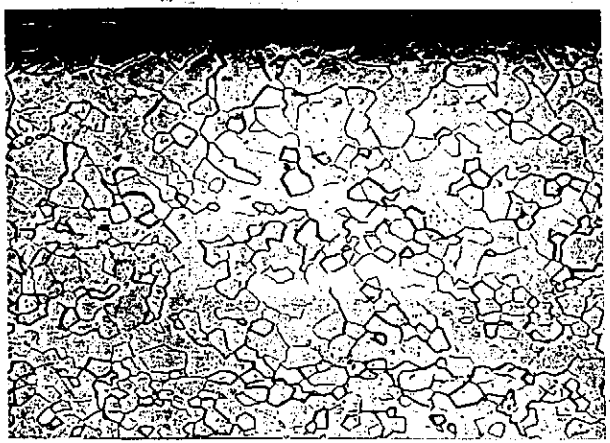

Abb. 1

Probe-Nr.: 1

Nb-Blech,
nicht titanisiert

100 : 1
II/ 21 509

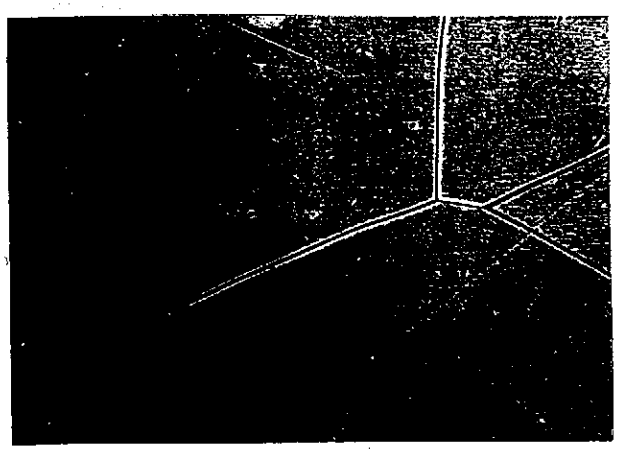

Abb. 2

Probe-Nr.: 2

Nb-Blech,
titanisiert
1400 °C/4h

100 : 1
II/ 21 510

MAN B&W

Untersuchungsbericht

Bearbeiter: Hengst/Dietrich

Nr. 95/0225a
Blatt 1
Datum: 09.02.95

Messung und Darstellung der Titan-Schichtdicke an Niob-Probe nach Vorgabe

Auftraggeber: Deutsches Elektronen-Synchrotron DESY
Auftrags-Nr. 004966/H.36.051.1/673/MKV

Werk-Nr. 2 720 899

Probe **D4 (27/95/1)** am 22.03.95 durch Herrn Hubert übergeben.

Ergebnis:

Mikrogefügeschliff mit Darstellung der titanisierten Randzone, Vergrößerung 500 : 1:

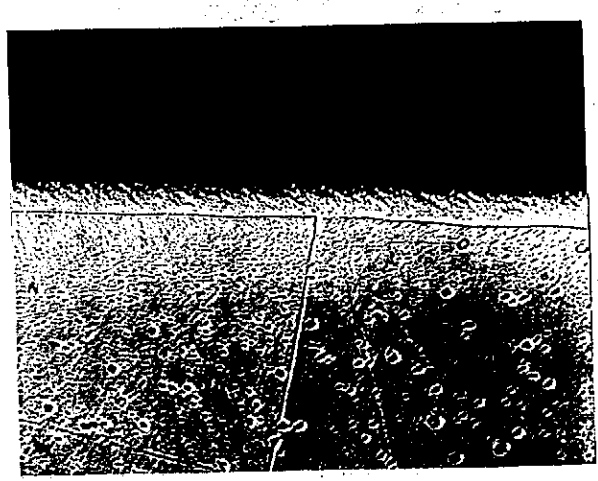

Abb.: 1

Vert.:
DESY
MBD/SRQ

MAN B&W Diesel
Aktiengesellschaft
Werkstoffprüfung
Hengst

tesla 1995 08

Untersuchungsbericht

Bearbeiter: Hengst/Dietrich

Nr. 95/0225a

Blatt 2

Datum: 03.04.95

Messung und Darstellung der Titan-Schichtdicke an Niob-Probe nach Vorgabe

Nachtrag REM-Untersuchung:

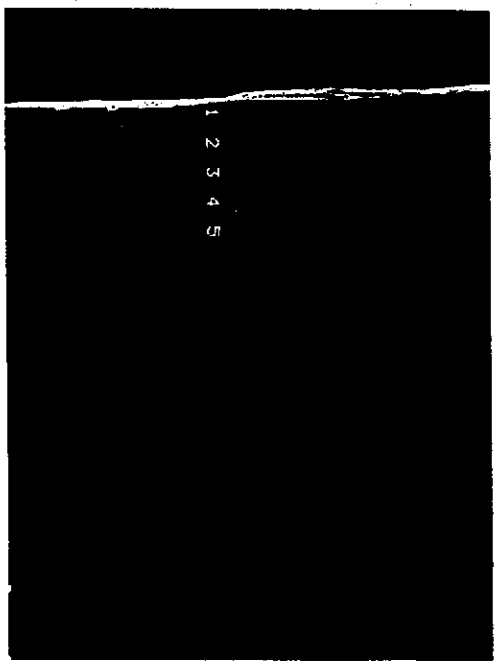

Abbildung der Ti-Schicht mittels Raster-Elektronenmikroskop (ca. 1300 : 1) mit den Meßpunkten der Spotanalysen, dargestellt in den nachfolgenden Diagrammen 1 - 5, Seite 3 - 7.
Ein Ti-Nachweis unterhalb der optisch sichtbaren Schicht ist nicht gegeben.

MAN B&W Diesel
Aktiengesellschaft
Werkstoffprüfung

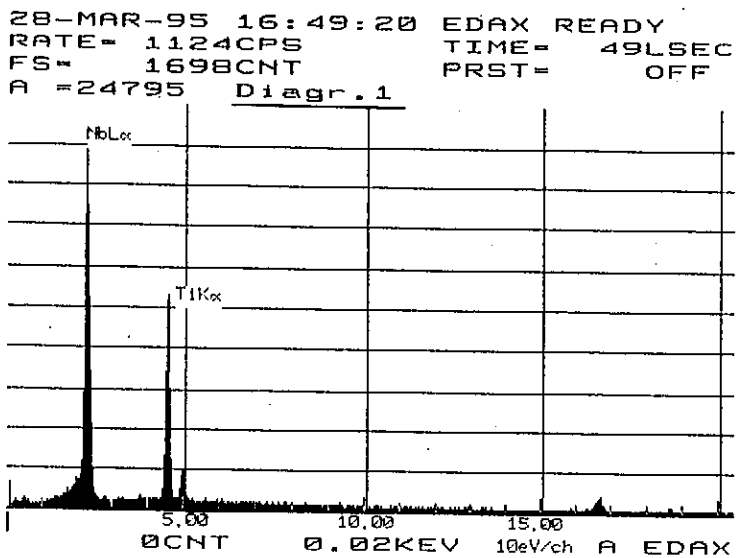

tesla 1996-03

28-MAR-95 18:00:31 EDAX READY
RATE= 1170CPS TIME= 49LSEC
FS= 2028CNT PRST= OFF
B =24795 Diagr.4

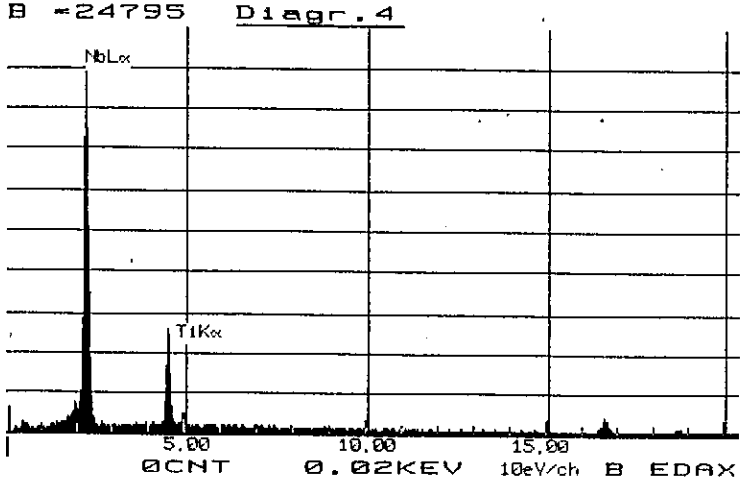

0CNT 0.02KEV 10eV/ch B EDAX

28-MAR-95 18:07:30 EDAX READY
RATE= 103CPS TIME= 49LSEC
FS= 1328CNT PRST= OFF
B =24795 Diagr.5

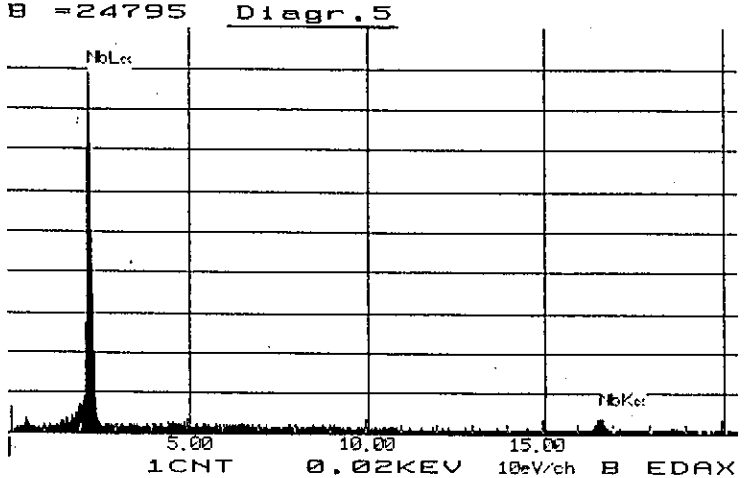

1CNT 0.02KEV 10eV/ch B EDAX

comparison of A

Methode		for 4 h at 1400 C eating, step heating
grinding	Probe-Nr.: 2	80-82 µm
SIMs		70-<90 µm
EDX (EMA)		0-3 µm
µ-SYXRF		80 µm

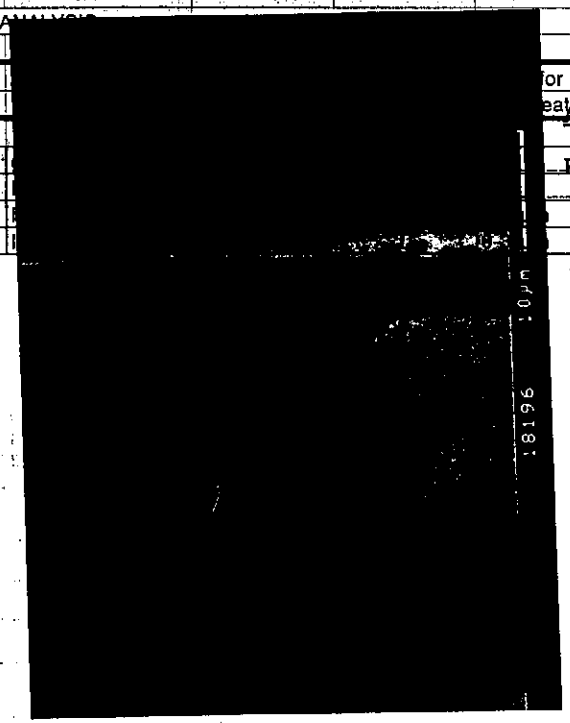

← Ti-Schicht
← "Schlagschatten"

← Grundgesfüge

Titan-Schichtdicke 4 µm

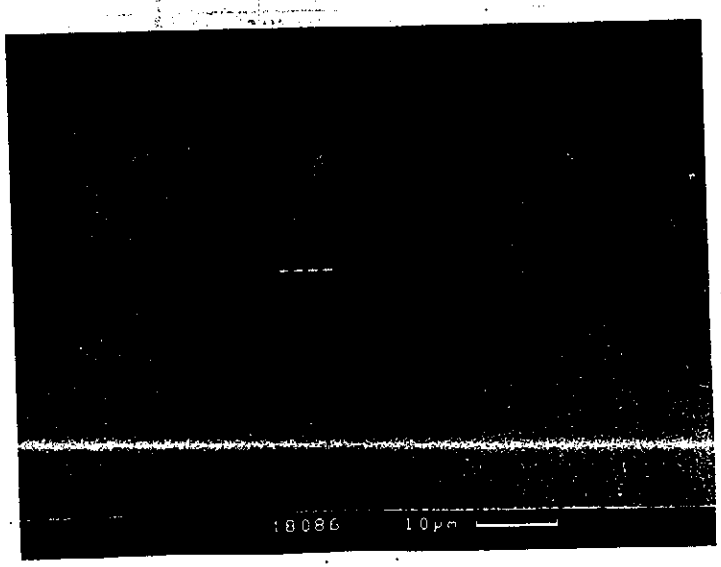

Abb. 7

Probe-Nr.: 3

Titan-Schichtdicke
ca. 5 µm

Abb. 9

Elektronenstrahl-Mikroanalyse der titanisierten Oberfläche
(Probe 2)

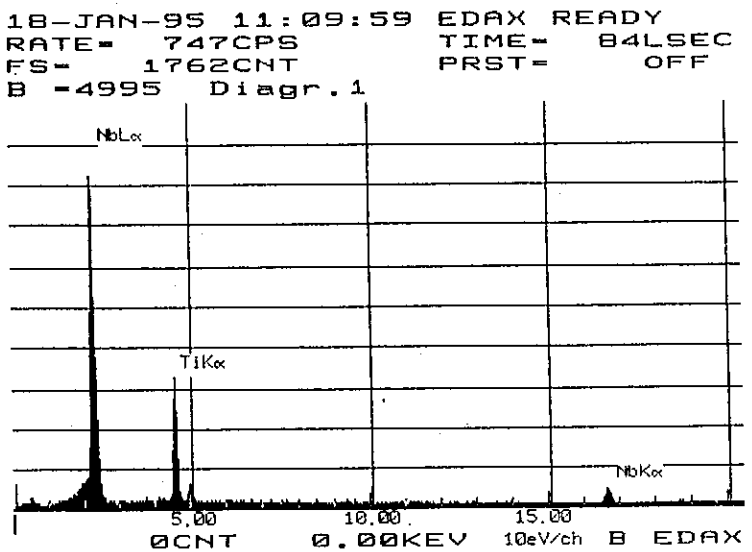

Analyse von Titan in Niobblech

Im nachfolgenden Experiment wurde die Diffusion von Titan in Niob hinein untersucht.

Der Meßplatz für hochortsaufgelöste Röntgenfluoreszenzanalyse (μ-SYXRF) am Hasylab wurde am Ablenkmagnetenstrahl L aufgebaut. Die weiße Strahlung wird durch eine Glaskapillare von $10\mu m$ Innendurchmesser kollimiert. Damit stehen folgende experimentellen Konditionen zur Verfügung:

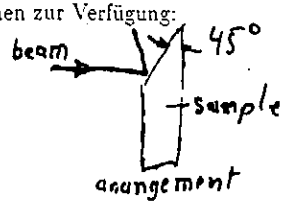

- Anregungsspektrum: $5 - 100keV$
- Strahlquerschnitt: kreisförmig $10\mu m$
- Ortsauflösung: besser als $10\mu m$
- Detektionssystem: HPGe der Firma DSG, Mainz (155 eV nominal)
- Nachweisempfindlichkeit für Titan: besser als 1%

Die Probe, welche schnell erhitzt wurde, wurde entlang der Schichtstruktur geschliffen und mit einer Rauhigkeit von weniger als $1\mu m$ poliert. Die andere Probe wurde nur gesägt und besitzt daher eine wesentlich rauhere Oberfläche. Während der Messungen steht die Probe unter 45° zum Strahl, damit der Detektor in der rechtwinkligen Geometrie wenig Streustrahlung bekommt.

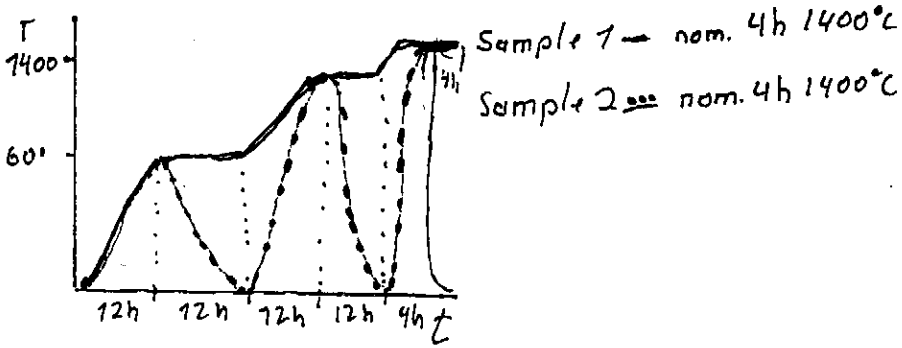

heattreatment on samples
to qualifie furnance

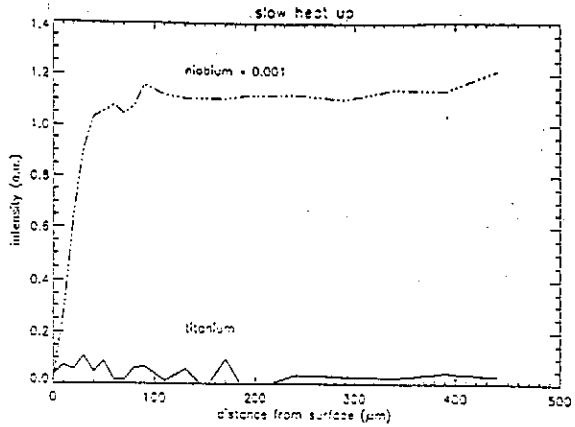

Abbildung 1:

Die Abb. 1 zeigt die Verteilung von Titan und Niob in der Probe. In den obersten $100\mu m$ erreicht das Titansignal wahrscheinlich gerade nicht aus, um mit drei Sigma Sicherheit (95%) nachgewiesen werden zu können. In tieferen Schichten ist der Rauschpegel zu hoch, um Titan nachweisen zu können.

Ti < 95% of Sigma probability

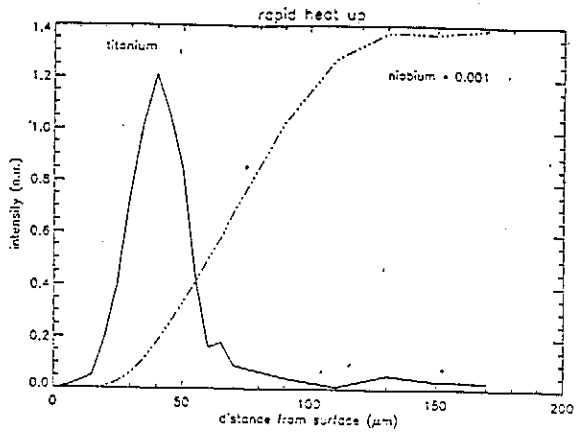

Abbildung 2:

Die Abb. 2 zeigt die Verteilung von Titan in Niob. Die oberste Schicht besteht aus nahezu reinem Titan. Die Titankonzentration nimmt mit zunehmender Schichttiefe ab und zeigt den typischen Verlauf eines Diffusionsprofils mit Poissontailing. Das Niobsignal steigt erst langsam mit zunehmender Tiefe an.

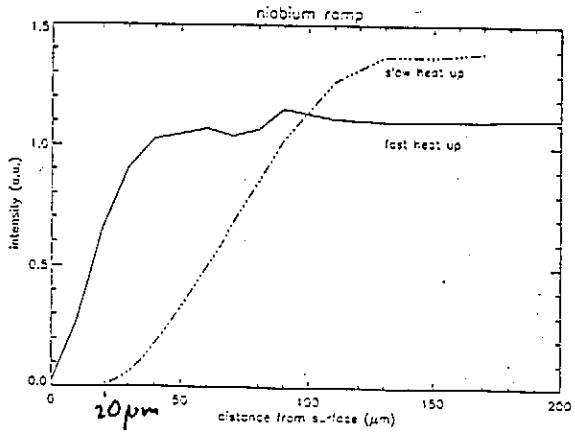

Abbildung 3:

Die Abb. 3 zeigt die beiden Niobsignale im Vergleich. Die Probe mit der langen Aufheizzeit zeigt eine Flanke von etwa $20\mu m$. Aus dem Strahlquerschnitt und einer in diesem Fall rauheren Oberfläche kann diese Anstiegsflanke leicht erklärt werden. Im Falle schneller Aufheizung hat die Flanke etwa $80\mu m$ Breite. Dieses Ergebnis ist völlig konform mit der gemessenen Titanschichtdicke von $70\mu m$.

Kai.

Creep in TTF Resonators

H. Kaiser

1.3.96

- creep measurements on 1-D samples

- creep of sag of resonators

- problems due to low strength of fired niobium

"Creep" is slow plastic deformation from prolonged exposure to stress.

creep = $\epsilon(\sigma, t)$

method: change in steps, then wait for plastic strain to occurr

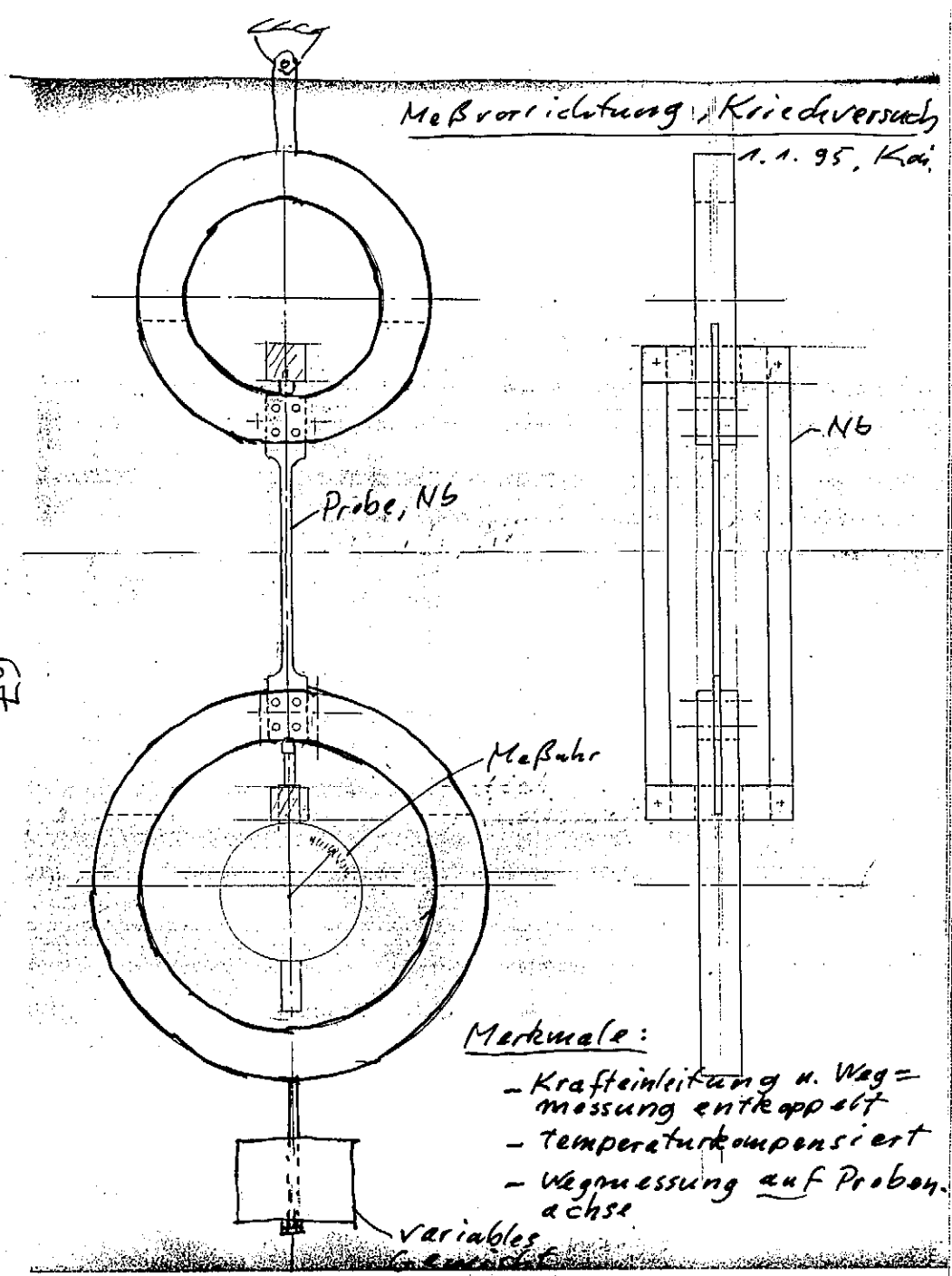
Meßvorrichtung Kriechversuch
1.1.95, Kai
Probe, N6
N6
Meßuhr
Merkmale:
- Krafteinleitung u. Weg-messung entkoppelt
- temperaturkompensiert
- Wegmessung auf Probenachse
variables

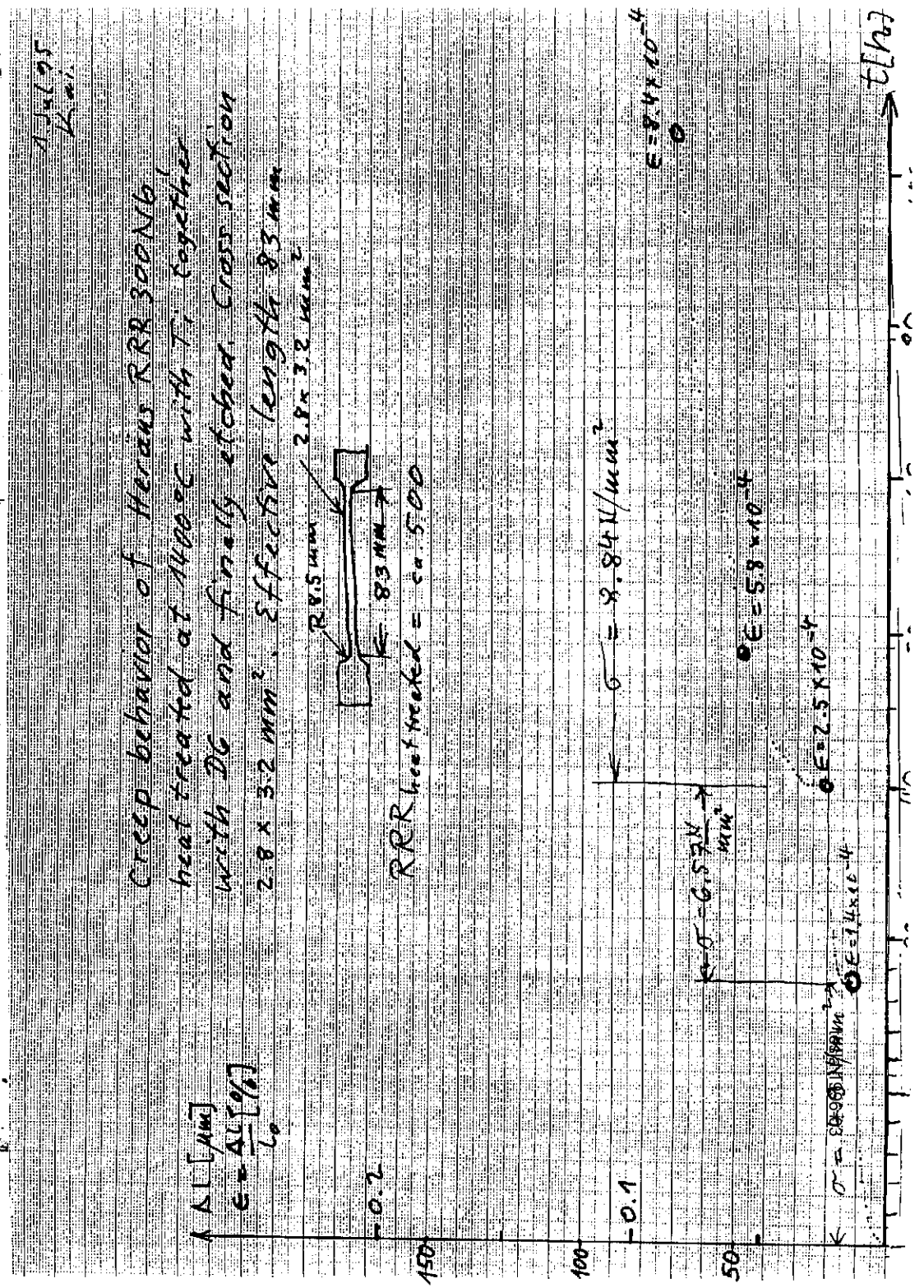
Creep behavior of Hereus RRR 300 Nb heat treated at 1400°C with Ti together with Dc and finally etched. Cross section
2.8 x 3.2 mm² Effective length 83 mm
2.8 x 3.2 mm²
R 0.5 mm
83 mm
RRR heat treated = ca. 500
ε = 8.84 10⁻⁴
ε = 5.8 x 10⁻⁴
ε = 2.5 x 10⁻⁴
σ = 8.84 N/mm²
σ = 5.5 N/mm²
σ = 2.5 N/mm²
ε = Δl/l₀
Δl [mm]
σ [N/mm²]
150
100
50
0.2
0.1

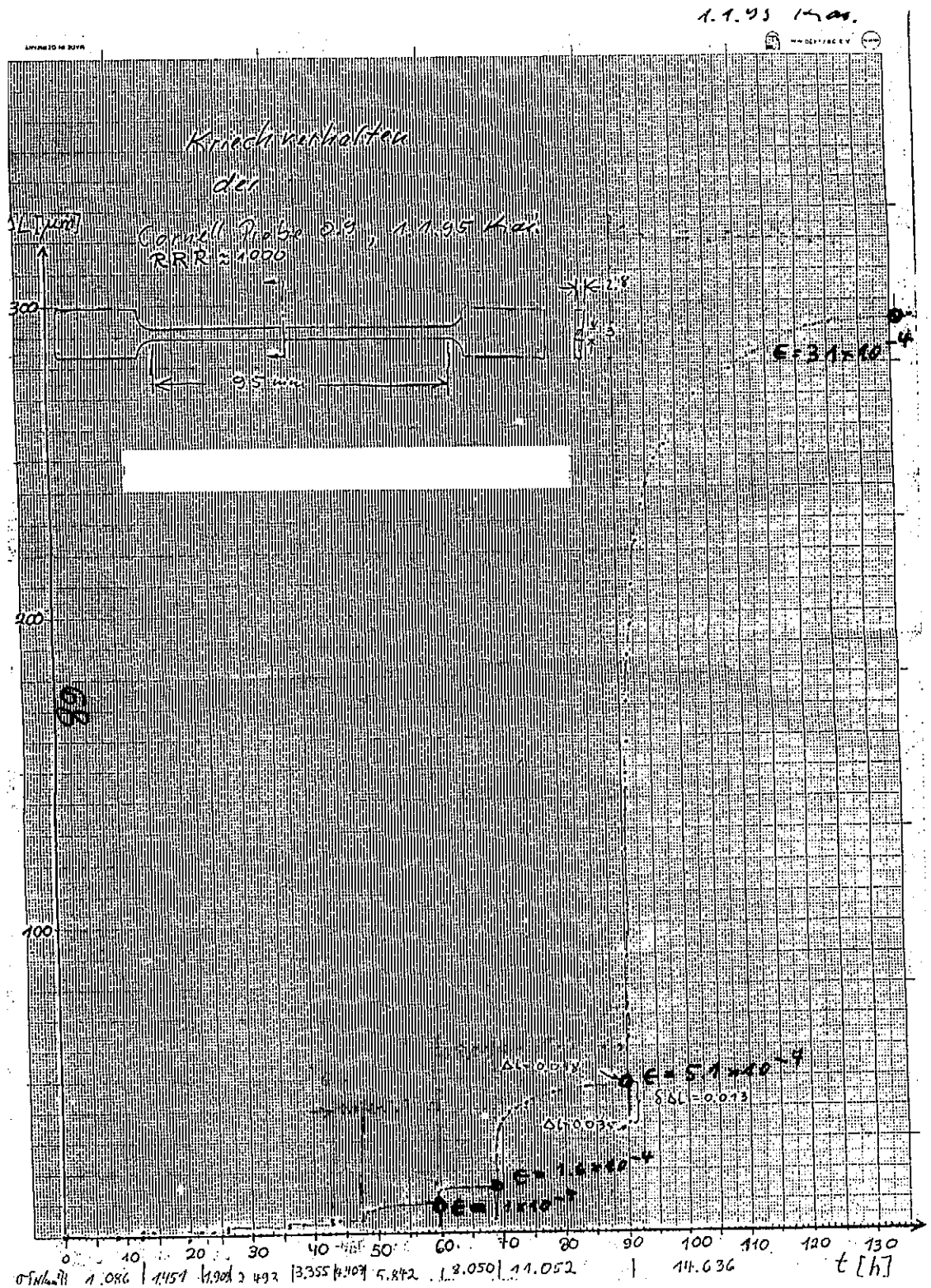

Problems due to low strength of Nb

- cavity shows plastic sagging
- necks for main coupler need a brace

- cavity flanges of cavity are deformed (up to 0.2 mm) by "Helicoflex" metal gaskets. ↷ frequent leaks

- handling of fired cavity can lead to deformation

- operation of tuner not fool-proof: Warming up fully compressed cavity will bend it.

Mittelhalbzelle

H.B. Peters
14.9.94

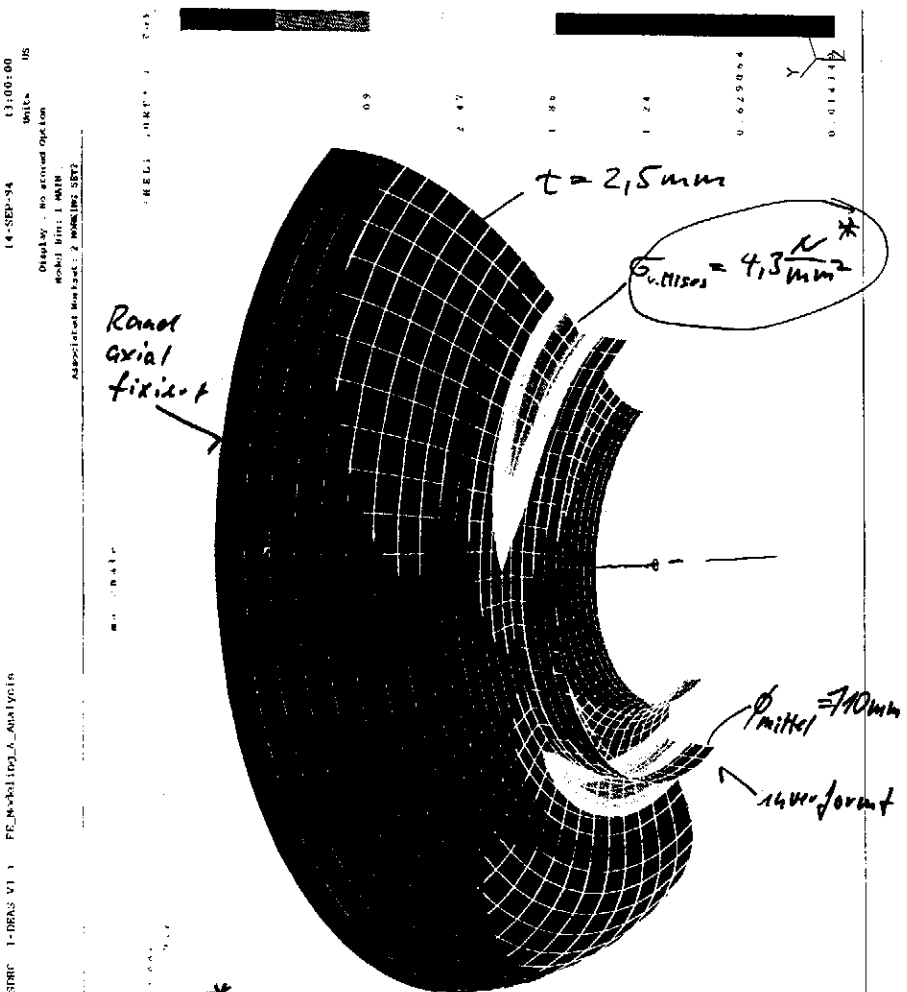

* Spannung gilt für Zwangskippung der Iris-Ebene gegenüber dem Äquator um 0,1 mrad. Hierfür erforderliches Biegemoment: 9986 Nmm (Vollquerschnitt)

cavity

$M_{b,max.} = 23072$ Nmm ↷ $\sigma_{max} = 9{,}9\ N/mm^2$

21.8.95 Ka:

Max Spannung im TTF-Resonator

Resonator im He Tank:

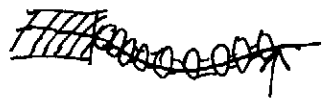

$\sigma_{max} = 9.93\ N/mm^2$

Resonator an Endflanschen unterstützt:

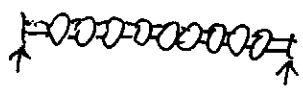

$\sigma_{max} = 14{,}2\ N/mm^2$

Resonator an Stützringen unterstützt:

$\sigma_{max} = 11{,}7\ N/mm^2$

Nach Ofenbehandlung:

$\sigma_{prop.} \approx 5\ N/mm^2$

Ka.. 4.9.95

Kriechen des Durchhangs von D3 nach Abstimmung, auf Endflanschen gelegert

tesla 1996-03

Kriechen des Durchhangs y

Creep of sag, D3 supported on endflanges

[mm]

o—— Meßpunkte

+—— $y = 0.15988\, E_{00}(0.337c4\, t)$, t[h]

y(1y) = 0,15 mm

y(100y) = 1,03 mm

D3, heat-treated

time [d]

Zeit

0.4
0.3
0.2
0.1
0

26.8.95 | 26.8. | 27.8. | 28.8. | 29.8. | 30.8. | 31.8. | 1.9. | 2.9. | 3.9. | 4.9.

0 1 2 3 4 5 6 7 8 9 10

232

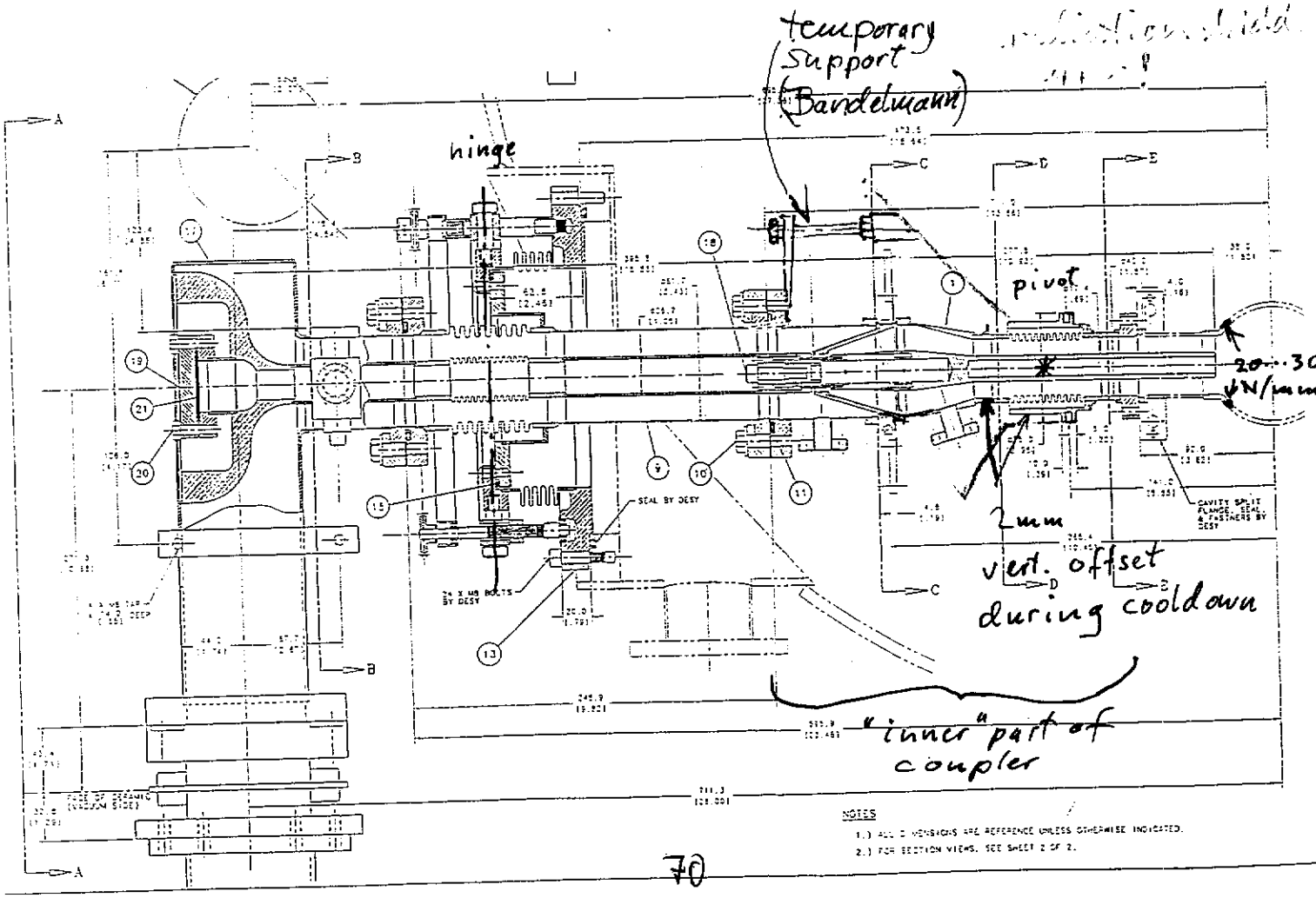

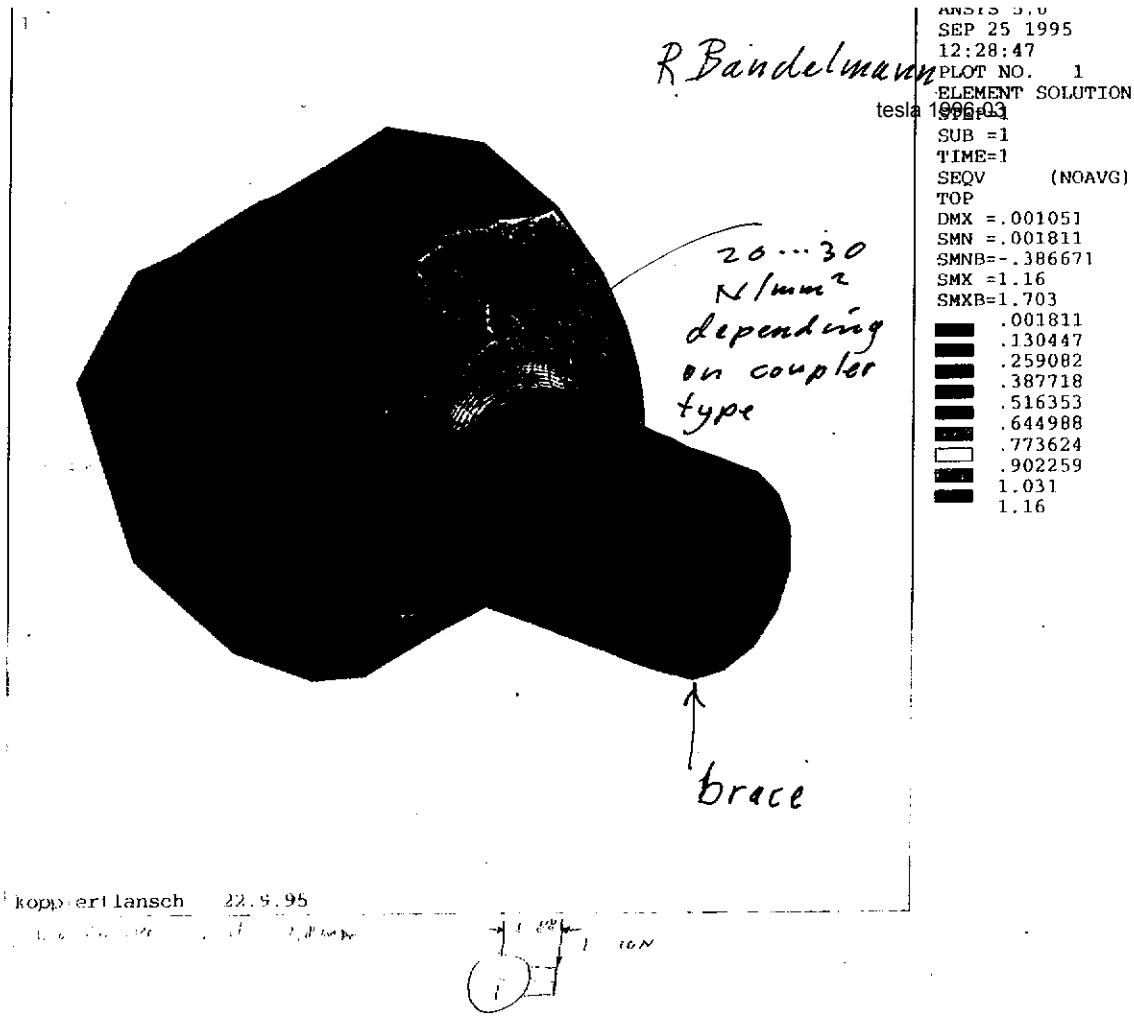
R Bandelmann
tesla 1996-03
ANSYS 5.0
SEP 25 1995
12:28:47
PLOT NO. 1
ELEMENT SOLUTION
STEP=1
SUB =1
TIME=1
SEQV (NOAVG)
TOP
DMX =.001051
SMN =.001811
SMNB=-.386671
SMX =1.16
SMXB=1.703
.001811
.130447
.259082
.387718
.516353
.644988
.773624
.902259
1.031
1.16
20…30 N/mm² depending on coupler type
brace
Koppelflansch 22.9.95

Understanding of Q degradation

Michael Pekeler
II. Institut für Experimentalphysik der Universität Hamburg

29 Feb 1996

Observation of Q degradation during:

- CWP (continious wave processing)
- HPP (high power processing)

In principle there is no difference in the processing mechanism between CWP and HPP. Two mechanisms are considered:

- Current I through emitting site heats up the emitter

$$I \sim \exp\left(-\frac{c}{\beta E}\right) .$$

  Strong heating $\Rightarrow$ Material evaporation

- Electric field causes Pressure P on emitting site

$$P = \frac{1}{2}\varepsilon_0(\beta E)^2$$

$$P = 10^2 \text{ N/(mm)}^2 \quad \text{for} \quad \beta E = 7 \text{ GV/m}$$

  If stress gets too high $\Rightarrow$ Material explosion

Example of Q-degradation during CW processing

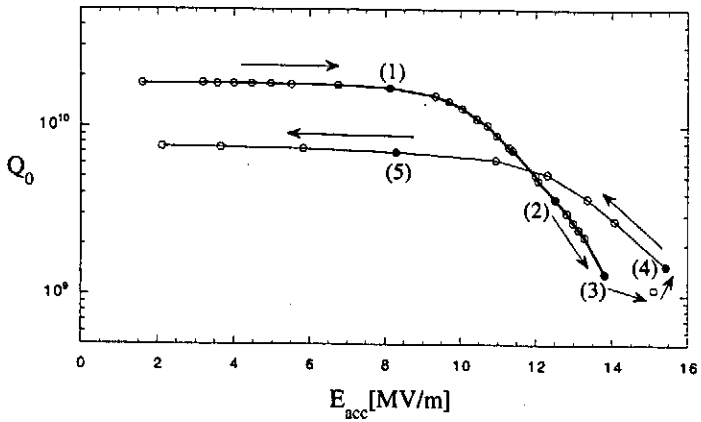

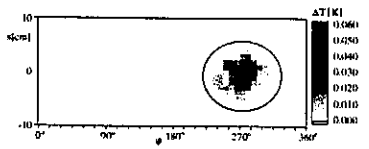

(1) $E_{acc} = 8.1\,\mathrm{MV/m},\ Q_0 = 1.7 \cdot 10^{10}$

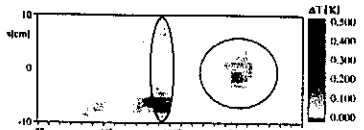

(2) $E_{acc} = 12.5\,\mathrm{MV/m},\ Q_0 = 3.7 \cdot 10^{10}$

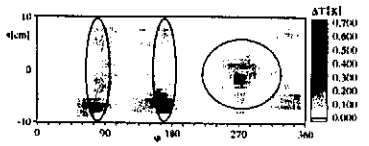

(3) $E_{acc} = 13.8\,\mathrm{MV/m},\ Q_0 = 1.3 \cdot 10^{9}$

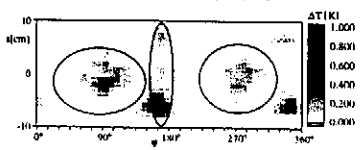

(4) $E_{acc} = 15.4\,\mathrm{MV/m},\ Q_0 = 3.8 \cdot 10^{9}$

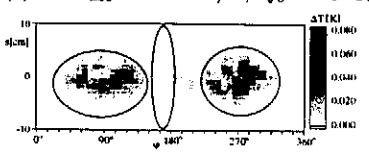

(5) $E_{acc} = 8.3\,\mathrm{MV/m},\ Q_0 = 7.0 \cdot 10^{9}$

Example of Q-degradation during HPP

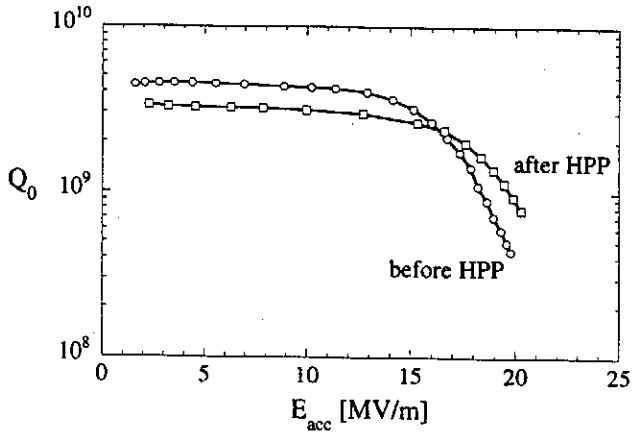

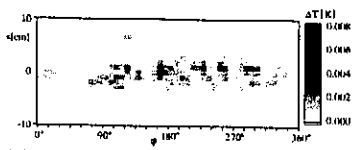

(1) $E_{acc} = 2.8\,\mathrm{MV/m},\ Q_0 = 4.5 \cdot 10^{9}$

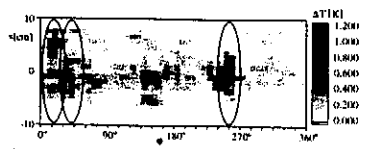

(2) $E_{acc} = 19.8\,\mathrm{MV/m},\ Q_0 = 4.4 \cdot 10^{8}$

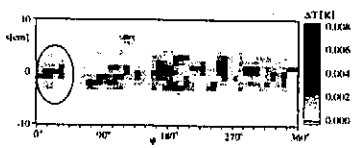

(3) $E_{acc} = 3.2\,\mathrm{MV/m},\ Q_0 = 3.3 \cdot 10^{9}$

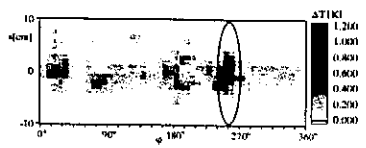

(4) $E_{acc} = 20.3\,\mathrm{MV/m},\ Q_0 = 7.8 \cdot 10^{8}$

Recovering of the Q ⇒ thermal cycle

- It is often observed, that thermal cycling to room temperature recovers Q
- sometimes HPP heats up the Cavity strong enough (Cavity in thermal breakdown), that the surface contamination changes, ex-specially, when HPP was performed at 4 K

Example for Q-recovery with HPP at 4K:

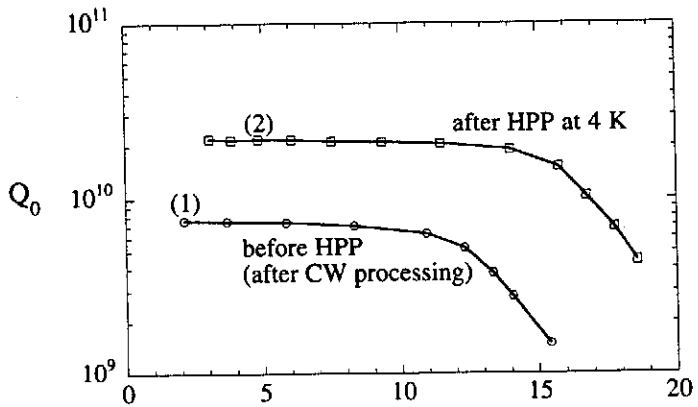

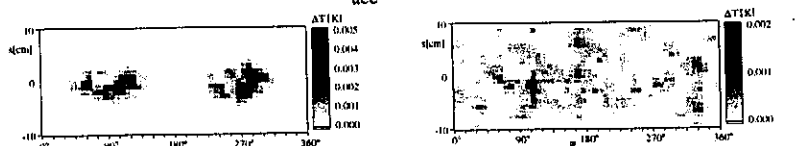

(1) $E_{acc} = 2.1\,\mathrm{MV/m},\ Q_0 = 7.6 \cdot 10^9$ (2) $E_{acc} = 4.8\,\mathrm{MV/m},\ Q_0 = 2.2 \cdot 10^{10}$

Example of Q-recovery with HPP at 2 K

(note: Starting Q verry low)

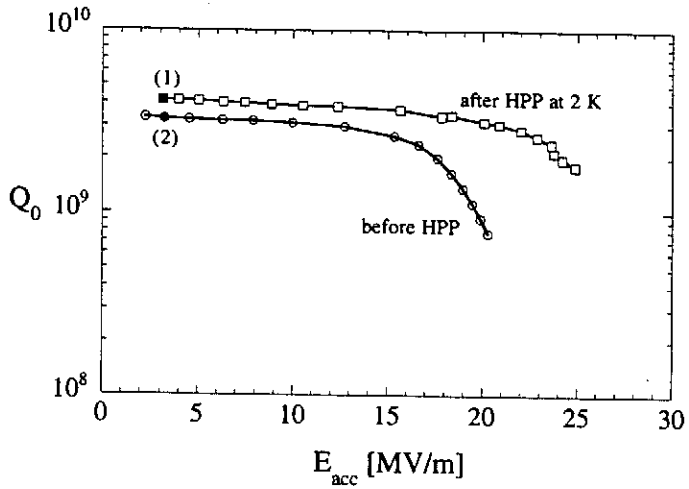

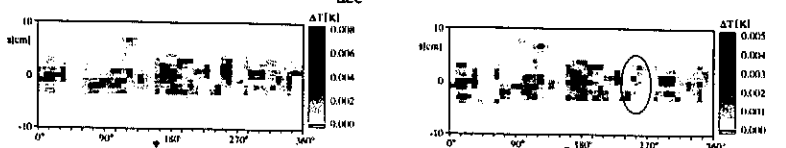

(1) $E_{acc} = 3.2\,\mathrm{MV/m},\ Q_0 = 3.3 \cdot 10^9$ max $\Delta T = 8$ mK

(2) $E_{acc} = 3.1\,\mathrm{MV/m},\ Q_0 = 4.1 \cdot 10^{10}$ max $\Delta T = 5$ mK

Danger of HPP:

- A lot of power has to go through coupler and exspecially through the ceramic and may produce outgasing which can influence the Q as well
- Field emission electrons hitting the ceramic may produce cantaminants which can act as new emitters.

  Japanese Q degradation (E. Kako et al.)

⇒ Design of coupler Fermi 1 safer than Fermi 3, electrons do not see the ceramic in the case of Coupler Fermi 1.

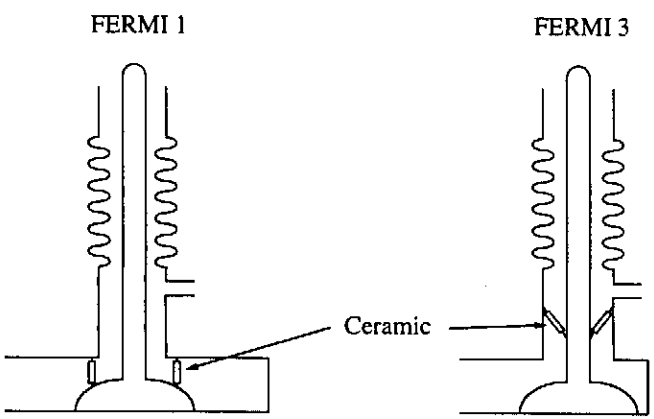

SA

Do we need HPP?

What did we learn from the 9-cell tests so far?

- If the cavity is not absolutely clean, only HPP can show the real potential of the cavity
- It is difficult to decide from the CW measurements, how good the flat-top-performance of the cavity is

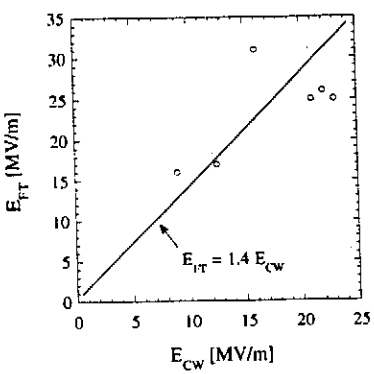

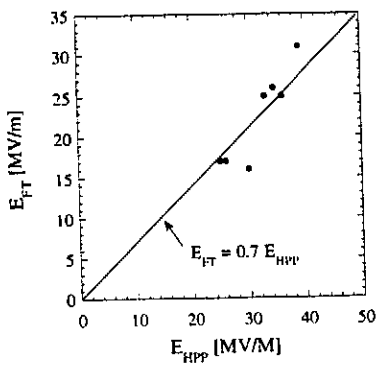

Field Emission (FE) Issues in TTF Superconducting RF Cavities (Production Series D1,...D6, C19)

Jozef Kuzminski
DESY/MHF-SL

Presented at R&D Meeting on 29-Feb-96 at DESY

Field Emission (FE), when present, is a serious factor limiting performance of superconducting RF cavity

FE signature:

- dramatic degradation of Q_0 during cavity excitation accompanied by intense X-rays (dose of > 1Gy/min were measured)
- Can be sometimes (?) cured in situ by High Power Processing (HPP). Example: D2_T2

Table 1 summarizes presently available data of TTF superconducting RF cavities from production series (D1,...,D6 and C19)

Performed tests suggests that FE presently is not a major concern because of careful cavities treatment and intense (triple) High Pressure Water (HPW) rinsing.

However it can be a problem if procedures are not strictly followed. Examples:

- "dirty " assembly - C19, D3
- "accidents" during testing D1

Cavity ID	Total Material Removed (μm)	HPW Rinsing	Initial RRR	Max. Oven Temp. (C)	Oven Time (min)	Final RRR	Low Eacc (MV/m)	Q_0 (10^9) at Low Eacc	Max. Eacc (MV/m)	Q_0 (10^9) at Max. Eacc	Max. Eacc Limited by	HPP (MV/m)	File	Comment
D1	155	3	281	1400	240	535	0.86	34.40	23.70	14.70	TB		07dec95qe03	No FE seen. Very flat excitation function.
D1							1.04	17.60	21.60	2.65	AP		13dec96qe06	Heavy FE observed for Eacc>15 MV/m as a results of FNAL coupler processing
D2	135	1	289	1400	240	348	3.18	18.10	14.00	1.24	TB		16mar95qe01	Heavy FE observed for Eacc>7 MV/m
D2							1.72	9.91	21.90	3.68	TB	35(HPP)	16mar95qe02	FE cured by HPP
D3	100	3	288	1400	60	520	1.53	25.20	11.50	2.20	TB		23jan96qe01	High FE. Cavity assembling problems.
D4	300	3	265	1400	240	525	0.90	28.90	13.50	15.60	TB		09feb96qe01	No FE seen (Q switch)
D5	130	3	265	1400 1250	60 180	465	0.70	30.30	8.00	3.70	TB		27feb96qe01	No FE seen (Q switch)
D6	200	1	265	1400	240	534	1.40	25.80	12.90	11.00	TB		24oct95qe15	FE seen in mode 8/9π Q switch. Hot spot seen in cell #5 (T-map, grinding.)
C19	150	1	250	1300	960	590	1.14	38.40	13.30	1.70	TB		02jun95qe01	Heave FE.
C19		1					1.07	19.20	21.60	1.75	TB	22(HPP)	12jun95qe08	FE Cured by HPP
C19		1					1.29	28.60	7.88	0.69	AP		07sep95qe01	Heavy FE ("dirty assembly")
C19		1					1.15	27.90	17.90	9.19	TB		06 oct95qe01	FE for Eacc>15MV/m

Cavity D1
Test 01

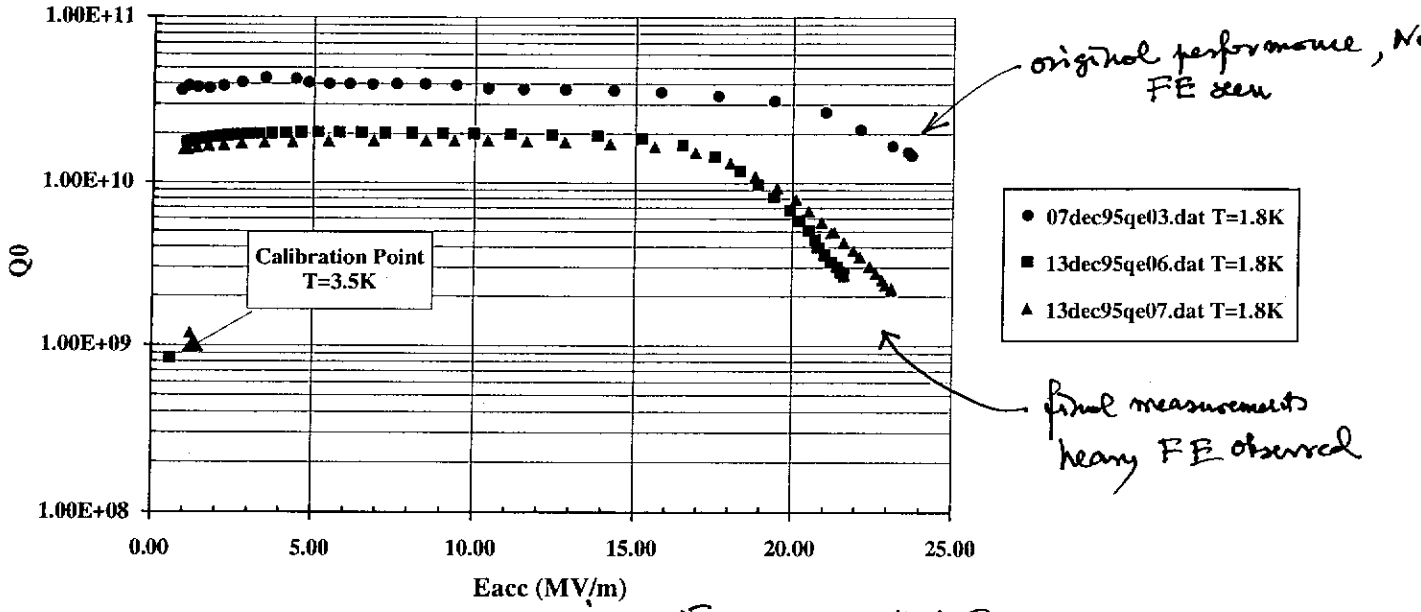

Performance degradation after/during High Power coupler processing

Cavity D2
Test 02

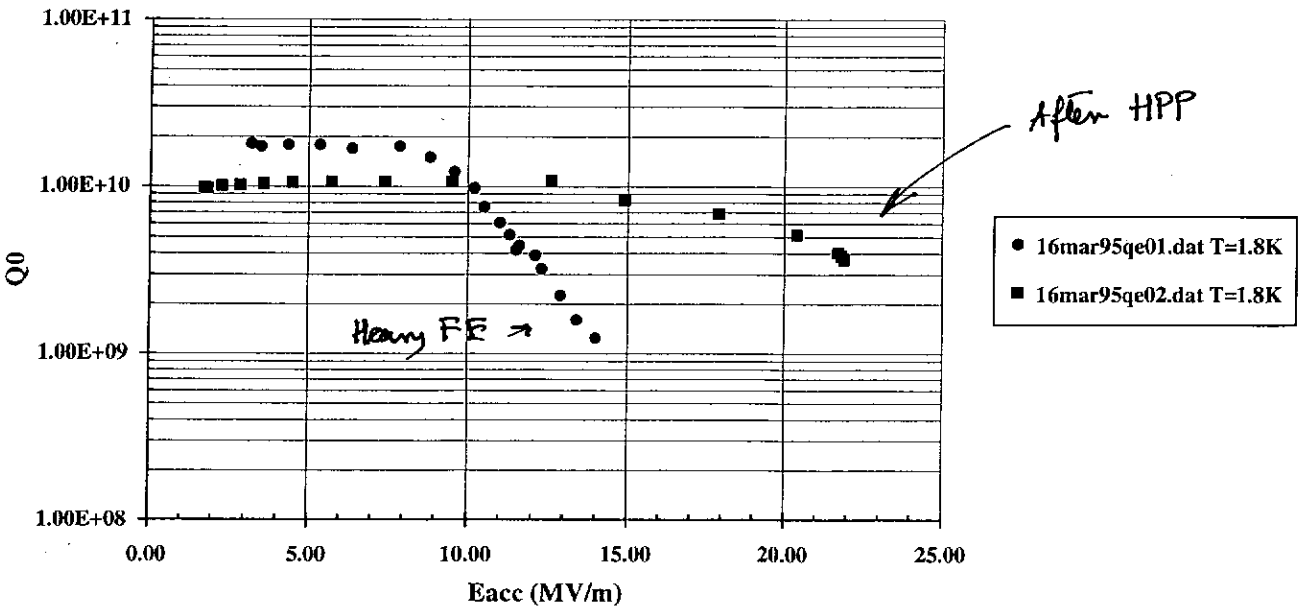

Example of 'in-situ' recovery by High Power Processing (HPP)

Cavity C19
Test 03

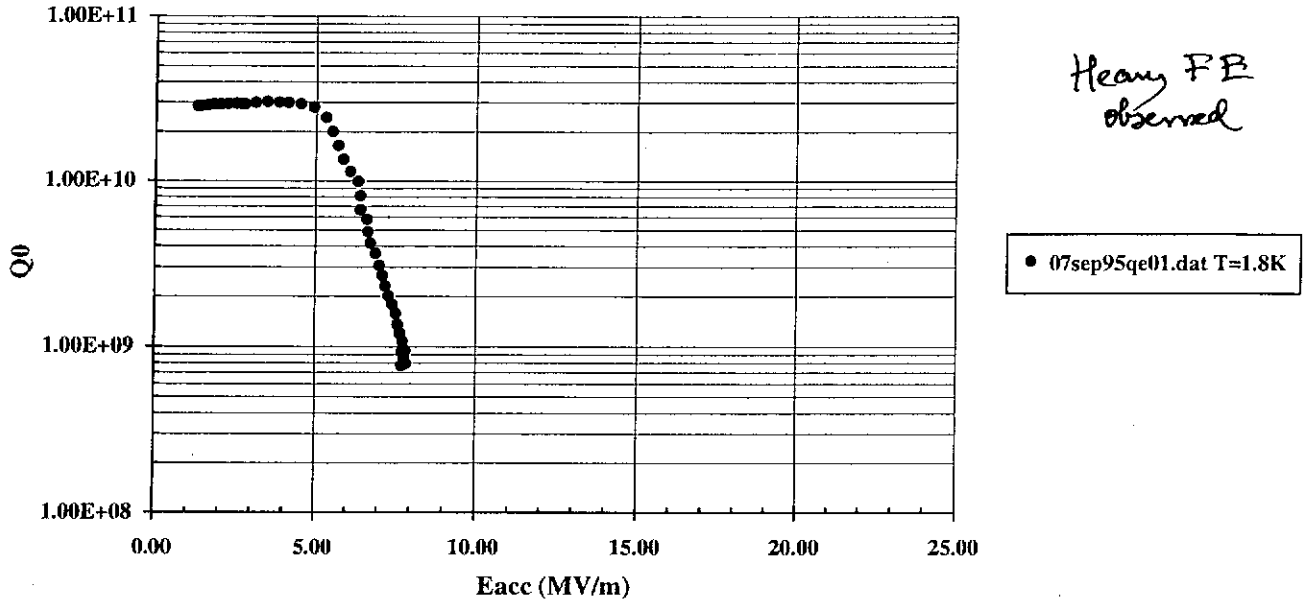

Heavy FE observed

"Dirty" assembly of C19 in CHECHIA (No local Clean Room)

Cavity D3
Test 01

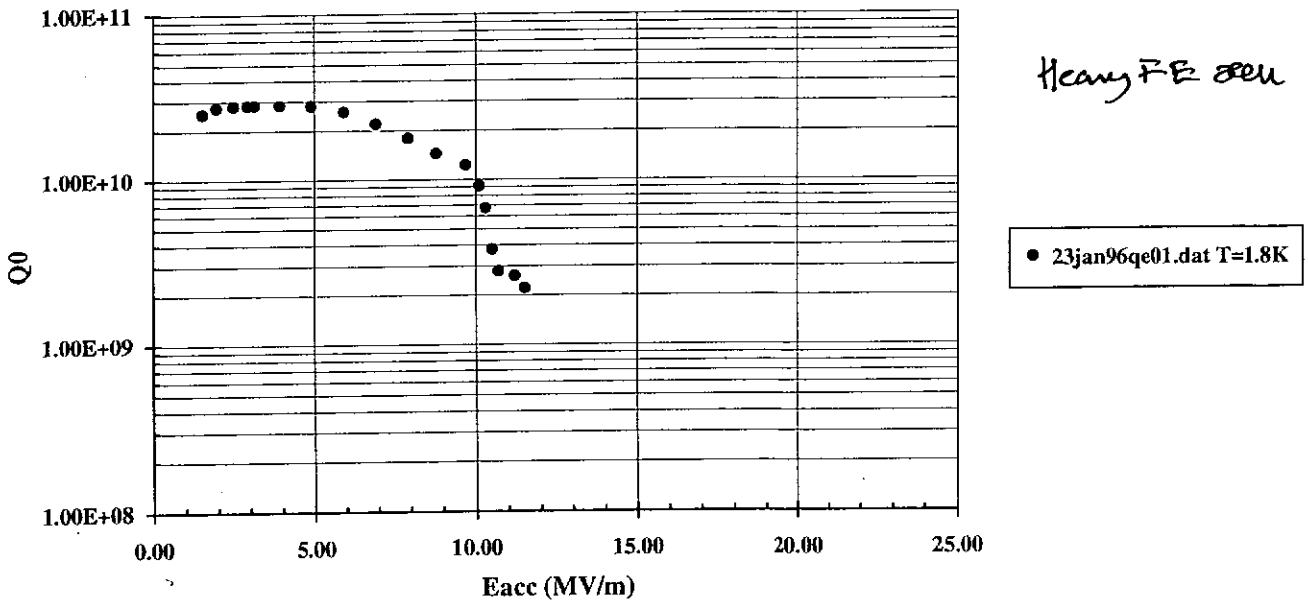

Heavy FE seen

"Dirty" assembee (leak on HOM coupler flange)

File: C19_T5_16nov95qe01.plt

Date: 25/2/96 21:52

Cavity C19
Test 05 (CHECHIA)

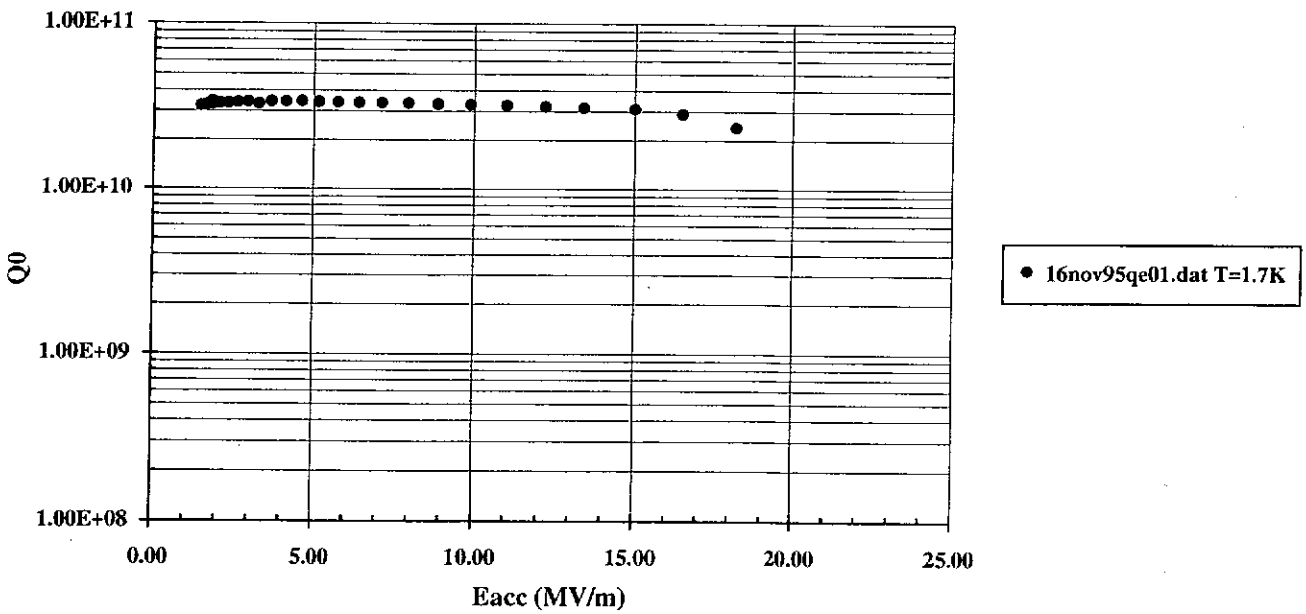

FE cured by High Pressure Water (HPW) rinsing

DC Field Emission from naturally rough Particles

T. Habermann

Univ. Wuppertal

Sample preparation (PK4):

- ≈ 10 µm BCP (1:1:1)
- rinsing in a container with deionized, filtered water
- rinsing with a water jet (deionized, filtered water)
- drying in chemistry room (without air-filtration)
- heat treatment at 400°C, 15 min
- FE-scans, emitter-analysis (FN, SEM, AES, EDX)
- 16 nm Au - vapor-deposition
- emitter-analysis (FN, SEM, AES, EDX)

change of electronical surface properties e.g. of secondary electron emission by Au-deposition

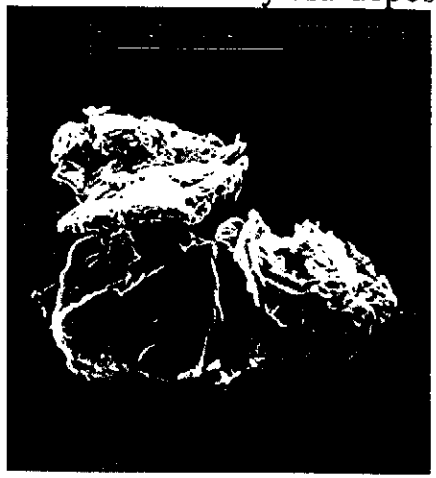

before Au deposition

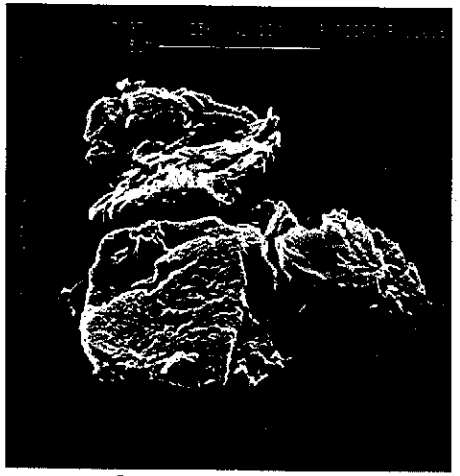

after Au deposition

82

Proof of uniform deposition thickness

thickness, calculated for ΔAu = 16 nm:

//

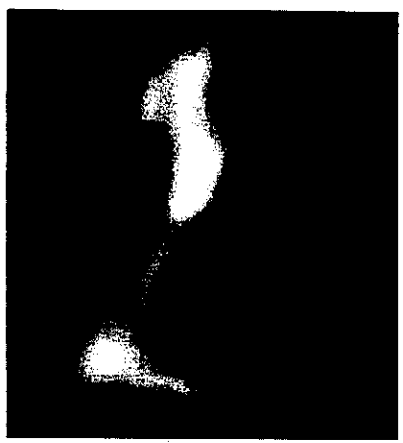

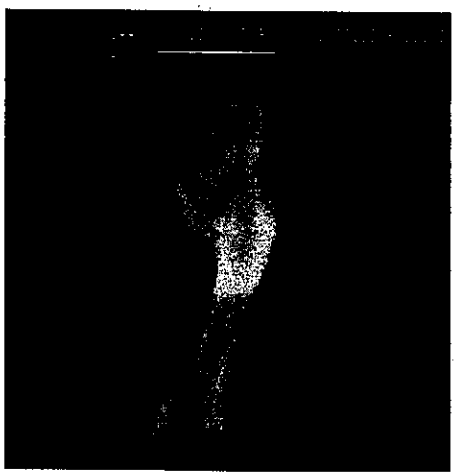

What changes by the Au-deposition?

Protrusion-Model:

$\beta i \approx hi/\pi$

$\beta \leq \beta 1 * \beta 2$

$S \approx r2^2 \pi$

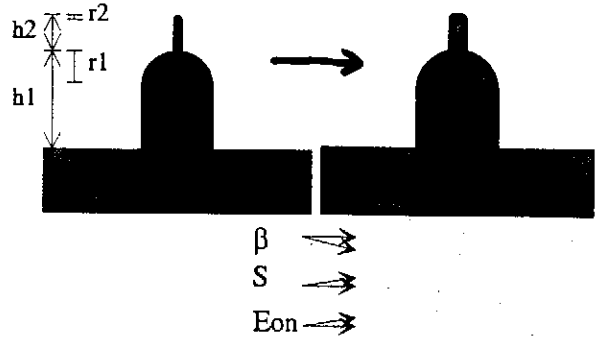

MIV-Model:

no enhanced field emission after Au-deposition

MIV + geometric field enhancement:

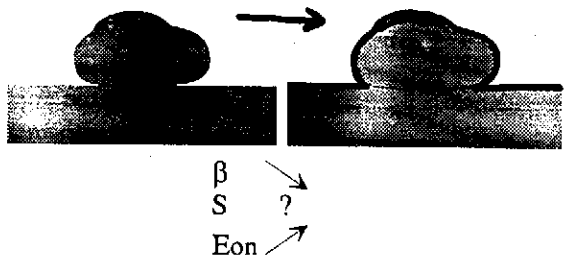

Antenna-Model (MIM):

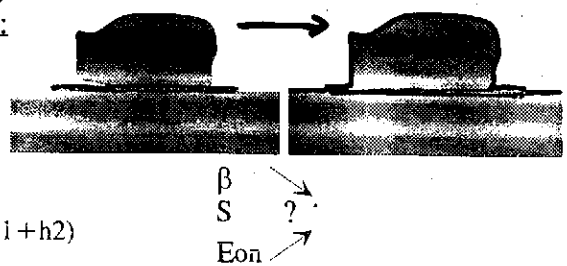

bef. Au-depos: $\beta_{FN} \sim (h1 + h2)$

tesla 1996-03

Estimation of β_{geo} from SEM-micrographs according to the "protrusion on protrusion model":

single protrusion:

$$\beta = h/r + 3\cos\theta$$

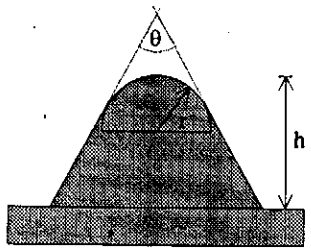

protrusion on protrusion:

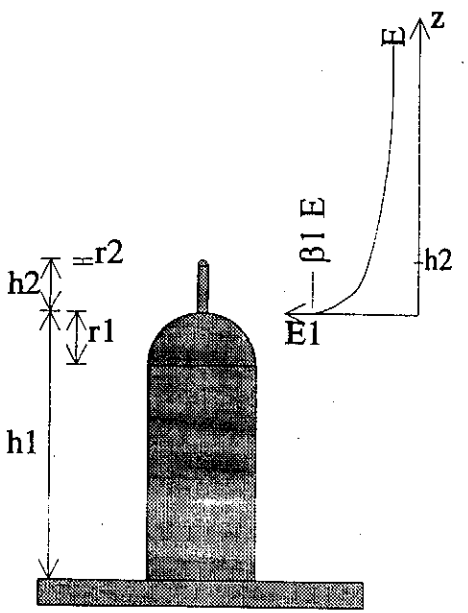

h2<<h1:

β1=10: calculations Saclay[1])

β1>10: calculations Wuppertal

h2 ≈ h1:

β1 = 2

$$\Rightarrow \beta_{geo} = \beta_2 \left\{ 2 + (\beta_1 - 2) \cdot \exp\left[-\left(\beta_1 \cdot h_2 / h_1 \right)^{(1.2367 - 0.0285 \cdot \beta_1)} \right] \right\}$$

[1]) M.Jiminez et al., J.Phys.D.: Appl.Phys. 27 ,1038 (1994)

After Au-deposition:

geometrical field enhancement

Comparision of β_{FN} and β_{geo} after Au-deposition leads to:

$\Phi_{Au} \approx 4.05$ eV

in Literature: $\Phi_{Au} = 4.3 - 4.9$ eV

Φ -Variation by adsorbates and geometry

Comparison of $\beta_{FN,\Phi=4.0eV}$ and β_{geo} before Au-deposition

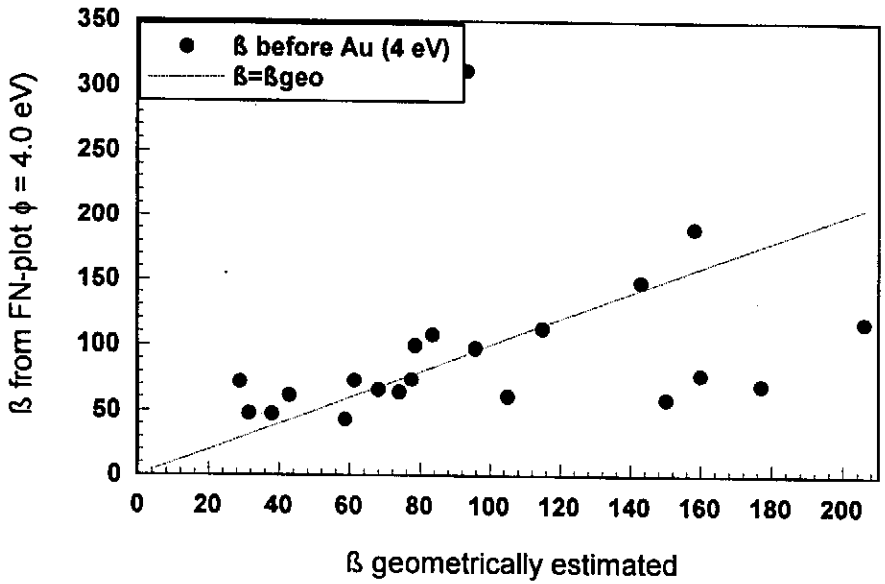

if geometric field enhancement: $\beta_{FN} \approx \beta_{geo}$

Comparison of $\beta_{FN,\Phi=4.05eV}$ and β_{geo} after Au-deposition

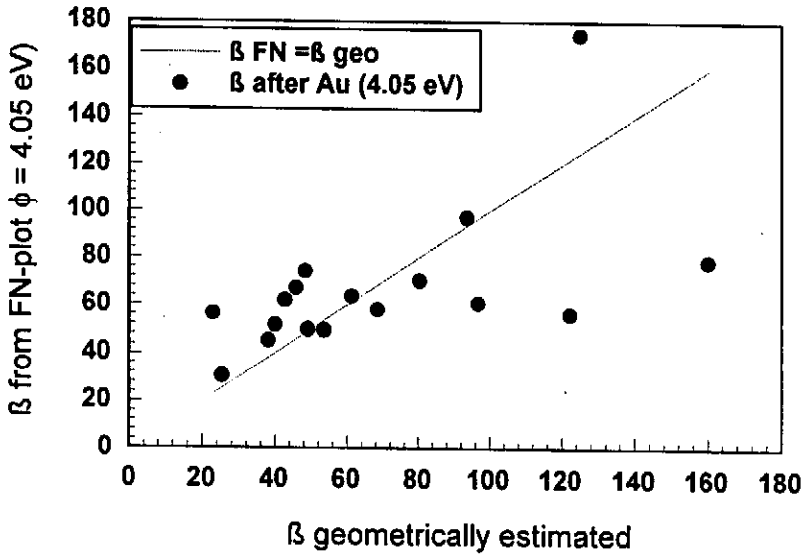

Comparison of the emitting areas from Fowler-Nordheim-analysis and from the geometry

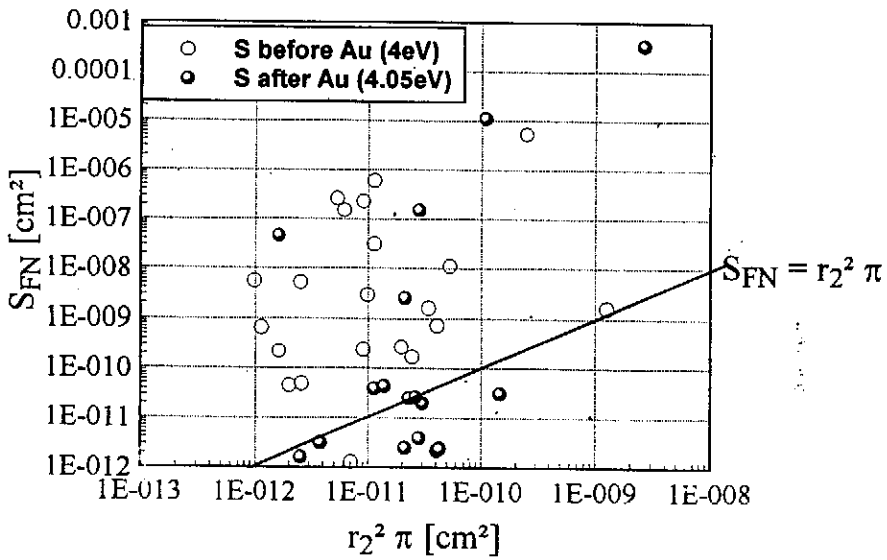

Protrusion-Model: $S_{FN} \leq r_2^2 \cdot \pi$

Emitters with β_{FN} in good agreement with estimated geometrical β_{geo}:

before Au deposition:

$\beta_{FN} = 112 = \beta_{geo} = 115$

$= 5*10^{-11}cm^2 \sim S_{geo} = 3*10^{-12}cm^2$

after Au deposition

$\beta_{FN} = 51 \sim \beta_{geo} = 40$

$S_{FN} = 3*10^{-9}cm^2 \neq S_{geo} = 2*10^{-11}cm^2$

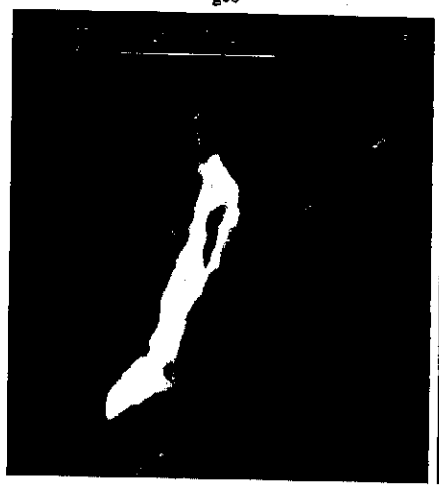

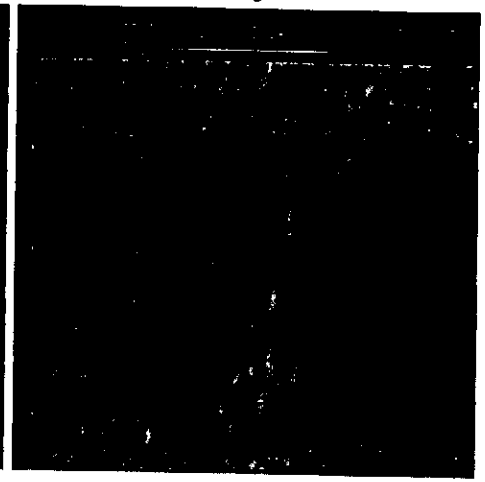

before Au:

$\beta_{FN} = 64 \sim \beta_{geo} = 74$

$S_{FN} = 6*10^{-9}cm^2 \neq S_{geo} = 1*10^{-12}cm^2$

after Au:

$\beta_{FN} = 49 = \beta_{geo} = 49$

$S_{FN} = 3*10^{-11}cm^2 \sim S_{geo} = 3*10^{-12}cm^2$

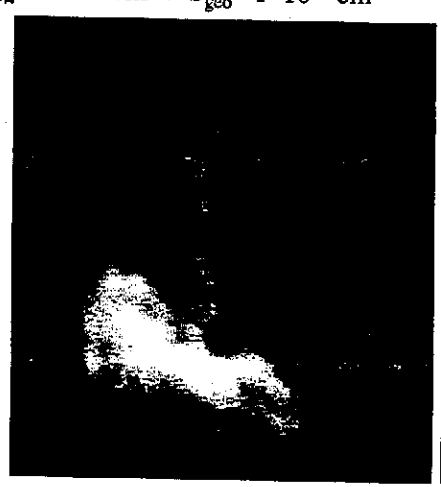

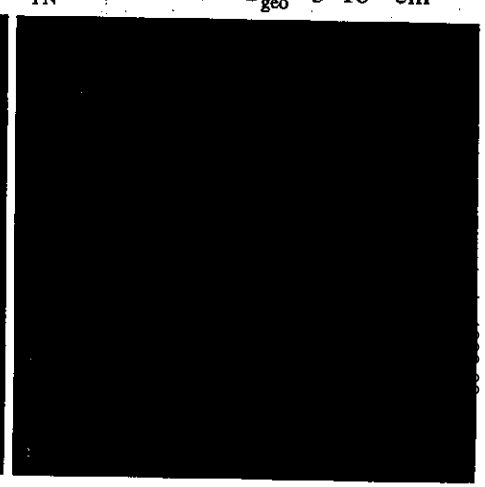

Emitters with β_{FN} strongly different from estimated geometrical β_{geo}:

before Au deposition:

$\beta_{FN} = 100 \neq \beta_{geo} = 79$

$S_{FN} = 3*10^{-10}cm^2 \sim S_{geo} = 3*10^{-11}cm^2$

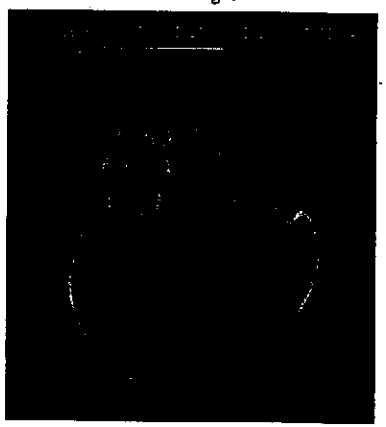

after Au deposition

$\beta_{FN} = 74 \neq \beta_{geo} = 48$

$S_{FN} = 2*10^{-12}cm^2 \sim S_{geo} = 4*10^{-11}cm^2$

98

before Au:

$\beta_{FN} = 61 \neq \beta_{geo} = 105$

$S_{FN} = 3*10^{-9}cm^2 \neq S_{geo} = 1*10^{-11}cm^2$

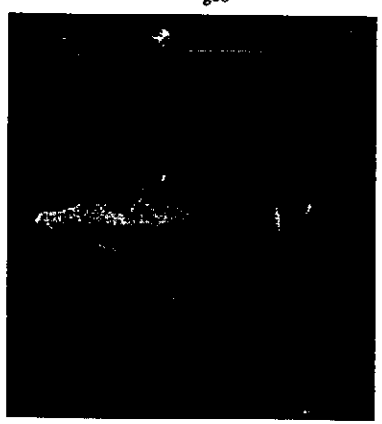

after Au:

$\beta_{FN} = 58 \neq \beta_{geo} = 68$

$S_{FN} = 3*10^{-11}cm^2 \sim S_{geo} = 1*10^{-11}cm^2$

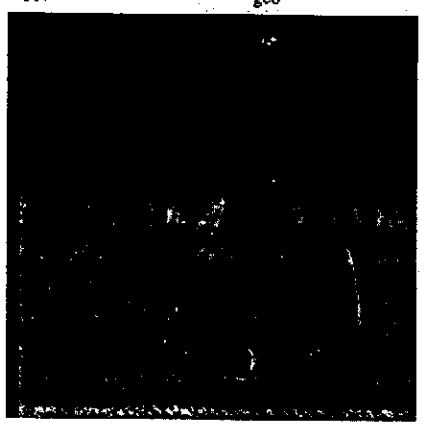

Change of E_{on} by Au-deposition:

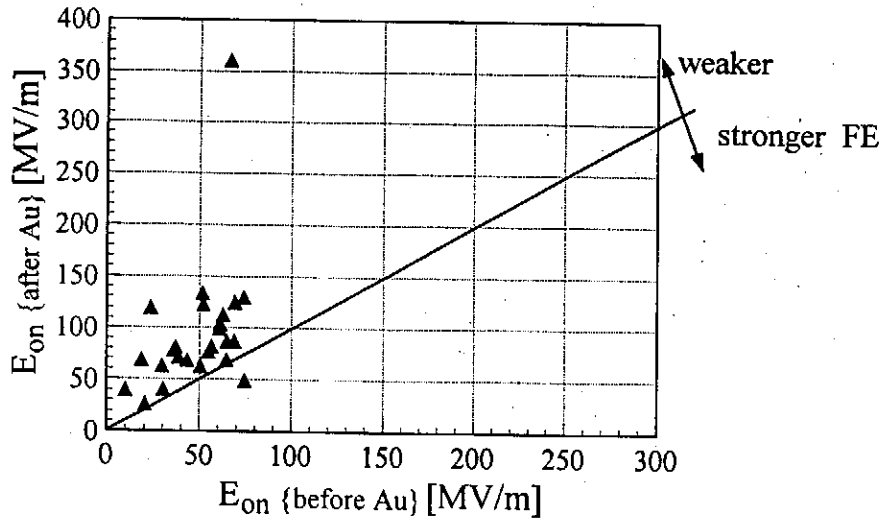

A slight increase of E_{on} by Au-deposition

Change of β_{FN} by Au-deposition:

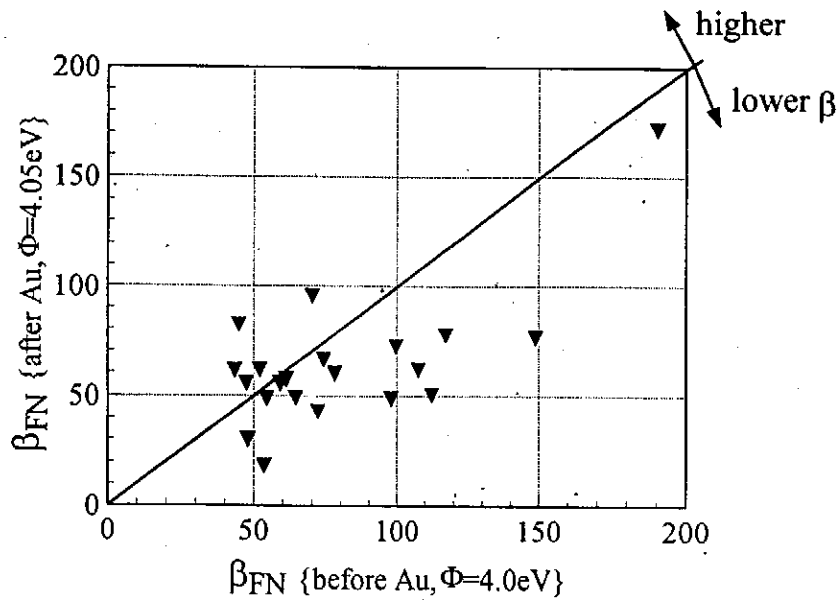

Change of S_{FN} by Au-deposition:

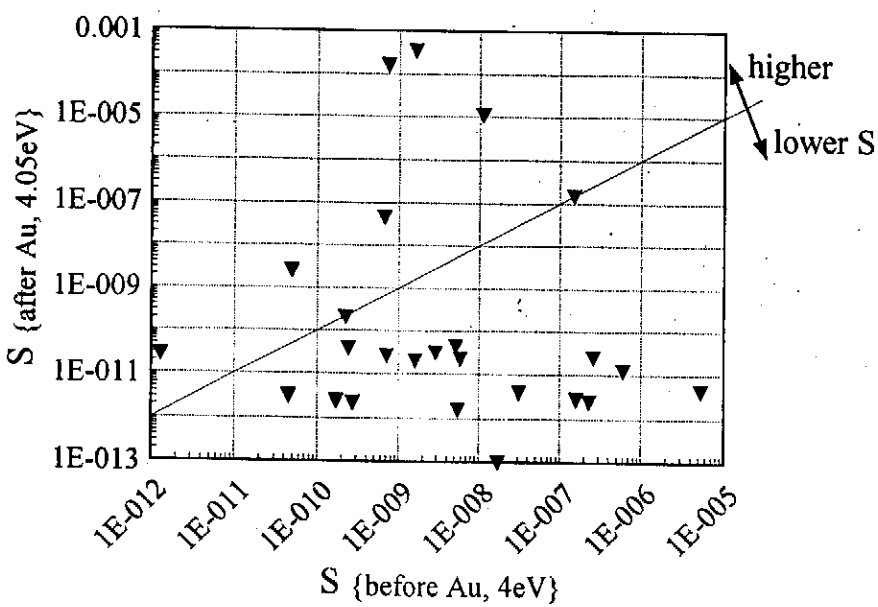

48

tesla 1996-03

Summary:

- very good agreement between β_{geo} and β_{FN} before gold-deposition
  → *geometric field enhancement sufficient for the observed FE*
- smaller spread of S_{FN}-values after Au-deposition, S_{FN} tend to more realistic values
  → *spread of S_{FN} probably due to adsorbates*
- assuming protrusion-model after Au-deposition the work function is changed
  → *influence of adsorbates and geometry*
- E_{on} rises by Au-deposition
- the average β_{FN} decreases ($\Phi = 4.05$eV)
- the average S_{FN} also decreases ($\Phi = 4.05$eV)
- → no pure MIV-model
  → MIM-model possible
  → geometric field enhancement can play a main role as emission mechanism

Outlook:

- Preparation of Nb-samples in cavities at TTF
- Influence of current processing on EFE
- Influence of Ion-bombardement on EFE
-
-

C. Stolzenburg

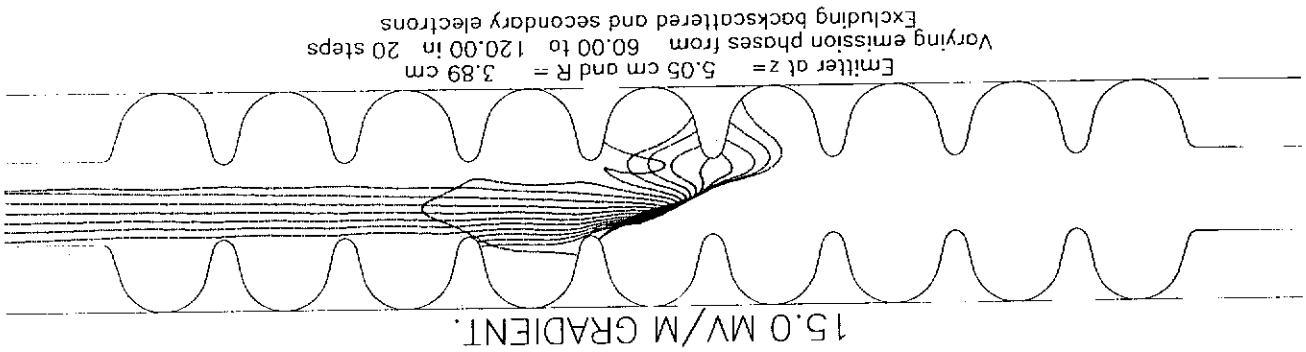

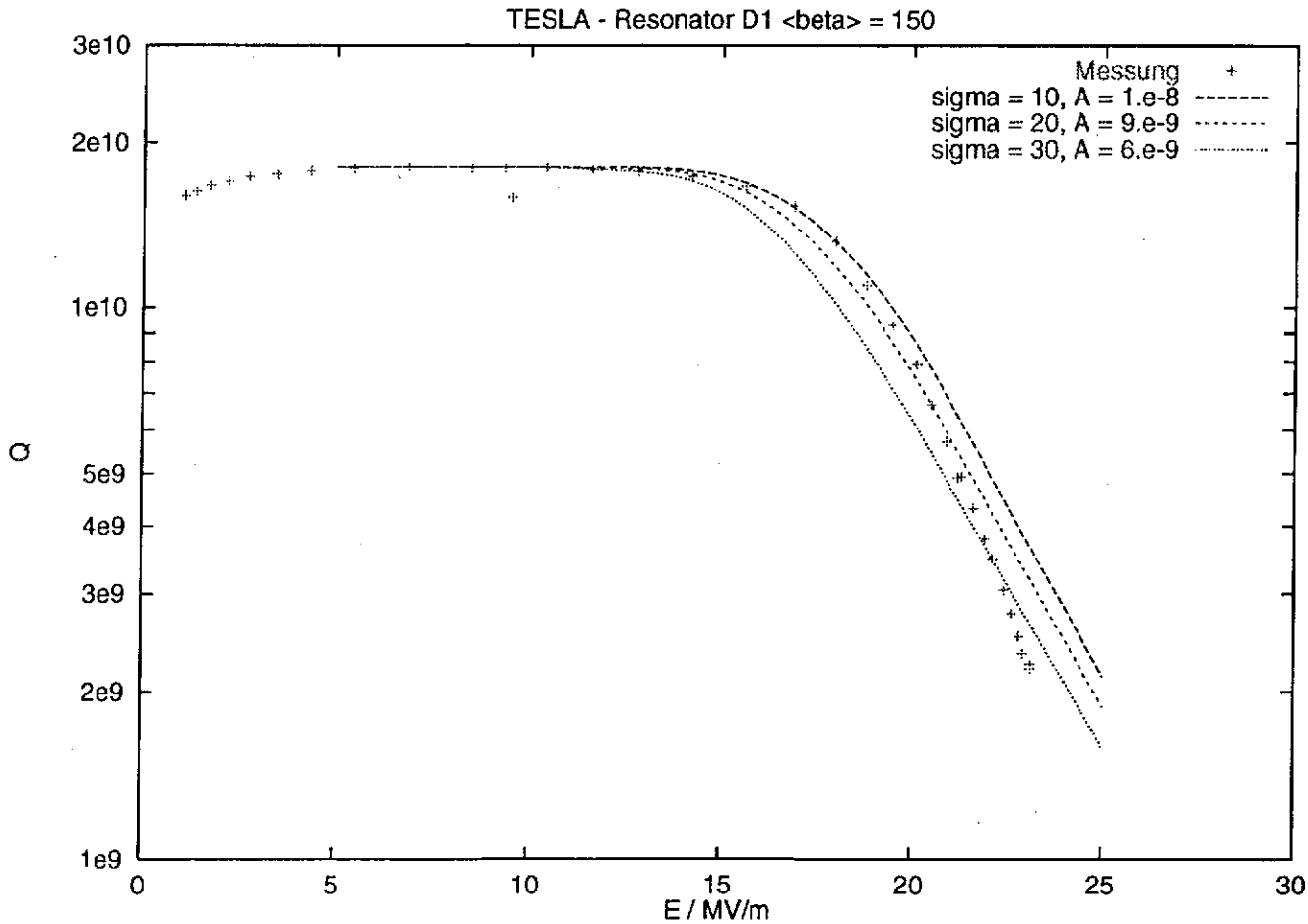

tesla 1996-03
E / MV/m
0
5
10
15
20
25
30
1e9
2e9
3e9
4e9
5e9
1e10
2e10
3e10
Q
Messung
beta = 80, A = 3.e-6
beta = 150, A = 9.e-9
TESLA - Resonator D1 <sigma beta> = 20

TESLA - Resonator D2, Test 2 Kurve 2 nach HPP
Messung vor HPP
Messung nach HPP
Q
3e10
2e10
1e10
5e9
4e9
3e9
2e9
1e9
0
5
10
15
20
25
30
E / MV/m

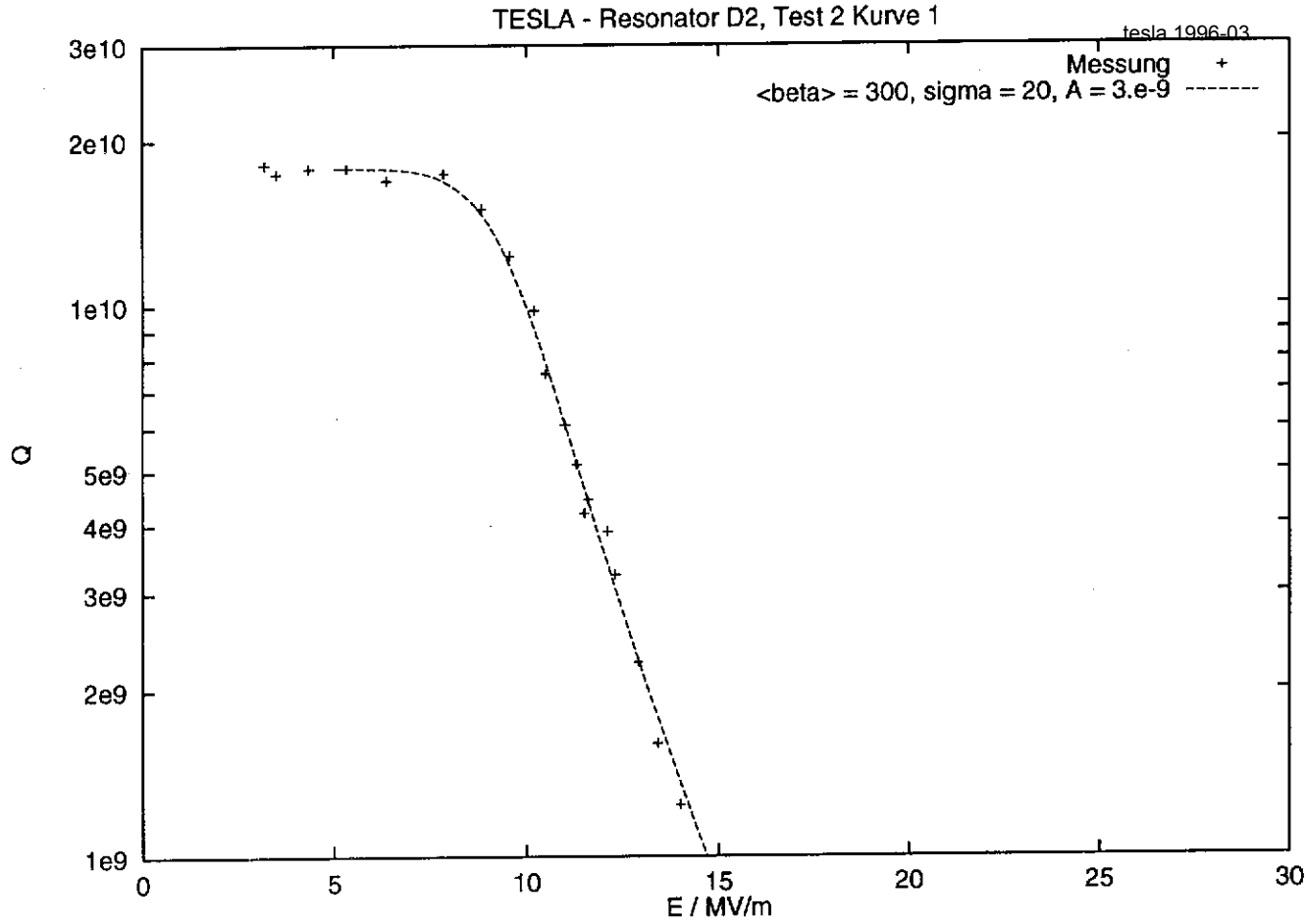
TESLA - Resonator D2, Test 2 Kurve 1
tesla 1996-03
Messung
<beta> = 300, sigma = 20, A = 3.e-9
Q
E / MV/m
3e10
2e10
1e10
5e9
4e9
3e9
2e9
1e9
0
5
10
15
20
25
30

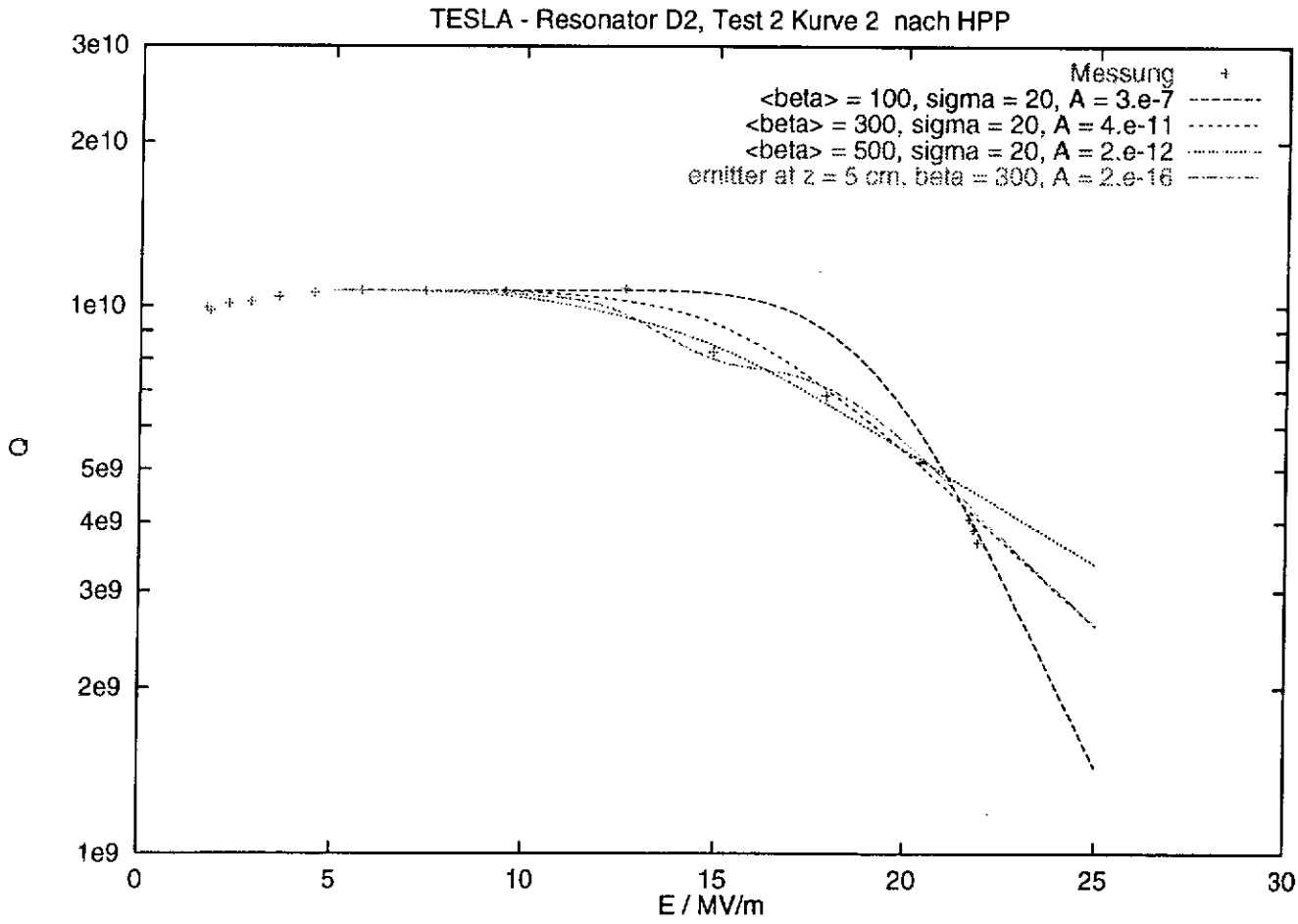
TESLA - Resonator D2, Test 2 Kurve 2 nach HPP
Messung
<beta> = 100, sigma = 20, A = 3.e-7
<beta> = 300, sigma = 20, A = 4.e-11
<beta> = 500, sigma = 20, A = 2.e-12
emitter at z = 5 cm, beta = 300, A = 2.e-16
Q
E / MV/m
3e10
2e10
1e10
5e9
4e9
3e9
2e9
1e9
0
5
10
15
20
25
30

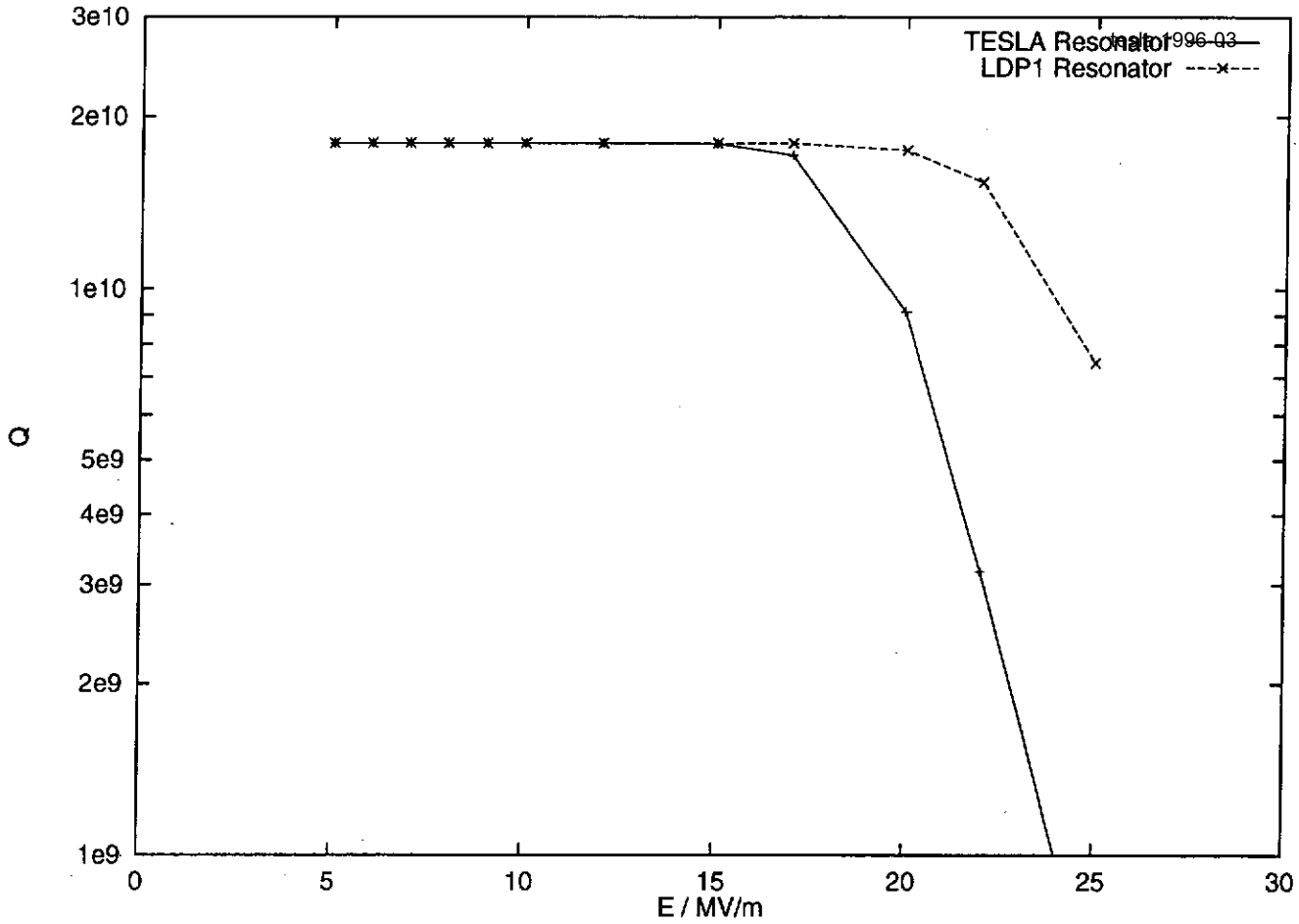
TESLA Resonator 1996-03
LDP1 Resonator
Q
3e10
2e10
1e10
5e9
4e9
3e9
2e9
1e9
0
5
10
15
20
25
30
E / MV/m